Description of Two Species of *Hoploscaphites* (Ammonoidea: Ancyloceratina) from the Upper Cretaceous (Lower Maastrichtian) of the U.S. Western Interior

Neil H. Landman, W. James Kennedy,
Neal L. Larson, Joyce C. Grier,
James W. Grier, and Tom Linn

Bulletin of the American Museum of Natural History

DESCRIPTION OF TWO SPECIES OF *HOPLOSCAPHITES* (AMMONOIDEA: ANCYLOCERATINA) FROM THE UPPER CRETACEOUS (LOWER MAASTRICHTIAN) OF THE U.S. WESTERN INTERIOR

NEIL H. LANDMAN
Division of Paleontology (Invertebrates), American Museum of Natural History, New York

W. JAMES KENNEDY
Oxford University Museum of Natural History, Oxford

NEAL L. LARSON
Larson Paleontology Unlimited, Keystone, South Dakota

JOYCE C. GRIER

JAMES W. GRIER
Department of Biological Sciences, North Dakota State University, Fargo

TOM LINN

BULLETIN OF THE AMERICAN MUSEUM OF NATURAL HISTORY
Number 427, 72 pp., 38 figures, 4 tables
Issued February 22, 2019

ISSN 0003-0090

CONTENTS

ABSTRACT

Two species of scaphitid ammonites (Ammonoidea: Ancyloceratina) from the Upper Cretaceous (lower Maastrichtian) of the Western Interior of North America are described. *Hoploscaphites macer*, n. sp., is medium size, with coarse ribs on the phragmocone, which become finer on the body chamber, and closely spaced ventrolateral tubercles. It occurs in the upper part of the *Baculites baculus* Zone and lower part of the overlying *B. grandis* Zone in the Pierre Shale in Montana, Wyoming, and Colorado, and in the Bearpaw Shale in Montana. *Hoploscaphites criptonodosus* (Riccardi, 1983) is larger and more coarsely ornamented, including one or two rows of lateral tubercles on the flanks of the phragmocone. It occurs in the upper part of the *Baculites baculus* Zone and overlying *B. grandis* Zone in the Pierre Shale in Montana, Wyoming, Colorado, and possibly South Dakota, and in the Bearpaw Shale in Montana and Saskatchewan, Canada. Both species form part of an evolving lineage of *Hoploscaphites* that first appears in the Western Interior of North America in the middle Campanian.

INTRODUCTION

The Upper Cretaceous Western Interior of North America contains a rich assemblage of scaphitid ammonites (hereafter referred to as scaphites for short). *Hoploscaphites* appears in the Western Interior in the middle Campanian *Baculites asperiformis* Zone and persists to the upper Maastrichtian *Hoploscaphites nebrascensis* Zone (fig. 1). It is represented by approximately 15 species, many of which have yet to be described. All of them are endemic to North America, with closely related species in western Greenland (Birkelund, 1965). They have occasionally been reported from Western Europe, but only as fragments (Machalski et al., 2007). Such rare occurrences are probably due to postmortem drift. In contrast, *Hoploscaphites constrictus* Sowerby, 1817, which is present in the Maastrichtian of Europe, is absent in North America.

Many of the species of *Hoploscaphites* in the Western Interior are very well preserved, retaining their original shell material and buccal apparatus. Their excellent preservation is due to their rapid burial in muddy to silty sediments that are nearly impermeable to groundwater penetration during postdepositional history. In addition, the ammonites commonly occur in early diagenetic concretions that preserve their three-dimensional shape. The shell material is also preserved with its original mineralogy and microstructure and is, thus, suitable for carbon and oxygen isotope analyses. The results of these studies suggest that species of *Hoploscaphites* lived close to the bottom in well-oxygenated environments (Landman et al., 2012a).

GEOLOGIC SETTING

Williams and Stelck (1975) and Landman et al. (2016) reviewed the paleogeography of the Western Interior Seaway during the early Maastrichtian. The western margin of the Seaway was bordered by a north-south trending unstable cordillera, whereas the eastern margin was formed by the low-lying stable platform of the eastern part of the coterminous United States and Canada (Cobban et al., 1994). The shoreline cut across the eastern half of Montana (fig. 1), forming a peninsula at the southeastern corner of the state that is referred to as the Sheridan Delta (Reiskind, 1975). The delta extended along the Montana-Wyoming border as far east as the Black Hills and separated the Mosby Embayment to the west from the rest of the Western Interior Seaway to the east (fig. 1). This deposit may not have comprised a single delta, but rather multiple deltas, reflecting shedding of sediments from regional uplifts in the area of the Big Horn and Granite Mountains (Krystinik and DeJarnett, 1995). The shoreline continued southwestward as a series of embayments as far as the northwestern corner of Colorado, and then cut southeastward across the middle of the state.

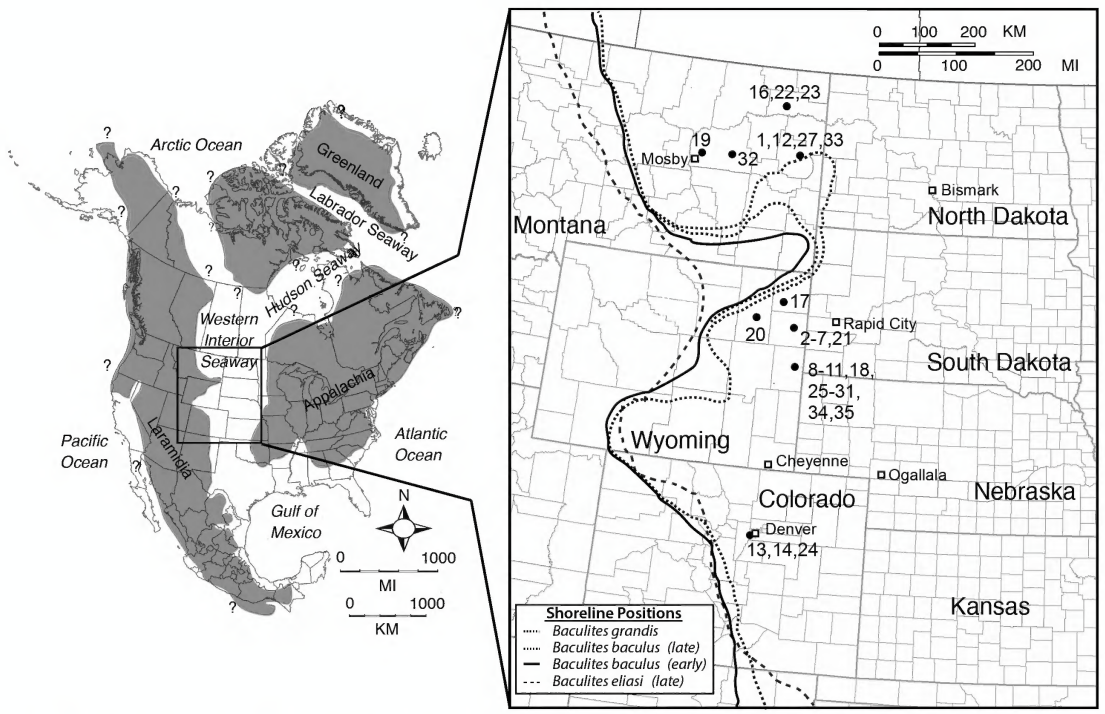

FIGURE 1. Overview of the Late Cretaceous Western Interior Seaway (left) and close-ups of the strandlines (right) during the deposition of the upper Campanian–lower Maastrichtian *Baculites eliasi–B. grandis* zones (modified from Landman et al., 2016). The numbered dots indicate U.S. localities cited in the text, as listed in the appendix.

The fossil localities in this study are close to the western margin of the Seaway, probably less than 100 km from shore, according to the paleogeographic maps produced by Cobban et al. (1994) and modified by Slattery et al. (2013). The depth of the Seaway during this time is difficult to precisely establish, but recent studies have suggested that it was less than 100 m deep (Gill and Cobban, 1966; Kauffman and Caldwell, 1993; Sageman and Arthur, 1994). Based on the fauna, sedimentology, and distance from shore on the Cedar Creek Anticline in east-central Montana, we estimate that the depth of deposition in this area was possibly even less, perhaps ≤50 m.

The sedimentary record of the Seaway contains a rich molluscan fauna that is used to subdivide the Upper Cretaceous strata of this area into numerous biostratigraphic zones (fig. 2). This zonation has been integrated with radiometric dates derived from interbedded bentonites (Cobban et al., 2006). The Maastrichtian Stage in the Western Interior Basin has been subdivided into six ammonite zones (Gill and Cobban, 1966; Landman and Waage, 1993a; Larson et al., 1997). They are, from lowest to highest, the *Baculites baculus*, *B. grandis, B. clinolobatus, Hoploscaphites birkelundae, H. nicolletii,* and *H. nebrascensis* zones (fig. 2). Walaszczyk et al. (2001) further refined the zonation using inoceramids. The *B. baculus* Zone is subdivided into the *Endocostea typica* Zone below and the *"Inoceramus" incurvus* Zone above, and the *B. grandis* Zone coincides with the *Trochoceramus radiosus* Zone (fig. 2). The Campanian-Maastrichtian boundary is placed at the base of the *B. baculus* Zone coincident with the base of the *E. typica* Zone (Walaszczyk et al., 2001; Cobban et al., 2006).

Hoploscaphites macer, n. sp., occurs in the upper part of the *Baculites baculus* Zone and lower part of the *B. grandis* Zone in the Pierre

Stage		Western Interior of North America	
		Ammonite Zones	Inoceramid Zones
Maastrichtian	upper (part)	***Hoploscaphites nebrascensis***	
		Hoploscaphites nicolletii	
		Hoploscaphites birkelundae	
	lower	***Baculites clinolobatus***	***"Inoceramus" balchii***
		Baculites grandis	***Trochoceramus radiosus***
		Baculites baculus	***"Inoceramus" incurvus***
			Endocostea typica
Camp. (part)	upper (part)	***Baculites eliasi***	***"Inoceramus" redbirdensis***

FIGURE 2. Biostratigraphic chart of the Upper Cretaceous (Campanian and Maastrichtian) of the Western Interior of North America showing ammonite and inoceramid zones (modified from Cobban et al., 2006).

Shale in Montana, Colorado, and Wyoming, and the Bearpaw Shale in Montana. *Hoploscaphites criptonodosus* (Riccardi, 1983) occurs in the upper part of the *B. baculus* Zone and overlying *B. grandis* Zone in the Pierre Shale in Montana, Colorado, Wyoming, and possibly South Dakota, and in the Bearpaw Shale in Montana. It has also been reported from the *B. baculus* Zone in the Belanger Member of the Bearpaw Shale in southwestern Saskatchewan, Canada (Riccardi, 1983). The presence of this species in both the United States and Canada testifies to the broad extent of the Western Interior Seaway during the deposition of the lower Maastrichtian *B. baculus* Zone. In contrast, no ammonites are known from Canada in the overlying *B. grandis* Zone, implying that the Seaway must have retreated from this area by the late early Maastrichtian (Riccardi, 1983; Landman et al., 2017).

STRATIGRAPHY

Old Woman Anticline, Wyoming

Many of the specimens in this study are from the Old Woman Anticline at Red Bird, Niobrara County, Wyoming. This section has been extensively documented by Gill and Cobban (1966), Hicks et al. (1999), and Slattery et al. (2018), and we briefly review it here (fig. 3). The *Baculites baculus* and *B. grandis* zones occur in the upper unnamed member of the Pierre Shale. This unit conformably overlies the Kara Bentonitic Member. It is 207 m thick and consists of variably sandy and silty shale containing many layers of fossiliferous limestone concretions. Several beds of bentonite and bentonitic shale occur in the middle of the unit. The sediments become progressively sandier and siltier toward the top of the section. The contact with the overlying Fox Hills Formation is marked by a 0.37 m thick bentonite overlain by a 4 m thick bed of glauconitic sandstone (unit 112, Gill and Cobban, 1966) containing a few phosphatic nodules and phosphatized internal molds of *Baculites* (see Gill and Cobban, 1966: 37).

Cedar Creek Anticline, Montana

Most of the other specimens in this study are from the Cedar Creek Anticline in east-central Montana (figs. 4, 5). The geology of the Upper

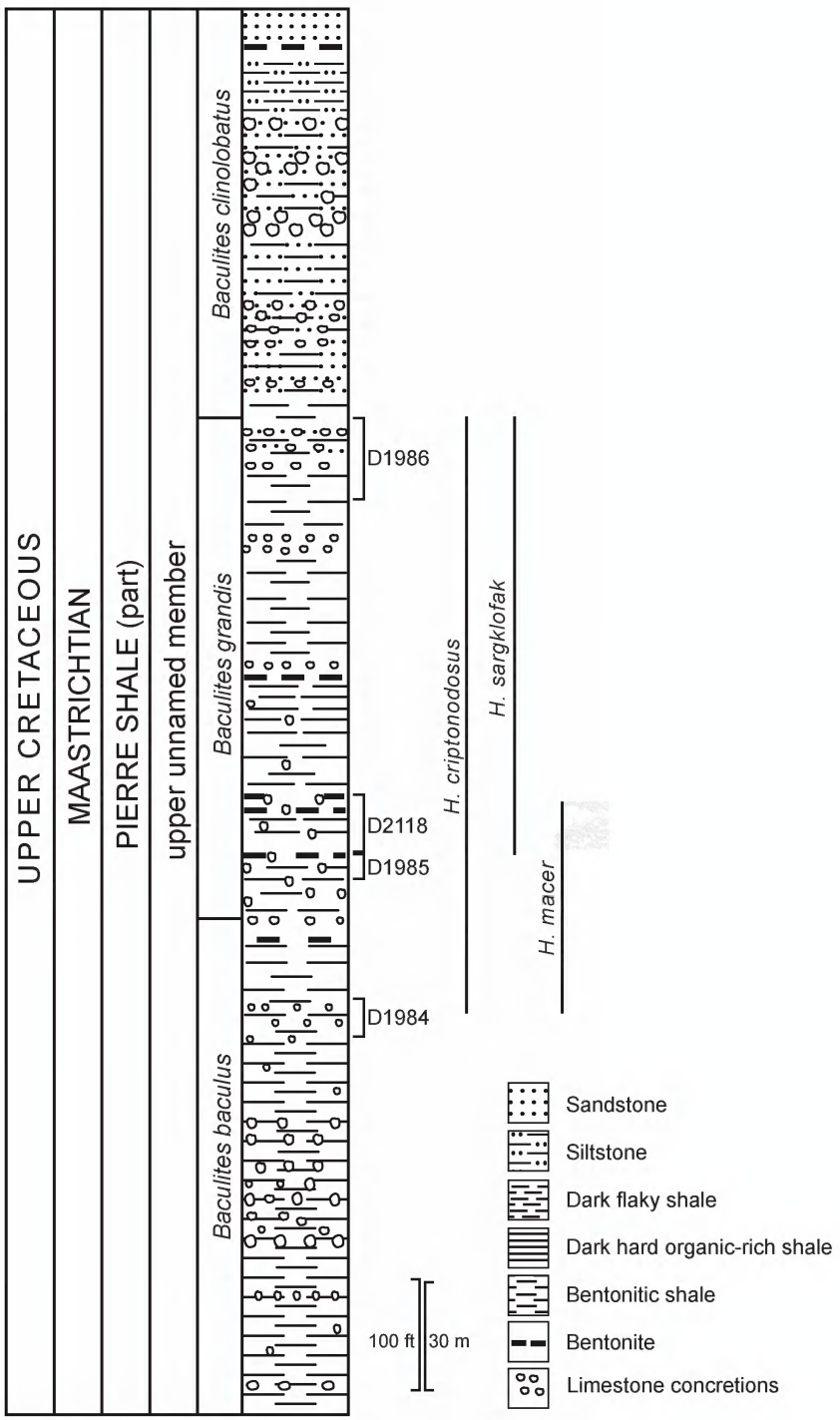

FIGURE 3. Stratigraphic section of the Pierre Shale at Red Bird, Niobrara County, Wyoming (modified from Gill and Cobban, 1966), showing the ranges of three species of *Hoploscaphites* The D numbers refer to USGS Mesozoic localities cited in the text.

Cretaceous section on the anticline has been described by Calvert (1910), Coryell and Salmon (1934), Erdmann et al. (1936), DeWolf and West (1939), Gries (1954), Robinson et al. (1959), Bishop (1967, 1973), Gill and Cobban (1973), Clement (1986), Grier et al. (1992, 2007), Grier and Grier (1998), Walaszczyk et al. (2001), Vuke et al. (2003), Linn (2010), and Landman et al. (2015a, 2018b). As a result of renewed study of this section in the last several years, we present a modified version of the stratigraphic column originally published by Bishop (1967, 1973).

The Cedar Creek Anticline occupies parts of Dawson, Wibaux, Prairie, and Fallon counties, Montana, and Bowman County, North Dakota (fig. 1). The Pierre Shale in this area consists of light to dark gray fissile, silty or sandy shale 60–65 m thick interbedded with bentonites and bentonitic shale. It contains iron manganese (Fe-Mn), limestone, and sandy-bedded concretions, some of which are abundantly fossiliferous. The Pierre Shale becomes progressively siltier up section and is overlain by the Fox Hills Formation (fig. 5A), which is overlain in turn by the Hell Creek Formation. The Pierre Shale is late Campanian to early Maastrichtian in age and contains the upper part of the *Baculites eliasi, B. baculus*, and lower part of the *B. grandis* zones (fig. 4). The section is equivalent in age to the lower one-half of the upper unnamed shale member of the Pierre Shale at Red Bird, Wyoming, as described by Gill and Cobban (1966).

The lower part of the Pierre Shale in the northern area of the Cedar Creek Anticline is 10 m thick and consists of dark gray shale with seven thin bentonite layers and several layers of Fe-Mn concretions (Bishop, 1967, 1973; Linn, 2010). It is overlain by approximately 11 m of gray shale with additional Fe-Mn concretions and relatively abundant specimens of *Baculites eliasi* Cobban, 1958. Approximately 15 m above this interval are two layers of brownish-tan to yellowish sandy-bedded concretions (fig. 5E, F), commonly coated with cone-in-cone structure, which Bishop (1967, 1973) referred to as the "bedded concretions." The upper layer is more persistent than the lower layer and is a reliable stratigraphic marker in this area.

Small, white, spherical to flat, sparsely fossiliferous carbonate concretions occur just below, in between, and just above the sandy-bedded concretions. Specimens of *Baculites eliasi* occasionally occur up to 2 m below the bedded concretions. Both the bedded and small white concretions occur in light gray sandy shale. A few large specimens of *B. baculus* Meek and Hayden, 1861, appear in the same horizon as the upper layer of sandy-bedded concretions (fig. 5F) in association with *Endocostea typica* (Whitfield, 1877) (fig. 6A) and *Eurysalenia minima* Kier, 1966 (7B). A cold methane seep deposit also occurs at this horizon and represents the highest occurrence of such deposits in the U.S. Western Interior (Delaney et al., 2018). The top layer of sandy-bedded concretions marks the base of the *B. baculus* and *E. typica* zones, which represents the Campanian-Maastrichtian boundary in this area.

An interval of gray septarian concretions occurs approximately 2 m above the upper layer of sandy-bedded concretions. Many of these septarian concretions contain barite crystals and invertebrate fossils including species of *Hoploscaphites* and *Endocostea typica* (fig. 6A). Another layer of concretions occurs approximately 1 m above the septarian concretions. They contain a diverse fauna with several species of *Hoploscaphites*, which Bishop (1967, 1973) aptly called the "scaphite concretions." This is the source of the concretion studied in detail by Landman et al. (2015a). The septarian and scaphite concretions occur in gray fissile shale. The scaphite concretions are overlain, in turn, by a 2 m thick interval of bentonitic shale capped by a 7–8 cm thick bentonite (fig. 5C, D). On fresh exposures, the bentonite is pale yellow in color, but upon weathering, it turns light gray and develops a popcorn texture, with scattered gypsum crystals on top (fig. 5D). A few concretions occur within the bentonitic shale and contain species of *Hoploscaphites* and *Endocostea typica*. The top of the bentonite is approximately 8 m above the top of the upper layer of andy-bedded concretions (fig. 4).

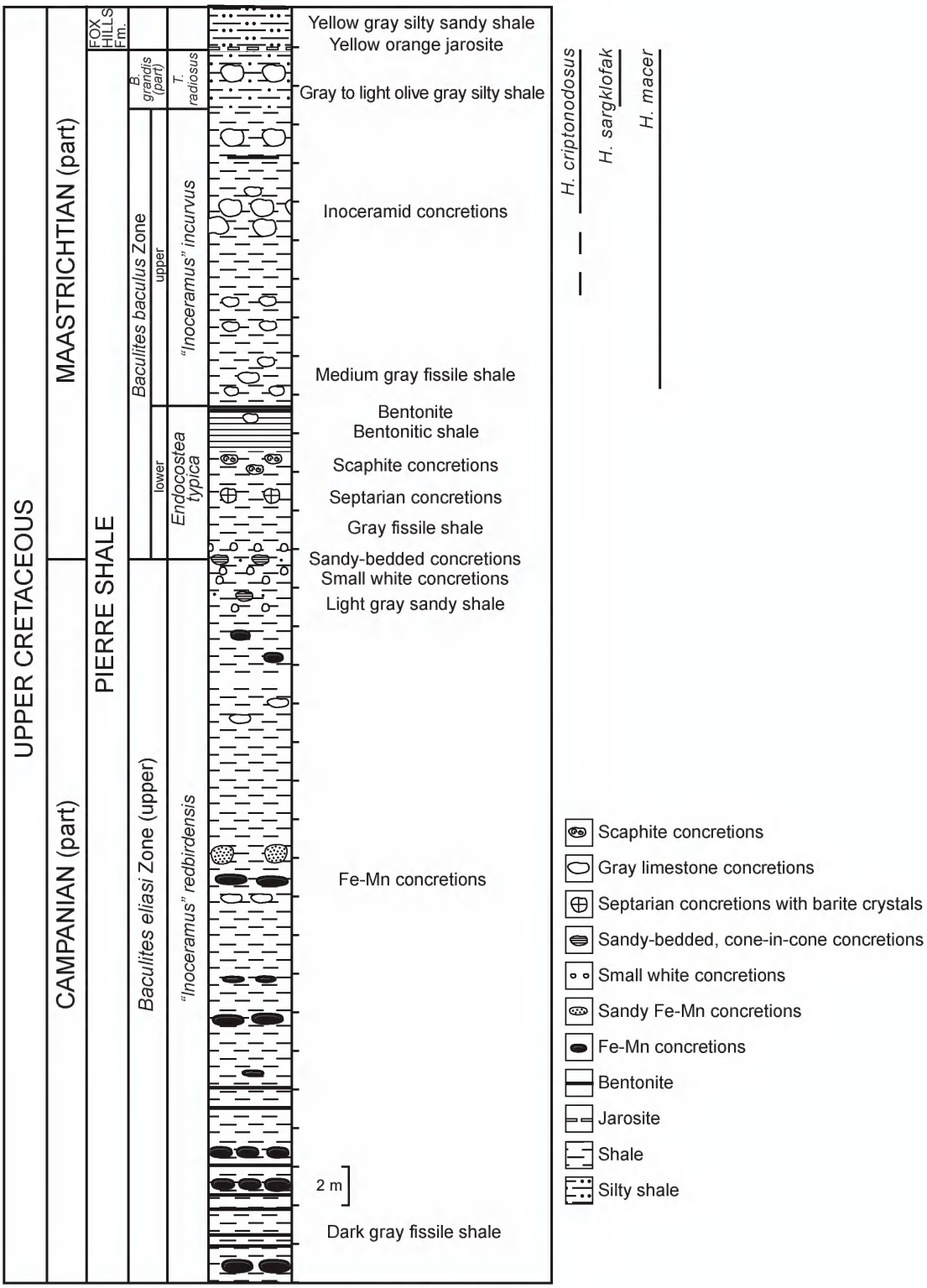
UPPER CRETACEOUS
CAMPANIAN (part)
MAASTRICHTIAN (part)
PIERRE SHALE
FOX HILLS Fm.
Baculites eliasi Zone (upper)
Baculites baculus Zone
lower
upper
"Inoceramus" redbirdensis
Endocostea typica
"Inoceramus" incurvus
B. grandis (part)
T. radiosus
Yellow gray silty sandy shale
Yellow orange jarosite
Gray to light olive gray silty shale
Inoceramid concretions
Medium gray fissile shale
Bentonite
Bentonitic shale
Scaphite concretions
Septarian concretions
Gray fissile shale
Sandy-bedded concretions
Small white concretions
Light gray sandy shale
Fe-Mn concretions
2 m
Dark gray fissile shale
H. criptonodosus
H. sargklofak
H. macer
Scaphite concretions
Gray limestone concretions
Septarian concretions with barite crystals
Sandy-bedded, cone-in-cone concretions
Small white concretions
Sandy Fe-Mn concretions
Fe-Mn concretions
Bentonite
Jarosite
Shale
Silty shale

Immediately above the bentonite are approximately 15 m of medium gray fissile shale with intermittent gray limestone concretions 0.3–1.0 m in diameter. The lowest layer of concretions above the bentonite contains "*Inoceramus*" *incurvus* Meek and Hayden, 1856, marking the base of the "*I.*" *incurvus* Zone (= upper *Baculites baculus* Zone) (fig. 7A, C). Because the concretions in this zone contain numerous inoceramids, we refer to them as inoceramid concretions. However, they also contain a wide variety of other faunal elements including other bivalves, gastropods, and scaphites. The species of *Baculites* in this interval appear to be intermediate between *B. baculus* and *B. grandis* (see Bishop, 1967; Linn, 2010).

The sediment coarsens toward the top of the Pierre Shale and consists of a 3 m thick interval of gray to light olive-gray, silty shale (fig. 4). Gray limestone concretions contain *Baculites grandis* Hall and Meek, 1855, and, very rarely, *Trochoceramus radiosus* (Quaas, 1902) (fig. 6B). The lowest occurrence of *B. grandis* and *T. radiosus* marks the base of the *B. grandis* and *T. radiosus* zones, respectively. *Hoploscaphites macer*, n sp., is relatively abundant in this interval, along with fewer specimens of *H. criptonodosus* and *H. sargklofak* Landman et al., 2015b.

The Pierre Shale is conformably overlain by the Fox Hills Formation (figs. 4, 5A). The base of this formation is marked by a layer of yellow-orange jarosite nodules (Bishop, 1967, 1973; Linn, 2010) (fig. 5B). Occasionally this layer contains rare phosphatized internal molds of *Baculites* (fig. 6C–K). Because of the compressed shape of these internal molds, we attribute them to *B. clinolobatus* Elias, 1933. The presence of these phosphatized specimens indicates a lag deposit possibly associated with a transgression post-dating the deposition of the *B. clinolobatus* Zone and prior to the final retreat of the Western Interior Seaway (Gill and Cobban, 1966). The Fox Hills Formation is as much as 32 m thick and consists of yellowish gray silty, sandy shale in the lower part and yellowish-gray shale alternating with sandy shale and sandstone in the upper part. The top of the Fox Hills Formation culminates in a light-colored, nearshore sandstone called the Colgate Member that is up to 40 m thick (Vuke et al., 2003). The Hell Creek Formation, where present, conformably overlies the Fox Hills Formation.

MODE OF LIFE AND HABITAT OF SCAPHITES

The mode of life and habitat of scaphites, principally species of *Hoploscaphites*, has been reviewed by Landman et al. (2012a). The adult stage is indicated by the uncoiling of the body chamber and consists of a shaft and hook, which recurves backward. The uncoiling of the body chamber can be viewed as a morphogenetic countdown reflecting the growth of the reproductive organs and the attainment of maturity. The countdown begins at the point at which the shell departs from the spiral coil and develops into the shaft. This marks the beginning of an essentially irreversible process, unless a fatal injury intervenes, culminating in the formation of the adult shell. It involves a sequence of morphogenetic events that proceed step by step and terminate with the cessation of growth. Internally, the initiation of the morphogenetic countdown is indicated by closer spacing of the last two or three septa.

The shape of the aperture at maturity is an important clue to the mode of life of scaphites. The apertural opening is reduced in size relative to the whorl section at the point of recurvature. The shape of the aperture is visible in specimens in which the body chamber is broken in half. The aperture is kidney shaped with an elongate, broadly rounded projection along the dorsum (fig. 8C, D). This projection probably impeded unrestricted movement of the soft body outside

FIGURE 4. Stratigraphic section of the Pierre Shale and Fox Hills Formation on the Cedar Creek Anticline, east-central Montana (modified from Bishop, 1967, 1973; Landman et al., 2018b), showing the ranges of three species of *Hoploscaphites*.


A
B
C
D
E
F

of the aperture. Therefore, it is unlikely that scaphites were equipped with long arms or tentacles. In addition, the ventral and lateral sides of the aperture are bordered by a deep constriction that ends in a thin lip (fig. 9), further reducing the size of the aperture.

Because of the uncoiling of the body chamber, adult scaphites are poorly designed for swimming. Jacobs et al. (1994) investigated swimming efficiency in *Scaphites whitfieldi* Cobban, 1952, from the Turonian Carlile Shale of South Dakota. They did flow tank experiments on models of actual juvenile and adult specimens. They plotted the coefficient of drag versus Reynolds number (a proxy for the rate of flow). They demonstrated that the coefficient of drag is higher in adults than in juveniles during horizontal swimming. Thus, the uncoiling of the body chamber at maturity increases the coefficient of drag and decreases the hydrodynamic efficiency. In addition, scaphites lack a midventral sinus, implying that they could not have easily recurved their hyponome backward. As a result, they were probably limited to backward or downward swimming.

The musculature in scaphites also provides some insights into the swimming ability of these animals. Only two types of muscle scars are present in scaphites. The unpaired midventral scar appears a few millimeters adoral of the midventral saddle in the external lobe (fig. 8A, B). It is small and oval in shape. The dorsal muscle scar is wedge shaped and drapes over the umbilical shoulder on either side of the midline just adoral of the last suture. No lateral muscle scars are present. If *Nautilus* is used as a model for swimming in scaphites, the lack of large retractor muscles implies that little propulsive power was available for strong swimming.

Scaphites probably lived in well-oxygenated environments near the bottom. Sessa et al. (2015) studied the isotopic composition of species of *Discoscaphites* from the upper Maastrichtian Owl Creek Formation of Mississippi. The isotopic values of the scaphites at this site are more similar to those of benthic rather than planktic foraminifera, suggesting that the scaphites lived close to the bottom. Slattery et al. (2018) recently investigated the record of faunal communities, including scaphites, along the western margin of the Western Interior Seaway during the early Maastrichtian. They demonstrated that changes in faunal communities during this time interval reflected a number of environmental factors such as distance from shore, level of oxygen, and water depth. Scaphites are more common in the more nearshore, better oxygenated settings. In addition, observations of the kind and incidence of shell injuries suggest that scaphites were sometimes attacked by animals that lived close to the bottom, indicating that scaphites probably lived in the same habitat as these predators (Landman et al., 2010).

FIGURE 5. Outcrops of the Pierre Shale and Fox Hills Formation on the Cedar Creek Anticline, east-central Montana. **A.** Overview of the contact between the Pierre Shale and Fox Hills Formation. The contact is marked by a color change from gray silty shale to yellowish gray silty sandy shale. The sagebrush in the foreground is 0.5 m high. **B.** Circular yellowish-orange jarosite nodules (arrow), approximately 14 × 16 cm in diameter, mark the base of the Fox Hills Formation. **C.** Photo from the top of the 2 m thick bentonitic shale, foreground, looking out over an adjacent part of the same outcrop. (The outcrop was cut through to make way for an oilfield transmission line.) The top of the bentonite coincides with the boundary between the upper and lower parts of the *Baculites baculus* Zone. **D.** The surface of the bentonite (pale yellow when freshly exposed) weathers to a light-gray popcornlike texture with irregular polygons, each approximately 4 cm × 4 cm in size. **E.** Upper layer of sandy-bedded concretions, which coincides with the boundary between the *B. eliasi* Zone below and the *B. baculus* Zone above, locally demarcating the Campanian-Maastrichtian boundary (length of hammer = 27 cm). **F.** Rare specimen (one of only four recovered from this interval) of *B. baculus* Meek and Hayden, 1861, from a light gray/tan concretion in the upper layer of sandy-bedded concretions (length of hammer = 32.5 cm).

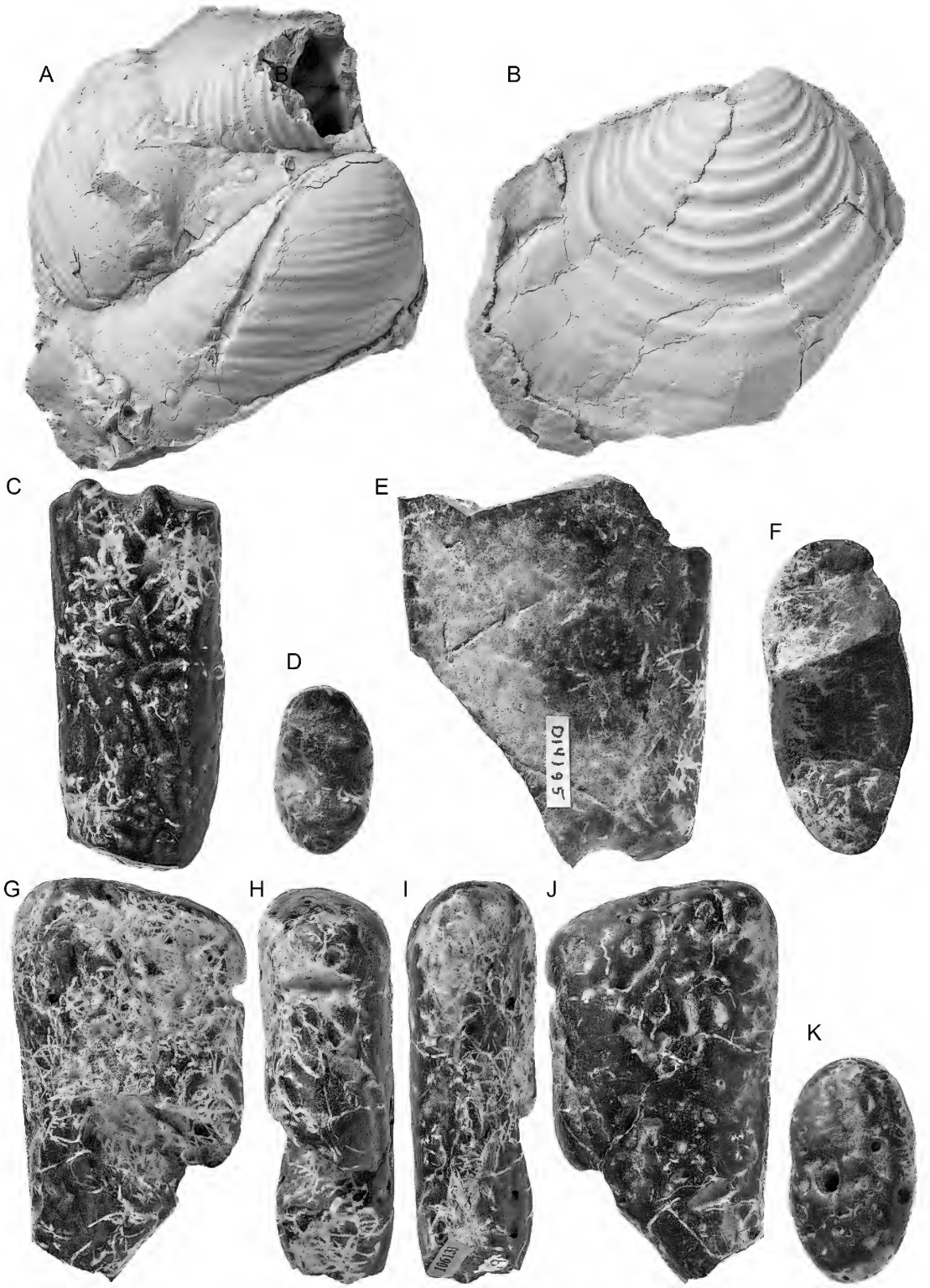
A
B
B
C
D
E
F
G
H
I
J
K

The limited swimming ability of scaphites, especially as adults, may have prevented them from migrating over long distances. Instead, they may have exploited a low-energy lifestyle, remaining at a single site for an extended period of time. The discovery of scaphites and other ammonites in cold methane seep deposits in the Upper Cretaceous Western Interior is consistent with this hypothesis (Landman et al., 2012b, 2018a). The scaphites at some of these sites are very well preserved and permit analysis of the carbon and oxygen isotopic composition of the shell material. The carbon isotopic composition of specimens in seep deposits is statistically lower than that of specimens at age equivalent nonseep sites, implying that some scaphites may have spent part or all of their lives at a single seep.

EVOLUTIONARY PATTERNS

Landman et al. (2010) redescribed species of *Hoploscaphites* from the Upper Cretaceous (upper Campanian) Western Interior of North America. They noted a high degree of variation within and between species. They compared *H. nodosus* (Owen, 1852) and *H. brevis* (Meek, 1876), which occur in the same ammonite zones (*Baculites compressus–B. cuneatus* zones). Although they treated these two species as separate, they noted that *H. nodosus* and *H. brevis* could be interpreted as representing the coarsely and finely ornamented end members, respectively, of the same species. Landman et al. (2010: 72–73) concluded that "it is entirely possible that all of the scaphites in the *Baculites compressus–B. cuneatus* zones represent a single very variable species" and argued that "the differences in size, degree of compression, and coarseness of ornament [among specimens] may simply reflect differences in the rate of growth and age at maturity, keyed to changes in the environment."

A similar argument could be made for *Hoploscaphites criptonodosus* and *H. sargklofak* (fig. 10). Both species occur in the same ammonite zone (*Baculites grandis* Zone). The pattern of ornamentation is the same in both forms, including the presence of lateral tubercles on the exposed phragmocone, but the ribs and tubercles are coarser in *H. criptonodosus* than in *H. sargklofak*. In addition, the size and degree of compression differ between the two species, with *H. criptonodosus* being larger and more robust than *H. sargklofak*. Thus, in theory, the two forms could represent the coarsely and finely ornamented end members, respectively, of the same species. However, because the two forms can be easily distinguished (perhaps owing to the lack of transitional specimens in our collections), and in deference to historical precedence, we maintain them as separate species.

One of the conspicuous trends in the evolution of scaphites in the Western Interior Seaway during the Maastrichtian is the directional change over time in whorl shape and tuberculation (Landman and Waage, 1993a, 1993b). The flanks of the body chamber are flatter and the incidence of tubercles on the exposed phragmocone is higher in geologically younger species. This is apparent in a comparison between older species from the lower part of the *Baculites baculus* Zone with younger species from the upper part of the *B. baculus* Zone and

FIGURE 6. **A.** *Endocostea typica* (Whitfield, 1877), AMNH 72834, Pierre Shale, 7 m below the crest of the 2 m-thick bentonitic shale, AMNH loc. 3921, Cedar Creek Anticline, east-central Montana. **B.** *Trochoceramus radiosus* (Quaas, 1902), AMNH 106046, Pierre Shale, highest layer of concretions below the base of the Fox Hills Formation, AMNH loc. 3921, Cedar Creek Anticline, east-central Montana. **C–K.** Phosphatized fragments of *Baculites* at the base of the Fox Hills Formation, Cedar Creek Anticline, east-central Montana. Because of their compressed whorl section, they are attributed to *Baculites clinolobatus* Elias, 1933. **C, D.** AMNH 106139, AMNH loc. 3921. **C,** Right lateral; **D,** whorl cross section at adapical end. **E, F.** USNM 723200, USGS Mesozoic loc. D14195. **E,** Right lateral; **F,** whorl cross section at adapical end. **G-K.** AMNH 106133, AMNH loc. 3921. **G,** Right lateral; **H,** dorsal; **I,** ventral; **J,** left lateral; **K,** whorl cross section at adapical end. Specimens ×1.

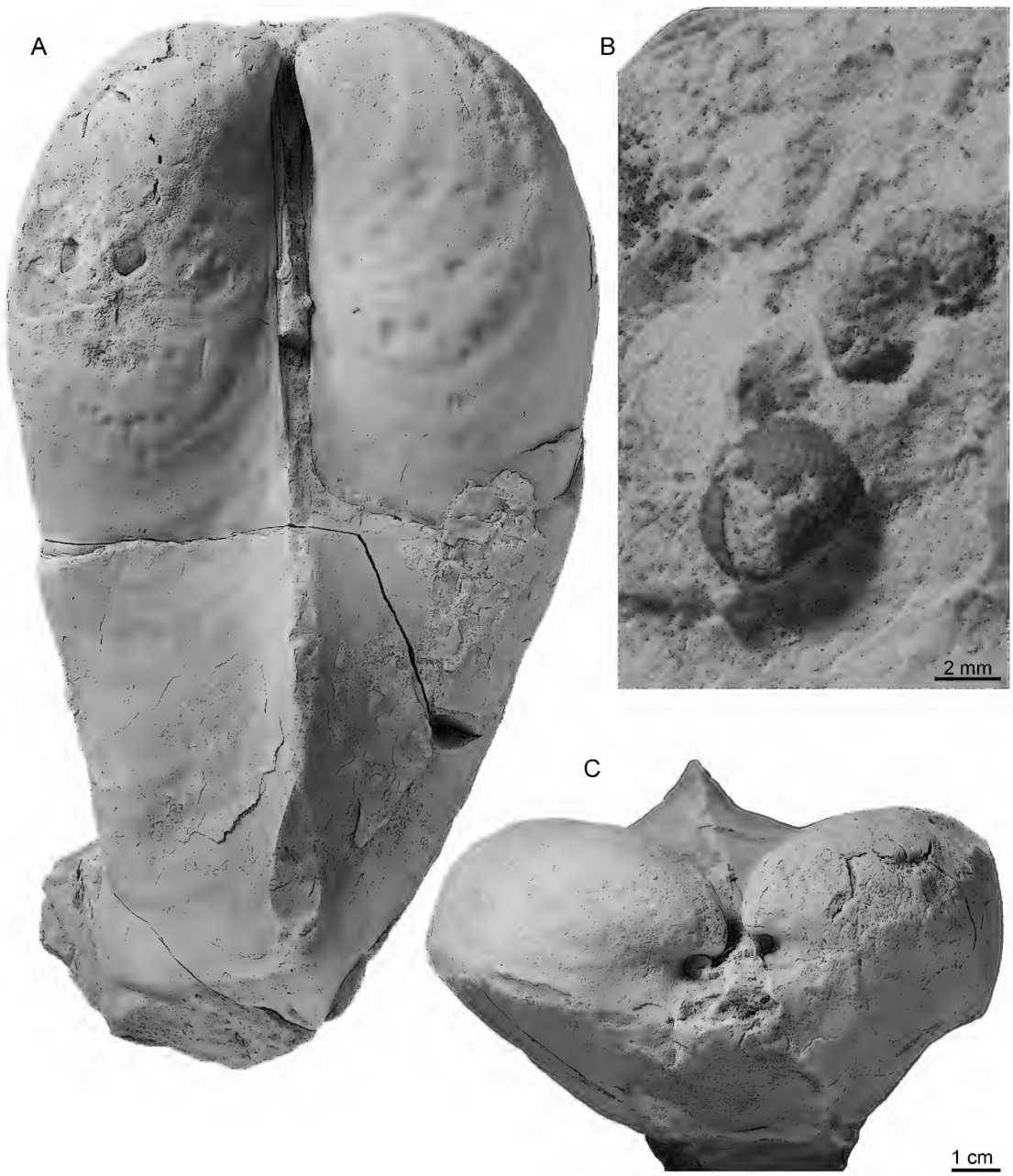

FIGURE 7. **A, C.** "*Inoceramus*" *incurvus* Meek and Hayden, 1856, AMNH 10659, AMNH loc. 3921, Pierre Shale, Cedar Creek Anticline, east-central Montana. **B.** Close-up of *Eurysalenia minima* Kier, 1966, AMNH 106132, in a small white concretion from the sandy-bedded concretionary interval, AMNH loc. 3921, Cedar Creek Anticline, east-central Montana.

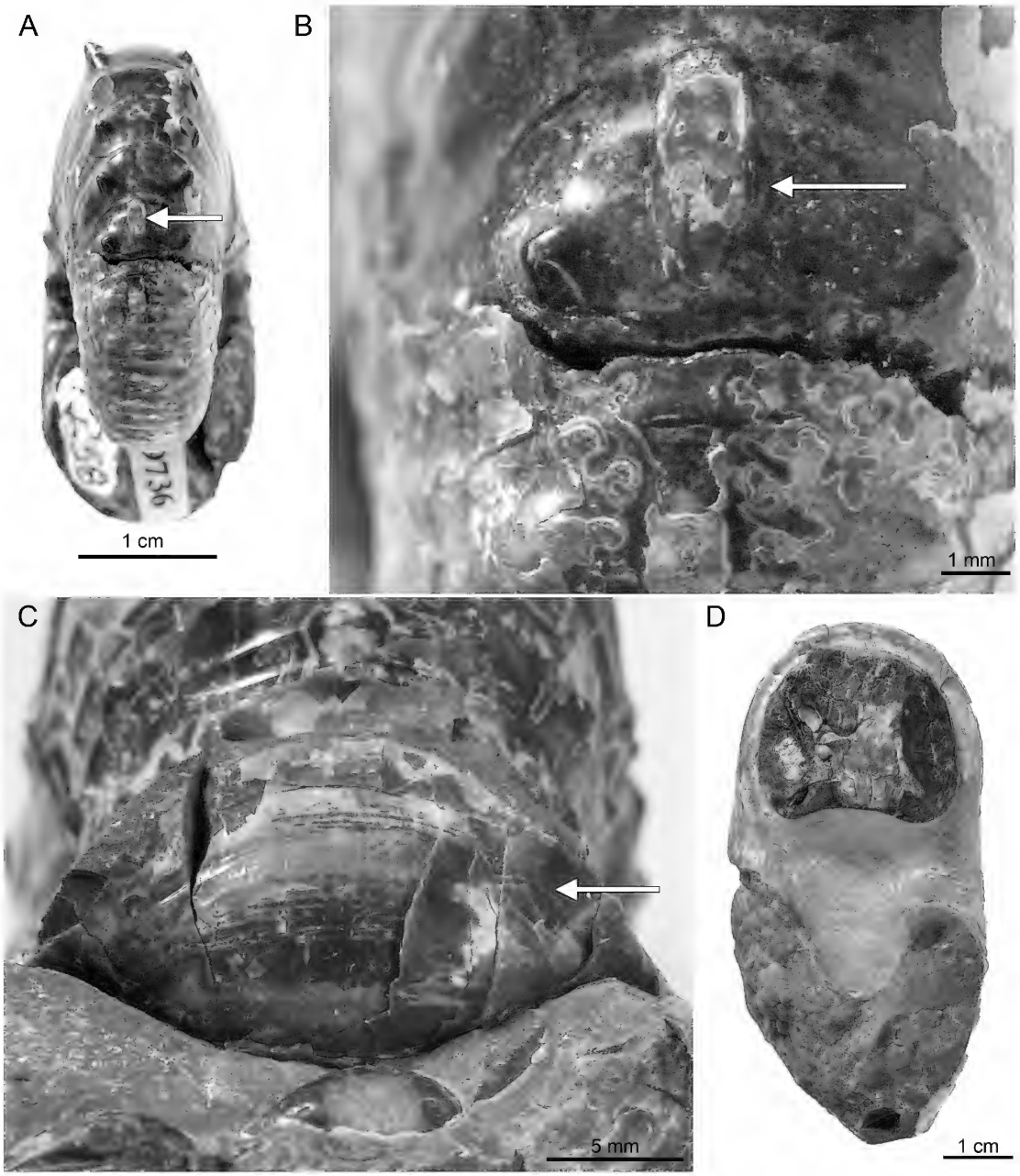

FIGURE 8. **A, B.** Unpaired ventral muscle scar (arrow) just adoral of the last suture, *Hoploscaphites macer*, microconch, AMNH 69736, AMNH loc. 3921, upper *Baculites baculus* or lower *B. grandis* Zone, Pierre Shale, Cedar Creek Anticline, east-central Montana. **C.** Apertural view of dorsal projection (arrow), *Hoploscaphites criptonodosus* (Riccardi, 1983), AMNH 108459, AMNH loc. 3278, *Baculites grandis* Zone, Pierre Shale, Weston County, Wyoming. The hook of the body chamber has broken off exposing the dorsal projection, which is plastered against the venter of the phragmocone. **D.** Kidney-shaped apertural opening showing the dorsal projection, *Hoploscaphites criptonodosus* (Riccardi, 1983), macroconch, AMNH 71830, AMNH loc. 3921, upper *Baculites baculus* or lower *B. grandis* Zone, Pierre Shale, Cedar Creek Anticline, east-central Montana.

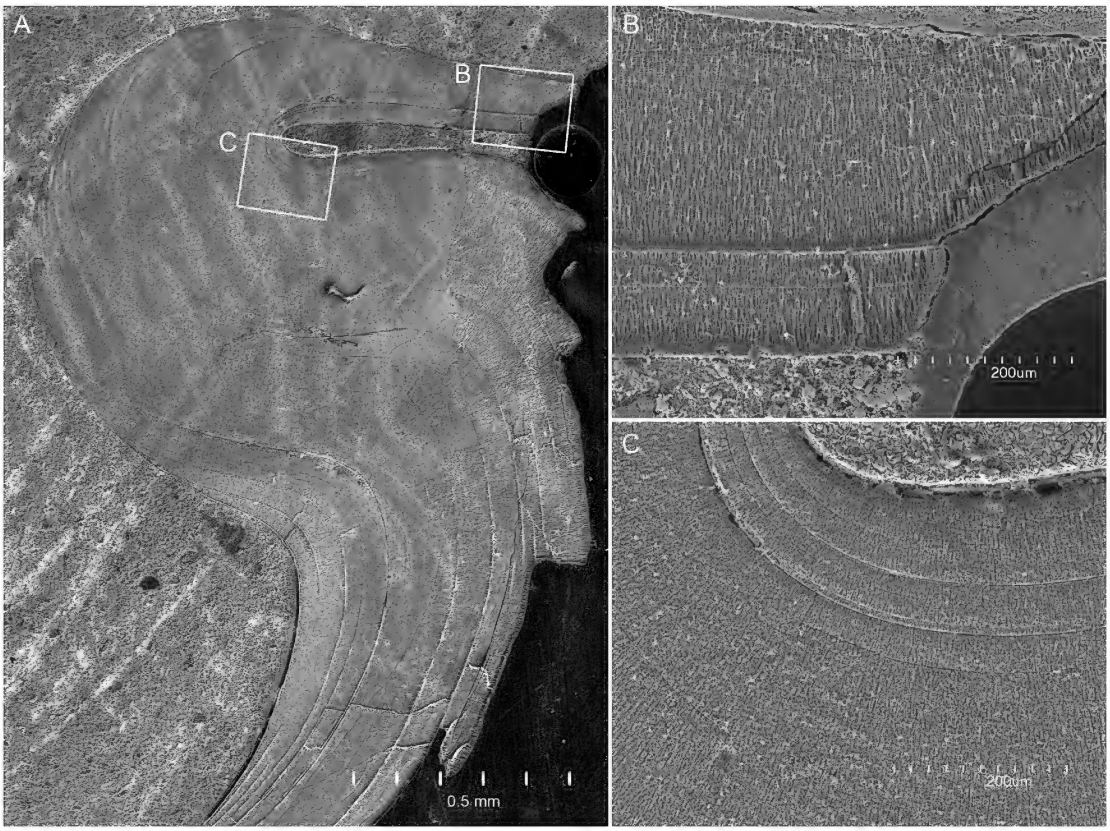

FIGURE 9. Cross section of the shell wall at the apertural margin of a mature macroconch of *Hoploscaphites criptonodosus* (Riccardi, 1983), AMNH 94676, AMNH loc. 3728, *Baculites grandis* Zone, Pierre Shale, Weston County, Wyoming. **A.** Overview of part of the apertural margin. The exterior direction is toward the right and the adoral direction is toward the top. The shell wall bends sharply inward at nearly a right angle forming a thick varix and then reflects outward terminating in a flared lip. During fossilization, sediments usually accumulate in the narrow gap behind the flared lip (for a rare example in which epizoans colonized this gap during the lifetime of the ammonite, see Landman et al., 2016). **B, C.** Close-ups of the shell wall showing the recurved layers of shell.

overlying *B. grandis* Zone. These patterns are further played out in the overlying *B. clinolobatus* Zone that contains two undescribed species in which the flanks of the body chamber are even flatter and the exposed whorls are covered with even more tubercles.

These changes in whorl shape and tuberculation can be captured in 3-D surface scans of ammonite specimens. We scanned six specimens with the help of Carolyn Merrill (AMNH) using an Arctec Space Spider scanner equipped with Artec Studio 12 software. The results of some of these scans are shown in figure 11. These images can be examined and manipulated in MeshLab and Geomagic. In collaboration with William Harcourt-Smith (AMNH), we are developing techniques to quantify the degree of tuberculation using spiral and radial transects that intersect the ribs and tubercles. Our preliminary results indicate that the "ridge and swale" topography produced by ribs can be distinguished from the "cinder cone" topography produced by tubercles, thus providing quantitative measures of the degree and kind of ornamentation.

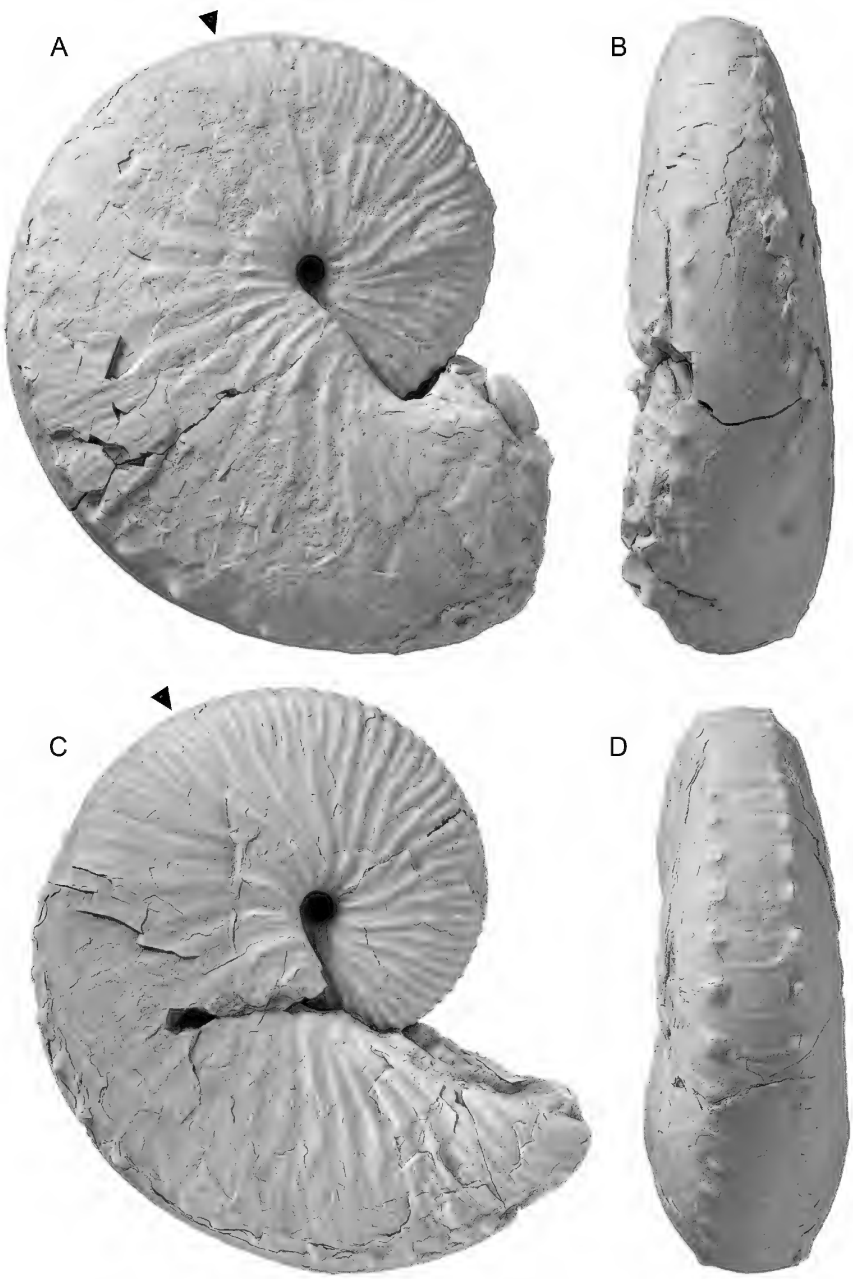

FIGURE 10. *Hoploscaphites sargklofak* Landman et al., 2015b, macroconchs. **A, B.** AMNH 108324, AMNH loc. 3264, lower *Baculites grandis* Zone, Pierre Shale, Weston County, Wyoming. **A,** Right lateral; **B,** ventral. **C, D.** AMNH 77027, *Baculites grandis* Zone, Pierre Shale, locality unknown. **C,** Right lateral; **D,** ventral. Arrows indicate the base of the body chamber. Specimens ×1.

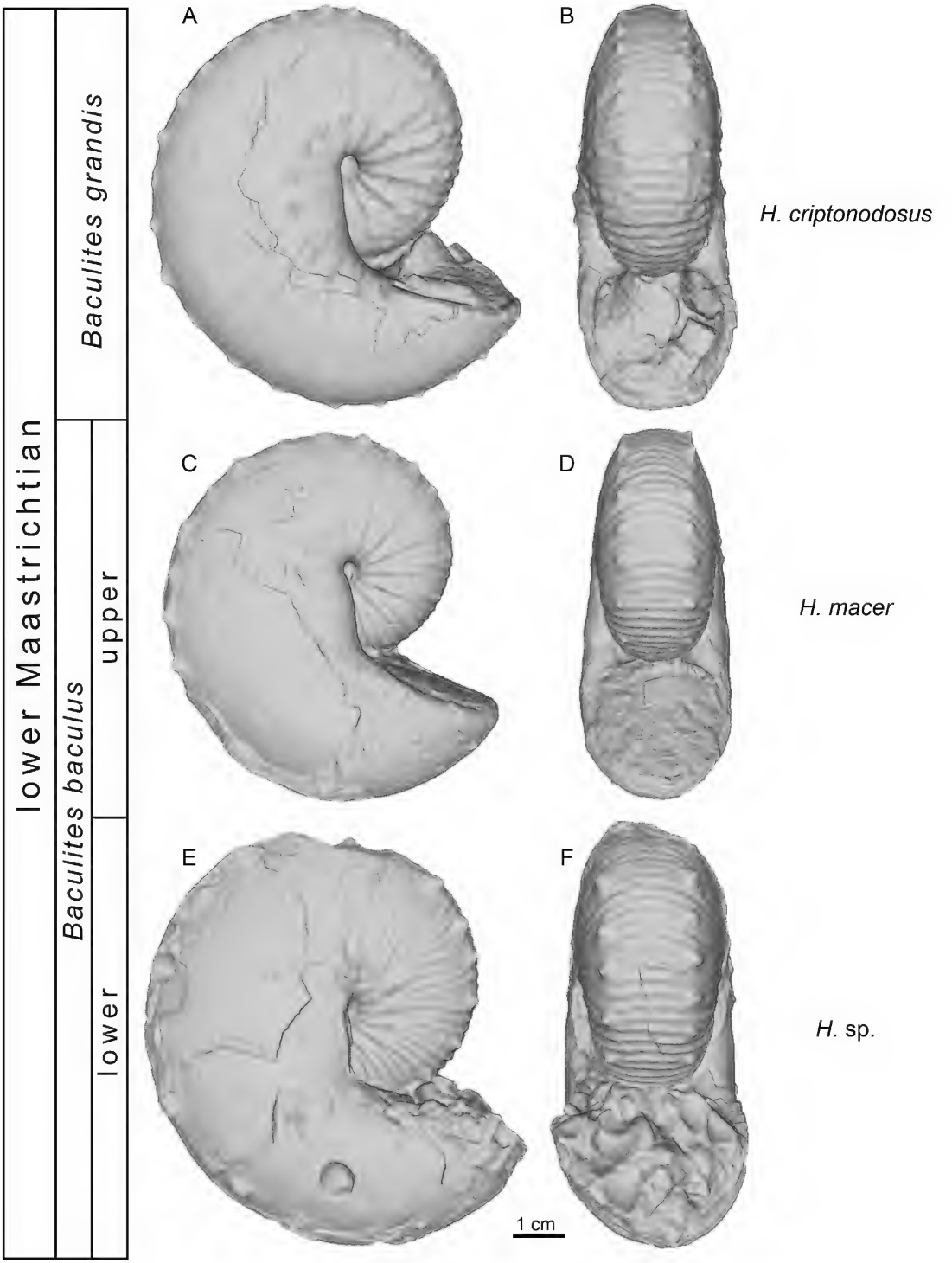
lower Maastrichtian
Baculites grandis
Baculites baculus
upper
lower
A
B
C
D
E
F
H. criptonodosus
H. macer
H. sp.
1 cm

The evolutionary changes in tuberculation and whorl shape are associated with changes in the environment in which the ammonites lived. As shown in the section on the Cedar Creek Anticline in east-central Montana, the sediments become siltier upsection from the *Baculites baculus* to the *B. grandis* zones (fig. 4). This trend is also apparent in the section on the Old Woman Anticline in northeast Wyoming, where it persists into the *B. clinolobatus* Zone (fig. 3). This change in lithology reflects the overall progradation of the shoreline eastward during the early Maastrichtian (although a brief transgression occurs during the deposition of the upper part of the *B. grandis* and lower part of the *B. clinolobatus* zones; see Slattery et al., 2018: fig. 13). Thus, both sites represent progressively more nearshore environments over time.

The increase in the number of tubercles may be related to an increase in the number and kinds of predators in these shallower water environments. Many studies have documented a relationship between ornamentation and predation in ammonites and other molluscs (Kröger, 2002; Larson, 2003; Keupp, 2006; Landman et al., 2010; Takeda et al., 2016). In *Hoploscaphites criptonodosus* and *H. sargklofak*, tubercles effectively increased the size of the shell, making it appear larger and less attractive to possible predators. The tubercles are also sharp and pointy, although in most specimens, the tips of the tubercles are now missing due to taphonomic factors. These conical projections probably made the shell more difficult to grasp by predators. Thus, the tubercles may have helped these scaphites elude predators or, in the event of an attack, may have limited the size of the damage to the shell.

This hypothesis is supported by an examination of injuries in other species of *Hoploscaphites* from the Western Interior Seaway. Landman and Waage (1986, 1993a, 1993b) studied the incidence of nonlethal injuries in two species of *Hoploscaphites* from the upper Maastrichtian Fox Hills Formation. They compared *H. spedeni* Landman and Waage, 1993a, from the Trail City Member with *H. nebrascensis* (Owen, 1852) from the overlying Timber Lake Member. The number of tubercle rows is higher in *H. nebrascensis* than in *H. spedeni* (nine versus seven rows of tubercles, respectively). The environment of these two species also changes from a more offshore to a more nearshore setting during this interval in response to the retreat of the Seaway during the Maastrichtian. At the same time, the incidence of injuries (number of injured specimens versus the total number of specimens in the sample) increased from 11.2% in *H. spedeni* to 25.8% in *H. nebrascensis*. One interpretation of these results is that *H. nebrascensis* became more successful at surviving attacks (Landman and Waage, 1986), possibly due to the presence of additional tubercles on the shell.

The change in whorl shape over time can also be interpreted in terms of an adaptation to shallower water environments. For example, the whorl section at midshaft is more compressed in *Hoplocaphites sargklofak* than in *H. macer*. The average value of W_S/H_S is 0.70 in *H. sargklofak*, as reported in Landman et al. (2015b), versus 0.77 in *H. macer* (table 1). This difference is consistent with hydrodynamic expectations. At higher Reynolds numbers (approximately equivalent to higher rates of flow) characteristic of higher energy environments, the coefficient of drag is lower in more compressed forms due to their smaller cross-sectional area. Jacobs et al. (1994) previously investigated this relationship in their study of scaphites from the Carlile Shale of South Dakota in which they utilized a flow

FIGURE 11. Surface scans showing the lateral and apertural views of macroconchs of three species of *Hoploscaphites* spanning the *Baculites baculus* to *B. grandis* zones. **A, B.** *Hoploscaphites criptonodosus,* AMNH 108313, AMNH loc. 3269, *B. grandis* Zone, Pierre Shale, Weston County, Wyoming. **C, D.** *Hoploscaphites macer*, BHI 4306, AMNH loc. 3921, upper *B. baculus* or lower *B. grandis* Zone, Pierre Shale, Cedar Creek Anticline, east-central Montana. **E, F.** *Hoploscaphites* sp., AMNH 108443, AMNH loc. 3921, lower *B. baculus* Zone, Pierre Shale, Cedar Creek Anticline, east-central Montana.

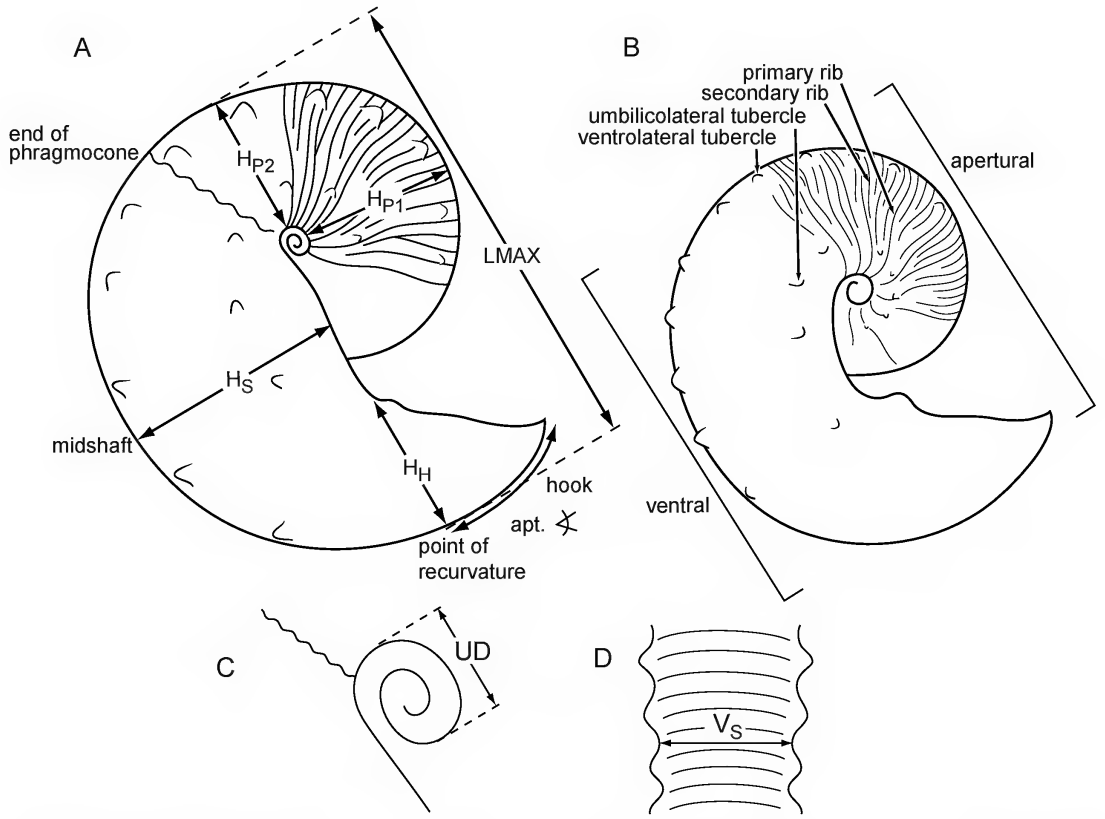

FIGURE 12. Scaphite terminology (after Landman et al., 2013: 9, fig. 3). **A.** Macroconch, right lateral view. Abbreviations: H_H = whorl height at the point of recurvature; H_{P1} = whorl height at the adapical end of the phragmocone; H_{P2} = whorl height at the adoral end of the phragmocone; H_S = whorl height at midshaft; LMAX= maximum length along the long axis; apt. <) = apertural angle. **B.** Microconch, right lateral view. **C.** Close-up of the umbilicus of the macroconch showing the umbilical diameter measured parallel to the long axis (UD). **D.** View of the venter of the body chamber at midshaft, with the adoral direction toward the top, showing the width of the venter (VS), as measured between the ventrolateral margins.

tank to measure coefficient of drag versus Reynolds number with casts of actual specimens.

TERMS, METHODS, AND REPOSITORIES

Most of the terms used to describe scaphites are reviewed by Landman et al. (2010). The adult shell consists of a closely coiled phragmocone and a slightly to strongly uncoiled body chamber (fig. 12). The adult phragmocone is the part of the phragmocone that is exposed in the adult shell, as compared to the part that is concealed inside. The point of exposure is the most adapical point of the adult phragmocone. The body chamber consists of the shaft, beginning near the last septum, and a hook terminating at the aperture. The point of recurvature is the point at which the hook curves backward.

Measurements of the adult shell are illustrated in figure 12. The maximum length of the adult shell (LMAX) was measured from the venter of the adult phragmocone to the venter of the hook. The umbilical diameter of the adult shell (UD) was measured through the center of the umbilicus parallel to the line of maximum length. Whorl width (W) and whorl

height (H) were measured at four points on the adult shell: (1) the adapical end of the phragmocone 90° adapical of the line of maximum length (W_{P1}, H_{P1}), (2) the adoral end of the phragmocone along the line of maximum length (W_{P2}, H_{P2}), (3) the body chamber at midshaft (W_S, H_S), and (4) the hook at the point of recurvature (W_H, H_H). The width of the venter at midshaft (V_S) was measured between ventrolateral margins on opposite sides of the venter. All measurements were made using electronic calipers on actual specimens, rather than on photos. We calculated several ratios to describe the shape of the adult shell and facilitate comparisons among specimens. The ratios of whorl width to whorl height were calculated at four points on the shell (W_{P1}/H_{P1}, W_{P2}/H_{P2}, W_S/H_S, W_H/H_H), as described above, and provide a measure of the degree of whorl compression. The ratio of ventral width to whorl height at midshaft (V_S/H_S) provides an additional measure of the degree of whorl compression. The ratio of maximum length to whorl height of the phragmocone along the line of maximum length (LMAX/H_{P2}) is a measure of the degree of uncoiling. The ratio of maximum length to whorl height at midshaft (LMAX/H_S) is a measure of the degree of curvature of the body chamber in lateral view. If the outline of the body chamber in lateral view is a semicircle, the ratio of LMAX/H_S equals 2. This ratio applies only to macroconchs because the umbilical seam of the body chamber usually coincides with the line of maximum length in these forms, and thus the whorl height is the distance from the line of maximum length to the venter of the body chamber (equivalent to the radius in the case of a semicircle). The apertural angle, as defined by Landman and Waage (1993a) and Machalski (2005), was measured on photographs of specimens in lateral view. A line was drawn along the umbilical shoulder and another line was drawn along the apertural margin. The apertural angle is the angle of intersection between these two lines, extending from approximately the point of recurvature to the aperture. We restricted this measurement to macroconchs, but even in these forms, it is sometimes difficult to know where to draw the line along the umbilical shoulder because the shoulder occasionally shows a bulge or sag.

A number of terms describe ornamentation. Primary ribs originate near the umbilicus, whereas secondary ribs originate on the flanks or venter, either by branching or intercalation. The density of ribs is measured by counting the number of ribs/cm on the venter at four points on the adult shell: (1) the adapical end of the phragmocone, (2) the adoral end of the phragmocone, (3) the midshaft, and (4) the hook. In addition to ribs, the ornamentation includes tubercles, which are small conical swellings. Umbilicolateral tubercles occur near the umbilicolateral margin, ventrolateral tubercles occur near the ventrolateral margin, and lateral tubercles occur on the flanks (fig. 12). The number of ventrolateral and umbilicolateral tubercles on the phragmocone and body chamber of the adult shell were counted. We recorded the distance between tubercles following the curvature of the shell, for example, along the umbilicolateral margin for umbilicolateral tubercles and along the ventrolateral margin for ventrolateral tubercles. We also recorded the number of ribs that loop between ventrolateral tubercles on opposite sides of the venter.

The repository of specimens described in the text is indicated by a prefix, as follows: Division of Paleontology (Invertebrates), American Museum of Natural History (AMNH), New York; Black Hills Institute of Geological Research (BHI), Hill City, South Dakota; Denver Museum of Nature and Science (DMNH), Denver; the Field Museum (FM), Chicago; Geological Survey of Canada (GSC), Ottawa; Mississippi Museum of Natural Science (MMNS), Jackson, Mississippi; Yale Peabody Museum (YPM), New Haven, Connecticut; and U.S. National Museum (USNM), Washington, D.C. The localities of the specimens are listed in the appendix.

SYSTEMATIC PALEONTOLOGY

Class Cephalopoda Cuvier, 1797

Order Ammonoidea Zittel, 1884

Suborder Ancyloceratina Wiedmann, 1966

Superfamily Scaphitoidea Gill, 1871

Family Scaphitidae Gill, 1871

Subfamily Scaphitinae Gill, 1871

Genus *Hoploscaphites* Nowak, 1911

[= *Mesoscaphites* Atabekian, 1979: 523 (nomen nudum) fide Kennedy, 1986; Wright, 1996; *Jeletzkytes* Riccardi, 1983: 14].

Type Species: *Ammonites constrictus* J. Sowerby (1817: 189, pl. A, fig. 1), by original designation.

Diagnosis: "Small to large scaphites, strongly dimorphic, with broad variation in degree of whorl compression ranging from slender to robust, with involute phragmocone, short to long shaft, and weakly recurved hook; apertural angle ranging from approximately 35° to 85°; aperture constricted with dorsal projection; ribs straight to flexuous, increasing by branching and intercalation, with weak to strong adoral projection on venter; adult shell with or without umbilicolateral, flank, and ventrolateral tubercles; suture fairly indented, with symmetrically to slightly asymmetrically bifid first lateral lobe" (Landman et al., 2010: 93).

Discussion: In their monograph on the scaphites of the "*nodosus* group," Landman et al. (2010) treated *Jeletzkytes* Riccardi, 1983, as a junior subjective synonym of *Hoploscaphites*. They argued that the shape of the shell, the pattern of ornamentation, and the complexity of the suture are the same in both genera, the only differences being the degree of compression and, as a result, the flexuosity of the ribs and the size of the tubercles. They noted that such variation already exists within the genus *Hoploscaphites*, as previously defined, and exemplified by the type species *H. constrictus*. Wright (1996: 261–262) cited the same reason for synonymizing the two genera: "Separation of the large and inflated species of the *nodosus* group as *Jeletzkytes* seems unnecessary, given the great variation within most scaphitid species." Later, Cooper (1994) erected the new subgenus *Karlwaageites* for derived members of *Jeletzkytes* from North America that bear lateral tubercles. However, the number and distribution of lateral tubercles can vary even within a single species, casting doubt on the utility of this character for subgeneric separation. Until a thorough phylogenetic revision of all scaphitid genera and subgenera is undertaken, we prefer to follow a more conservative approach and treat all these species in the genus *Hoploscaphites*.

Hoploscaphites macer, n. sp.

Figures 8A, B, 11C, D, 13–22, 23A–C, 24, 25

Diagnosis: Macroconchs oval to nearly circular in lateral view; cross section of shaft compressed subovoid with high whorls consisting of broadly rounded flanks and nearly flat venter; maximum width at adoral part of shaft; small umbilicus commonly with umbilical bulge; ribs coarse on phragmocone at the point of exposure, subsequently becoming finer; small, moderately closely spaced ventrolateral tubercles; small umbilicolateral tubercles on body chamber; occasional lateral tubercles on adapical part of phragmocone; apertural angle averaging 56°; microconchs oval in lateral view; cross section of shaft subovoid with broadly rounded flanks converging toward ventrolateral shoulder; large umbilicus exposing earlier whorls; closely spaced ventrolateral tubercles; relatively prominent umbilicolateral tubercles on body chamber; suture with broad, asymmetrically bifid first lateral saddle and narrow, symmetrically to asymmetrically bifid first lateral lobe.

Etymology: The name is derived from the Latin word *macer*, "thin," which is one's first impression of this species relative to other species in the same biostratigraphic zones. Upon inspection, however, the shell is slightly inflated. Nevertheless, this name has been used informally for the last 20 years, and for

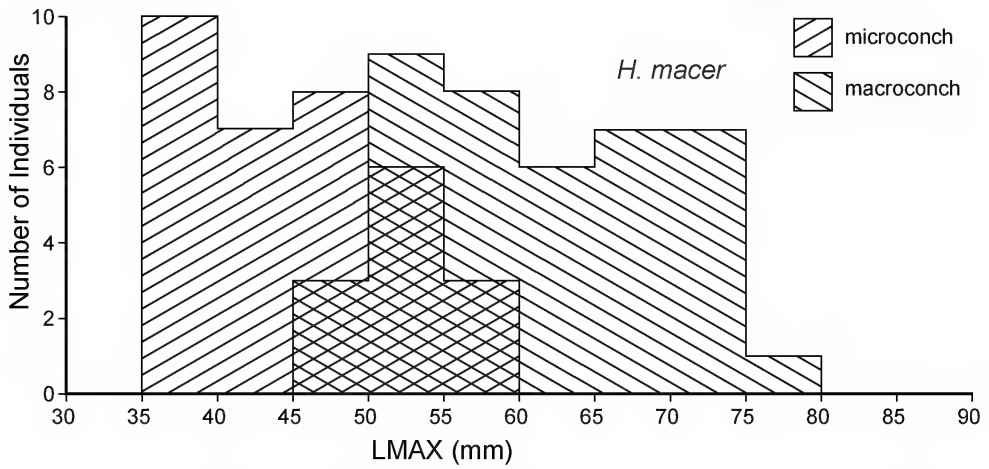

FIGURE 13. Size-frequency histogram of *Hoploscaphites macer*, n. sp., based on the samples in tables 1 and 2.

the sake of stability, we decided to retain the name for this species.

Types: The holotype is AMNH 71839 (figs. 19E–H, 23A), a macroconch, from the lower part of the *B. grandis* Zone of the Pierre Shale on the Cedar Creek Anticline, Montana. It is a steinkern with some attached shell 54.2 mm in diameter with a small umbilicus. The macroconch paratypes are AMNH 113323 (fig. 20D–F) and 113324 (fig. 20G–I), both from the upper part of the *B. baculus* Zone or the lower part of the *B. grandis* Zone of the Pierre Shale on the Cedar Creek Anticline, Montana, and USNM 713612 (fig. 17A–C) from the *B. grandis* Zone of the Bearpaw Shale in Roosevelt County, Montana. The microconch paratypes are AMNH 72634 (fig. 24M–P) and 108314 (fig. 24E–H) from the upper part of the *B. baculus* Zone or the lower part of the *B. grandis* Zone of the Pierre Shale on the Cedar Creek Anticline, Montana.

Material: The collection consists of approximately 100 specimens of which 75 comprise the measured set (40 macroconchs and 35 microconchs) (tables 1, 2). All the specimens in our collection are from the upper part of the *Baculites baculus* Zone or lower part of the *B. grandis* Zone of the Pierre Shale in Wyoming, Colorado, and Montana and the Bearpaw Shale in Montana.

Macroconch Description: In the measured sample, LMAX averages 61.4 mm and ranges from 45.2 to 76.0 mm (table 1). The ratio of the size of the largest specimen to that of the smallest is 1.68. The specimens form a broad size distribution, with a peak at 50–55 mm (fig. 13). Adults are slender with an oval to circular outline in side view. LMAX/H_S averages 2.05 and ranges from 1.86 to 2.25 (1.94 in the holotype). BHI 4346 (fig. 14A–D) is an example of a specimen with an oval outline (LMAX/H_S = 2.17) and AMNH 108487 (fig. 19A–D) is an example of a specimen with a more rounded, nearly perfectly circular outline (LMAX/H_S = 1.98).

The umbilicus is small and deep. The umbilical diameter averages 3.8 mm and ranges from 1.9 to 6.5 mm. UD/LMAX averages 0.06 and ranges from 0.04 to 0.12. In lateral view, the umbilical wall is straight and usually exhibits a pronounced umbilical bulge, so that part of the umbilicus of the phragmocone is concealed. All specimens are tightly coiled with little or no gap between the phragmocone and hook. LMAX/H_{P2} averages 2.78 and ranges from 2.55 to 2.98 (2.70 in the holotype). AMNH 76388 (fig. 18A–C) is an example of a tightly coiled specimen (LMAX/H_{P2} = 2.75) and BHI 4346 (fig. 14A–D) is an example of a more loosely coiled specimen (LMAX/H_{P2} = 2.89).

TABLE 1

Measurements of *Hoploscaphites macer*, n. sp., macroconchs

See figure 12 for description of measurements. All measurements are in mm except for apertural angle. * = close to *H. sargklofak*; ** = close to *H. criptonodosus;* b = *B. baculus* Zone; g= *B. grandis* Zone; b/g = *Baculites baculus* or *B. grandis* Zone; ub= upper *B. baculus* Zone; lg = lower *B. grandis* Zone; ub/lg= upper *B. baculus* or lower *B. grandis* Zone; [1] = suture; [2] = scanned.

Specimen no.	photo	Sample no.	Loc.	Zone	LMAX	LMAX/ H_{P2}	LMAX/ H_S	AA	UD	UD/ LMAX	W_{P1}/ H_{P1}	W_{P2}/ H_{P2}	W_S/ H_S	W_H/ H_H	V_S/H_S
AMNH 64680*	–	1236	3278	b/g	50.1	2.77	2.13	41.5	3.9	0.08	1.05	0.86	0.82	1.02	0.40
AMNH 71839[1] holotype	x	(JG385a)	3921	lg	52.3	2.70	1.94	44.5	2.7	0.05	0.99	0.84	0.80	1.11	0.38
AMNH 71861		(JG944)	3921	ub/lg	53.5	2.74	1.98	53.0	3.6	0.07	–	0.84	0.72	0.96	0.39
AMNH 71862		(JG460)	3921	lg	56.4	2.55	1.86	52.5	3.5	0.06	1.03	0.89	0.79	1.17	0.33
AMNH 71869		JG394	3921	ub/lg	54.2	2.81	1.96	–	3.0	0.06	0.93	0.91	0.84	1.06	0.34
AMNH 71872		(JG712)	3921	lg	56.9	2.55	1.96	–	4.7	0.08	1.02	0.96	0.87	–	0.50
AMNH 71931	x	(JG594)	3921	ub/lg	66.6	2.85	2.11	69	3.8	0.06	0.96	0.90	0.88	1.10	0.44
AMNH 74328	x	795	3921	ub/lg	57.5	2.86	2.05	57.5	3.9	0.07	1.00	0.90	0.77	1.13	0.41
AMNH 74330		710	3921	ub/lg	57.8	2.97	2.06	–	4.6	0.08	–	0.91	0.84	1.06	0.34
AMNH 74331 ontogeny	x	926	3921	ub/lg	52.5	2.81	2.03	52	1.9	0.04	–	0.89	0.91	1.04	0.50
AMNH 74332		234	?	b?	58.2	2.76	1.97	52	3.6	0.06	1.01	0.96	0.85	1.07	0.42
AMNH 74335	x	868	3921	ub/lg	71.0	2.83	2.02	66	3.5	0.05	–	0.78	0.74	0.99	0.38
AMNH 74337		706	3921	ub/lg	65.2	–	2.06	60	–	–	–	–	0.67	1.11	0.36
AMNH 74338		864	3921	ub/lg	45.2	2.70	2.00	40.5	3.2	0.07	0.95	0.82	0.80	1.02	0.43
AMNH 76267		(JG120)	3921	ub/lg	58.9	2.79	2.01	57	3.2	0.05	1.16	0.96	0.88	1.13	0.48
AMNH 76367		744 (JG256)	3921	ub/lg	71.2	2.83	1.98	68	–	–	–	0.76	0.72	1.00	0.30
AMNH 76387		742 (JG115)	3921	ub/lg	74.9	2.78	2.21	59	4.5	0.06	–	0.81	0.79	1.14	0.51
AMNH 76388	x	772 (JG119)	3921	ub/lg	61.3	2.75	2.06	42	3.2	0.05	0.98	0.96	0.95	1.10	0.38
AMNH 76394		975 (JG255)	3921	ub/lg	54.2	2.56	2.24	–	2.8	0.05	0.84	–	0.78	1.00	0.47

Specimen no.	photo	Sample no.	Loc.	Zone	LMAX	LMAX/ H_{P2}	LMAX/ H_S	AA	UD	UD/ LMAX	W_{P1}/ H_{P1}	W_{P2}/ H_{P2}	W_S/ H_S	W_H/ H_H	V_S/H_S
AMNH 76395		976 (JGn5)	3921	ub/lg	58.2	2.92	2.16	–	2.8	0.05	1.14	0.92	0.94	1.19	0.41
AMNH 76546		732 (JG181)	3921	ub/lg	61.3	2.79	–	63.5	2.9	0.05	0.90	0.90	–	1.13	–
AMNH 77032		169	3727	g	53.9	2.98	2.25	–	6.5	0.12	0.99	0.92	0.80	0.98	0.40
AMNH 108326		–	3921	ub/lg	74.5	2.58	–	–	3.8	0.05	0.82	0.74	–	0.94	–
AMNH 108444		384	?	?	64.5	2.88	2.07	–	4.2	0.07	1.07	0.89	0.79	1.04	0.35
AMNH 108458		860	3921	ub/lg	61.2	2.90	2.02	61	3.7	0.06	1.14	0.98	0.83	1.07	0.42
AMNH 108487	x	1245	3278	ub/lg	46.0	2.66	1.98	36	4.2	0.09	0.96	0.80	0.74	1.00	0.37
AMNH 113323 paratype	x	–	3921	ub/lg	63.7	2.78	1.94	63	3.6	0.06	1.00	0.90	0.84	1.03	0.39
AMNH 113324 paratype	x	–	3921	ub/lg	67.0	2.84	1.96	61	3.7	0.06	1.02	0.90	0.86	1.14	0.48
AMNH 116935		(JG2783)	3921	ub	76.0	–	2.11	–	–	–	–	–	0.80	–	–
AMNH 116937		(JG2785)	3921	lg	70.4	2.65	2.04	–	3.9	0.06	1.05	–	–	–	–
AMNH 116953		(JG2422)	3921	ub/lg	52.8	2.81	2.01	–	3.1	0.06	0.87	0.90	–	–	–
BHI 4306[2]	x	252	3921	ub/lg	72.1	2.80	2.00	58	3.7	0.05	–	0.93	0.83	1.07	0.40
BHI 4346**	x	793	3278	g	68.0	2.89	2.17	54.5	4.0	0.06	0.84	0.79	0.83	1.06	0.35
BHI 4786	x	870	3921	ub/lg	65.2	2.87	2.03	67	3.6	0.06	1.00	0.92	0.83	1.08	0.41
DMNH EPI 19920	x	–	1405	b/g	57.4	2.78	2.20	–	4.6	0.08	–	–	–	–	–
DMNH EPI 22915	x	–	1405	b/g	67.4	–	1.95	–	–	–	–	–	–	–	0.41
USNM 713612 paratype	x	154	5440	g	69.5	2.81	2.01	60.5	4.2	0.06	1.11	0.87	0.78	1.07	0.39
USNM 713613		227	10189	g	64.3	2.88	2.09	58	3.7	0.06	0.91	0.85	0.76	–	0.33
USNM 713623*		850	D2118	lg	51.6	2.72	2.07	–	4.5	0.09	–	–	0.77	1.03	0.33
USNM 713624*[1]	x	848	D2118	lg	72.2	2.85	2.10	55.5	4.6	0.06	0.97	0.85	0.77	1.07	0.36
Average					61.4	2.78	2.05	55.9	3.8	0.06	0.98	0.88	0.81	1.06	0.40
SD					8.1	0.11	0.09	8.7	0.8	0.02	0.11	0.06	0.06	0.06	0.05

TABLE 2

Measurements of *Hoploscaphites macer*, n. sp., microconchs

See figure 12 for description of measurements. All measurements are in mm. b = *B. baculus* Zone; g= *B. grandis* Zone; b/g = *Baculites baculus* or *B. grandis* Zone; ub= upper *B. baculus* Zone; lg = lower *B. grandis* Zone; ub/lg= upper *B. baculus* or lower *B. grandis* Zone; [1] = suture.

Specimen no.	Photo	Sample no.	Loc.	Zone	LMAX	LMAX/ H_{P2}	LMAX/ H_S	UD	UD/ LMAX	W_{P1}/ H_{P1}	W_{P2}/ H_{P2}	W_S/H_S	W_H/ H_H	V_S/H_S
AMNH 69736		(JG2258)	3921	ub/lg	40.8	2.71	2.31	2.5	0.06	0.84	0.77	0.81	1.00	0.36
AMNH 71898		(JG391)	3921	lg	39.8	3.22	2.64	3.3	0.08	1.02	0.95	0.96	0.93	0.42
AMNH 71905		(JG654)	3921	lg	35.8	2.75	2.40	3.9	0.11	0.84	0.82	0.82	1.07	0.32
AMNH 71921		1037 (JG185)	3921	ub/lg	38.6	2.97	2.32	3.0	0.08	0.82	0.81	0.80	0.87	0.37
AMNH 72555		(JG205)	3921	ub/lg	44.0	3.01	2.45	3.9	0.09	0.94	0.93	0.90	0.98	0.38
AMNH 72589		(JG314)	3921	ub/lg	37.5	2.74	2.35	3.5	0.09	0.95	0.83	0.82	0.94	0.37
AMNH 72590		(JG197)	3921	ub/lg	38.0	2.72	2.53	3.3	0.09	0.88	0.81	–	0.90	0.40
AMNH 72610		(JG 132)	3921	ub/lg	38.9	2.56	2.35	4.2	0.11	0.98	0.76	0.85	0.97	0.37
AMNH 72624	x	(JG335)	3921	ub/lg	54.3	3.19	2.40	4.2	0.08	0.87	0.98	0.93	1.13	0.50
AMNH 72634 paratype	x	(JG208)	3921	ub/lg	45.1	2.90	2.28	3.8	0.08	0.87	0.92	0.85	0.93	0.41
AMNH 74345		797	3921	ub/lg	48.5	2.88	2.35	3.7	0.08	1.07	0.97	0.95	1.04	0.53
AMNH 74350		1008	?	?	45.9	2.94	2.27	3.7	0.08	0.76	0.89	0.81	0.97	0.36
AMNH 74354		1046	3921	ub/lg	45.0	2.78	2.36	4.5	0.10	1.00	0.91	0.90	0.92	0.41
AMNH 74358		971	3921	ub/lg	44.9	2.78	2.24	3.3	0.07	0.90	0.77	0.84	1.01	0.38
AMNH 74361		954	3921	ub/lg	45.1	2.69	2.35	4.6	0.10	0.97	0.87	0.83	1.09	0.34
AMNH 76220		989 (JG363)	3921	ub/lg	50.0	2.96	2.58	3.7	0.07	0.98	0.95	0.85	0.99	0.40
AMNH 76279		(JG203)	3921	ub/lg	39.1	2.72	2.38	3.5	0.09	0.87	0.87	0.86	1.05	0.44
AMNH 76370		988 (JG171)	3921	ub/lg	51.6	2.91	2.34	3.9	0.08	0.84	0.88	0.90	1.00	0.45
AMNH 76381[1]		745 (JG128)	3921	ub/lg	56.6	3.20	2.68	5.6	0.10	1.16	1.00	0.84	0.89	0.34
AMNH 76382		264 (JG130)	3921	ub/lg	55.0	2.92	2.45	4.3	0.08	0.64	0.72	0.75	0.82	0.31
AMNH 76383	x	734 (JG131)	3921	ub/lg	45.6	2.90	2.54	4.0	0.09	0.77	0.79	0.87	0.98	0.46

Specimen no.	Photo	Sample no.	Loc.	Zone	LMAX	LMAX/ H_{P2}	LMAX/ H_S	UD	UD/ LMAX	W_{P1}/ H_{P1}	W_{P2}/ H_{P2}	W_S/H_S	W_H/ H_H	V_S/H_S
AMNH 76386		787	3921	ub/lg	44.2	3.04	2.41	4.2	0.10	1.08	1.01	0.92	1.12	0.54
AMNH 76417		1171 (JG388)	3921	ub	46.7	3.03	2.51	5.0	0.11	0.93	0.95	0.92	1.08	0.33
AMNH 95783		387	3921	ub/lg	51.5	3.05	2.48	3.3	0.06	0.88	0.94	0.97	1.00	0.38
AMNH 105894		(JP2747)	3921	ub/lg	54.5	2.88	2.43	3.3	0.06	0.89	0.74	0.75	0.99	0.46
AMNH 105895		(JP2816)	3921	ub/lg	51.8	2.72	2.44	3.2	0.06	0.71	0.70	0.84	0.88	0.53
AMNH 108314 paratype	x	–	3244	lg	43.4	2.96	2.44	3.2	0.07	0.93	0.82	0.83	0.94	0.42
AMNH 116943		(JG2791)	3921	lg	39.8	2.83	2.55	4.6	0.11	0.92	0.83	0.85	1.08	0.41
AMNH 116946		(JG2795)	3921	ub	40.1	2.79	2.53	3.6	0.09	0.96	0.93	0.99	1.17	0.50
AMNH 116949		(JG2798)	3921	ub	45.9	–	2.39	3.6	0.08	–	–	0.86	0.93	–
BHI 4321		235	3921	ub/lg	35.4	3.19	2.48	3.4	0.10	0.81	0.88	0.83	0.90	0.37
DMNH EPI 22907	x	–	1405	b/g	38.2	2.89	2.33	3.2	0.08	0.82	0.93	–	–	–
USNM 713625	x	388	3921?	ub/lg?	56.4	2.85	2.40	3.5	0.06	0.83	0.81	0.87	1.04	–
USNM 713639		–	D1047	b	47.3	–	–	–	–	–	–	0.85	1.00	–
YPM 35657	x	1034	A4745	b/g	42.0	2.86	2.45	3.6	0.09	0.74	0.74	0.86	0.93	0.34
Average					45.1	2.90	2.42	3.8	0.08	0.89	0.86	0.86	0.99	0.41
SD					6.0	0.16	0.10	0.6	0.02	0.11	0.09	0.06	0.08	0.06

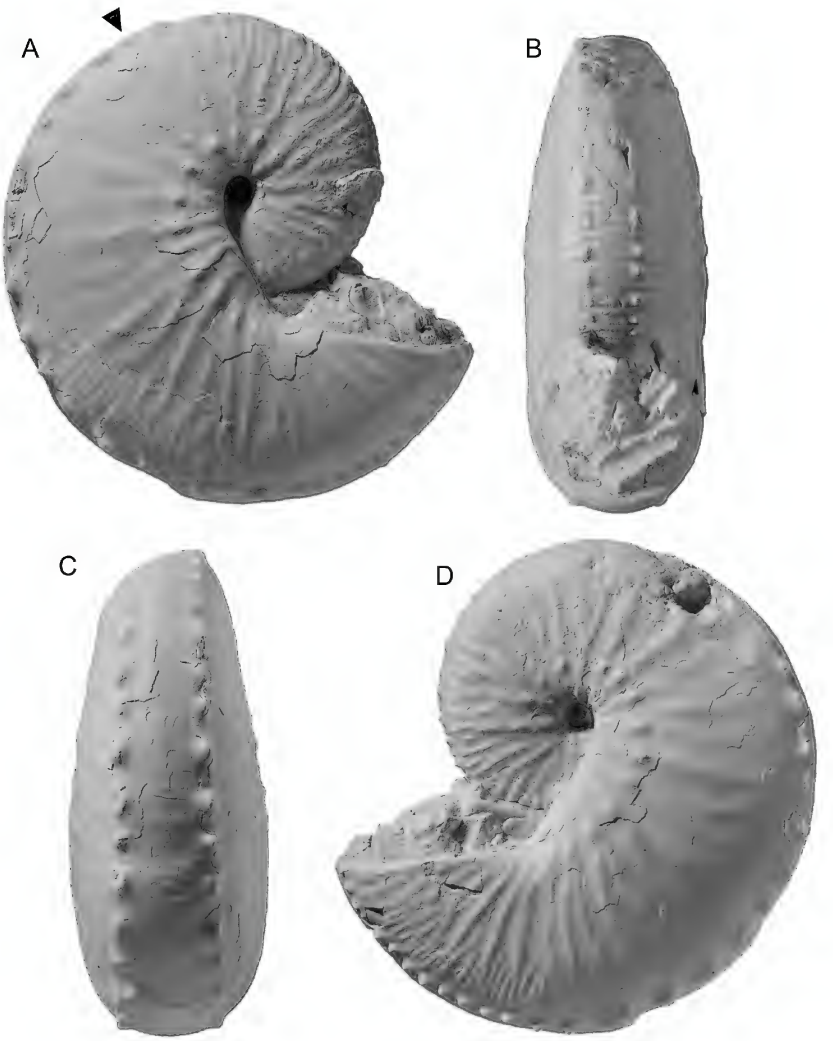

FIGURE 14. *Hoploscaphites macer*, macroconch. **A–D.** BHI 4346, AMNH loc. 3278, *Baculites grandis* Zone, Pierre Shale, Weston County, Wyoming. **A,** Right lateral; **B,** apertural; **C,** ventral; **D,** left lateral. Arrow indicates the base of the body chamber. Specimens ×1.

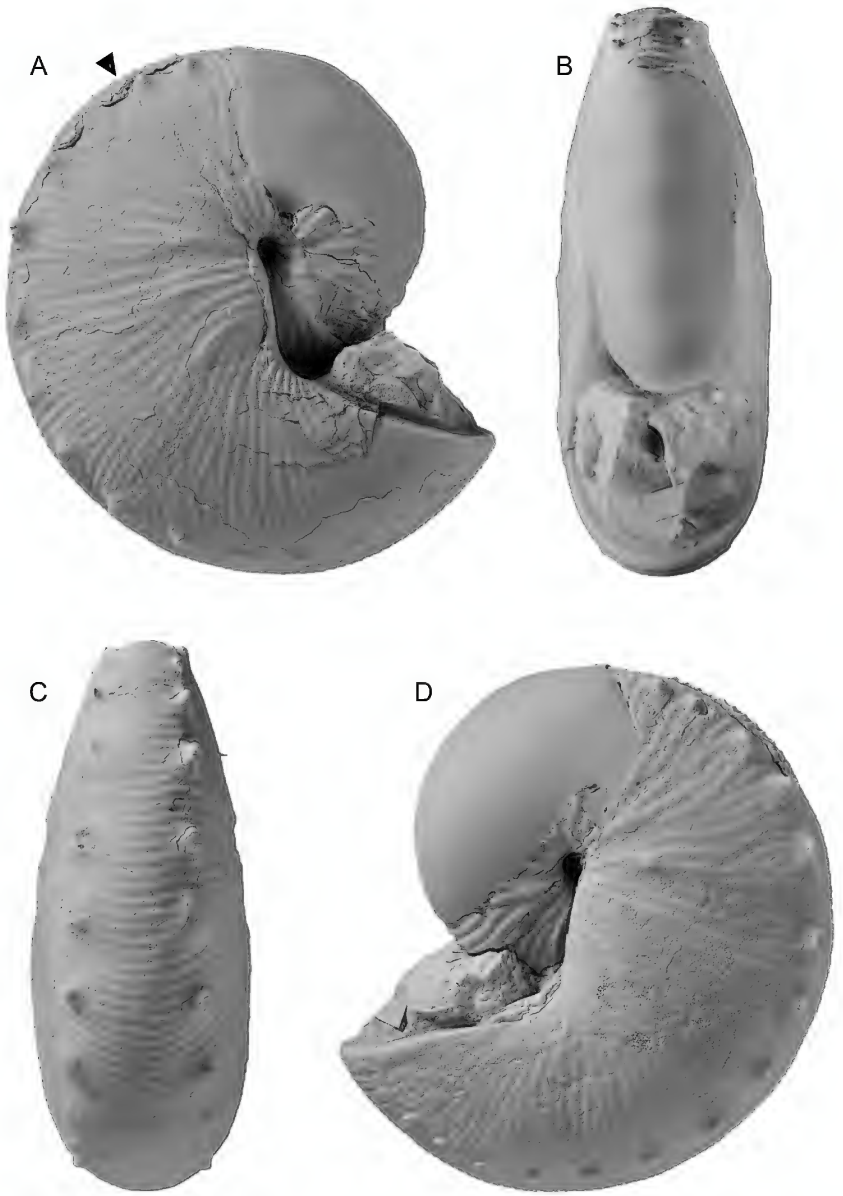

FIGURE 15. *Hoploscaphites macer*, macroconch. **A–D.** AMNH 74335, AMNH loc. 3921, upper *Baculites baculus* or lower *B. grandis* Zone, Pierre Shale, Cedar Creek Anticline, east-central Montana. **A,** Right lateral; **B,** apertural; **C,** ventral; **D,** left lateral. Part of the phragmocone is missing and is filled in with clay. Arrow indicates the base of the body chamber. Specimens ×1.

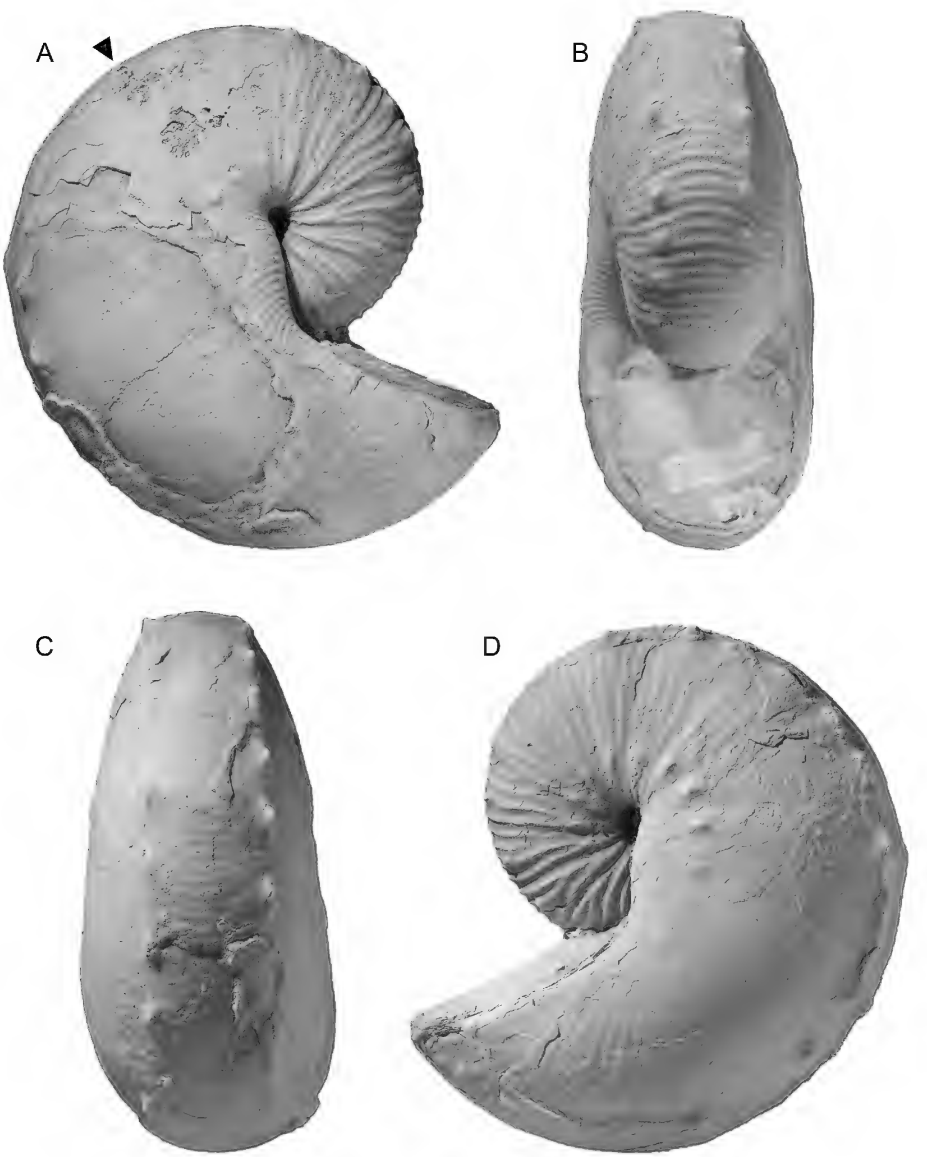

FIGURE 16. *Hoploscaphites macer*, macroconch. **A–D.** BHI 4306, AMNH loc. 3921, upper *Baculites baculus* or lower *B. grandis* Zone, Pierre Shale, Cedar Creek Anticline, east-central Montana. **A,** Right lateral; **B,** apertural; **C,** ventral; **D,** left lateral. Arrow indicates the base of the body chamber. Specimens ×1.

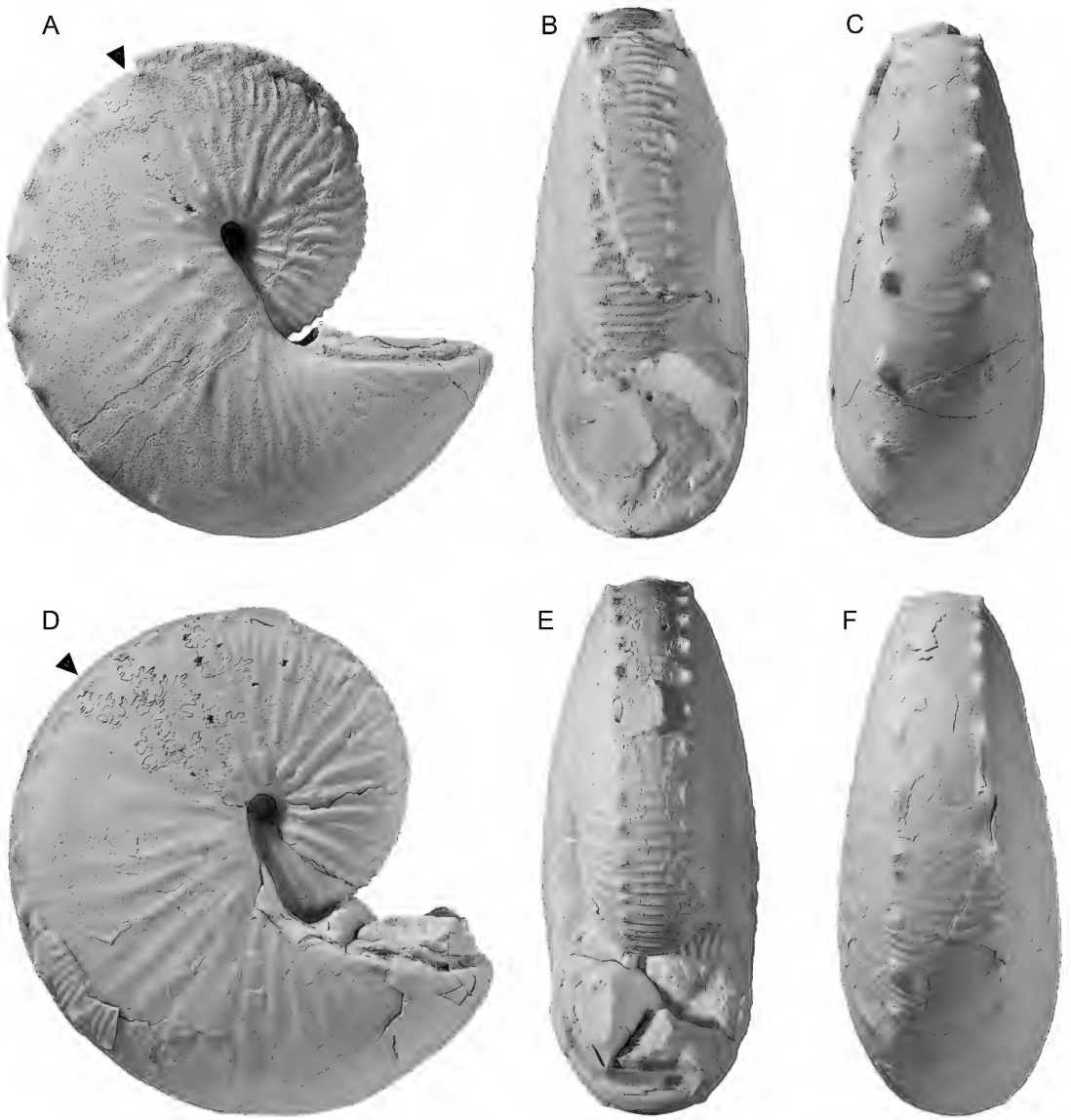

FIGURE 17. *Hoploscaphites macer*, macroconchs. **A–C.** USNM 713612, paratype, USGS loc. 5440, *Baculites grandis* Zone, Bearpaw Shale, Roosevelt County, Montana. **A,** Right lateral; **B,** apertural; **C,** ventral. **D–F.** USNM 713624, USGS Mesozoic loc. D2118, lower *Baculites grandis* Zone, Pierre Shale, Niobrara County, Wyoming. **D,** Right lateral; **E,** apertural; **F,** ventral. Arrows indicate the base of the body chamber. Specimens ×1.

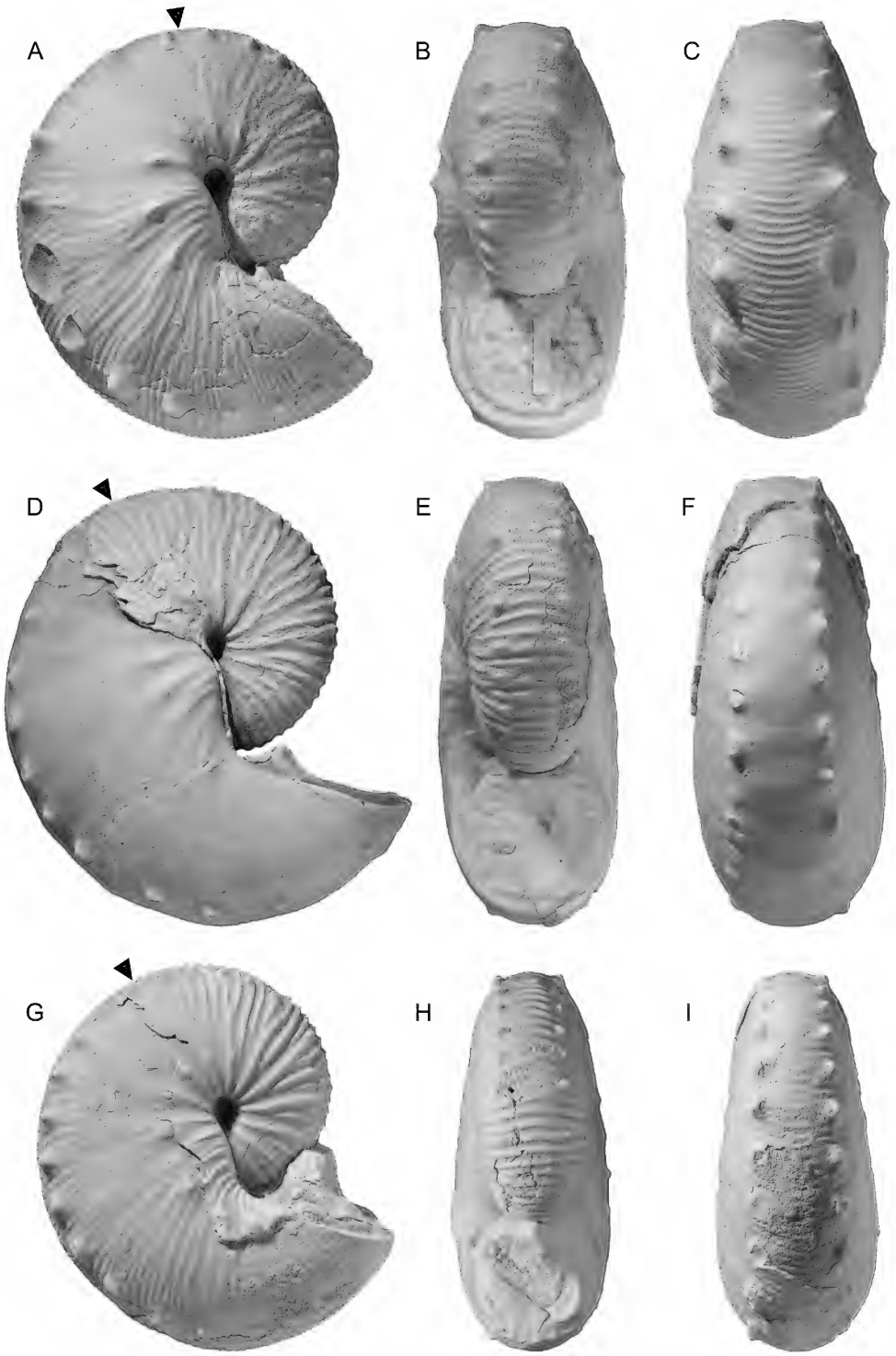
A
B
C
D
E
F
G
H
I

The exposed phragmocone occupies approximately one-half whorl and usually terminates just below the line of maximum length. AMNH 76367 (not figured) is an exception in which the phragmocone terminates just adapical of midshaft. An unpaired muscle scar appears on the venter just adoral of the end of the phragmocone (fig. 8A, B). The body chamber consists of a short shaft and recurved hook totaling slightly more than one-half whorl. The apertural lip is flexuous with a deep constriction, as in other scaphites (fig. 9). The apertural angle averages 55.9° and ranges from to 36.0° to 69.0° (44.5° in the holotype).

The whorl section of the phragmocone near the point of exposure is compressed subovoid with maximum whorl width at one-third whorl height. W_{P1}/H_{P1} averages 0.98 and ranges from 0.82 to 1.16 (0.99 in the holotype). The umbilical wall is steep and subvertical and the umbilical shoulder is sharply rounded. The flanks are broadly rounded and converge toward the venter starting at two-thirds whorl height. The ventrolateral shoulder is sharply rounded and the venter is broadly rounded. The whorl section of the phragmocone at the line of maximum length is more compressed than that at the point of exposure, reflecting a marked increase in whorl height. W_{P2}/H_{P2} averages 0.88 and ranges from 0.74 to 0.98 (0.84 in the holotype). In addition, the flanks are very broadly rounded and the venter is nearly flat.

As the shell passes from the phragmocone into the body chamber, the whorl width increases and reaches its maximum value on the adoral part of the shaft and, as a result, the shell forms a bulge in this area. Whorl height increases even more markedly during this transition and reaches its maximum value at midshaft. Thereafter, it diminishes to the point of recurvature and remains nearly the same up to the aperture. Because of these changes in whorl width and height, the whorl section at midshaft is only slightly more compressed than that along the line of maximum length (table 1). W_S/H_S averages 0.81 and ranges from 0.67 to 0.95 (0.80 in the holotype). The whorl section is subovoid with maximum whorl width at one-quarter whorl height. The umbilical wall is steep and subvertical and the umbilical shoulder is sharply rounded. The whorls are very high and broadly rounded and gently converge to the venter. The ventrolateral shoulder is sharply rounded and the venter is nearly flat. V_S/H_S averages 0.40 and ranges from 0.30 to 0.51 (0.38 in the holotype).

The whorl section at the point of recurvature is less compressed than that at midshaft, mainly due to a decrease in whorl height. W_H/H_H averages 1.06 and ranges from 0.94 to 1.19 (1.11 in the holotype). The whorl section at the point of recurvature is subovoid with maximum whorl width at one-half whorl height. The umbilical wall is slightly concave and the umbilical shoulder is sharply rounded. The flanks are broadly rounded and gently converge toward the venter.

At the adapical end of the exposed phragmocone, ribs emerge at the umbilical seam and strengthen across the umbilical wall and shoulder. They attain their maximum strength at one-third whorl height and in some specimens, such as AMNH 113324 (fig. 20G–I) develop into small umbilicolateral tubercles at this point. Ribs are rectiradiate to slightly prorsiradiate and weakly flexuous, bending slightly backward on the inner flanks, slightly forward on the midflanks, and slightly backward again on the outer flanks. They are widely spaced, with intercalation and branching occurring at one-third and two-thirds whorl

FIGURE 18. *Hoploscaphites macer*, macroconchs. **A–C.** AMNH 76388, AMNH loc. 3921, upper *Baculites baculus* or lower *B. grandis* Zone, Pierre Shale, Cedar Creek Anticline, east-central Montana. **A,** Right lateral; **B,** apertural; **C,** ventral. **D–F.** BHI 4786, AMNH loc. 3921, *Baculites baculus* or *B. grandis* Zone, Pierre Shale, Cedar Creek Anticline, east-central Montana. **D,** Right lateral; **E,** apertural; **F,** ventral. **G–I.** AMNH 74328, AMNH loc. 3921, upper *Baculites baculus* or lower *B. grandis* Zone, Pierre Shale, Cedar Creek Anticline, east-central Montana. **G,** Right lateral; **H,** apertural; **I,** ventral. Arrows indicate the base of the body chamber. Specimens ×1.

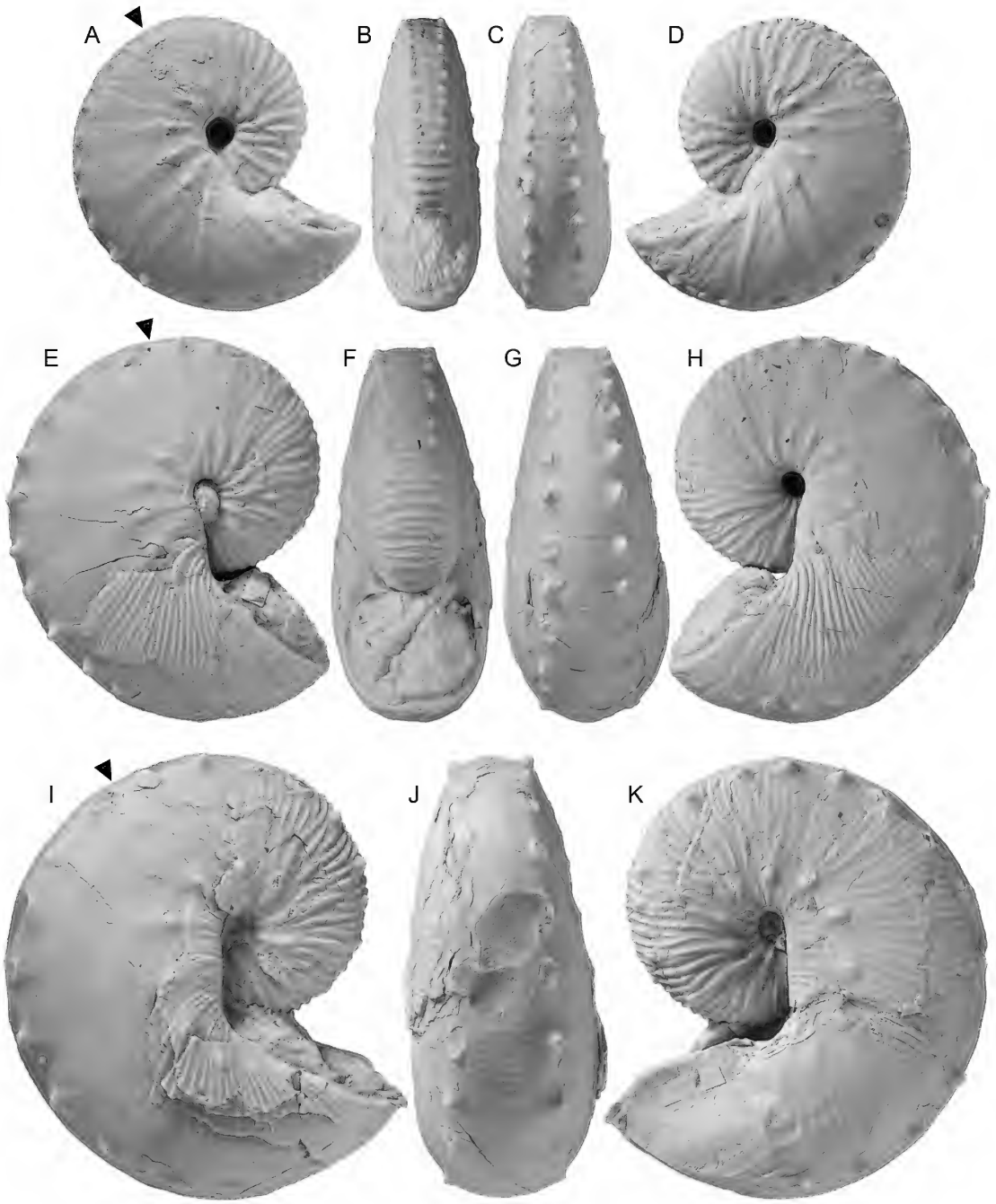
A
B
C
D
E
F
G
H
I
J
K

height, so that the outer flanks are more densely covered with ribs than the inner flanks. Ribs are uniformly strong on the venter, which they cross with a slight adoral projection. The rib density on the venter on the adapical end of the phragmocone ranges from 6 to 8 ribs/cm in our measured sample (7 ribs/cm in the holotype).

The same pattern of ribbing persists onto the adoral part of the phragmocone. However, because the whorl section is more compressed at this point than on the adapical part of the phragmocone due to an increase in whorl height and a flattening of the flanks, the ribs on the adoral part of the phragmocone are relatively longer and more closely spaced. The rib density on the venter on the adoral end of the phragmocone ranges from 6 to 9 ribs/cm in our measured sample (9 ribs/cm in the holotype).

On the body chamber, ribs arise at the umbilical seam and are rursiradiate on the umbilical wall and shoulder. They are adorally concave at one-third whorl height and in many specimens form small umbilicolateral tubercles at this point. The tubercles are evenly spaced and usually extend to the aperture. In the holotype, the distance between consecutive umbilicolateral tubercles at midshaft is 5 mm. Ribs are straight and prorsiradiate on the middle and outer flanks, with branching and intercalation occurring at two-thirds whorl height. As a result, the outer flanks are more densely covered with ribs than the inner flanks. Ribs cross the venter with a strong adoral projection. They become more closely spaced toward the aperture. In our measured sample, the rib density ranges from 7 to 10 ribs/cm on the midshaft versus 8 to 13 ribs/cm on the hook (10 versus 13 ribs/cm, respectively, in the holotype).

Ventrolateral tubercles develop early in ontogeny at a diameter of approximately 6 mm and persist onto the exposed phragmocone (fig. 22). Because the venter is broadly rounded, the tubercles occur slightly below the ventrolateral shoulder. The tubercles are widely and unevenly spaced on the adapical end of the exposed phragmocone, but become more closely and uniformly spaced toward the adoral end. In the holotype, the distance between consecutive tubercles on the exposed phragmocone, starting at the point of exposure, is 7, 6.5, 4.5, 3, 5, 3, 5, 3, 4, and 4 mm (fig. 19E–H). The total number of ventrolateral tubercles on the exposed phragmocone ranges from 6 to 13 in our measured sample (11 tubercles in the holotype). The tubercles are conical in shape and change from slightly radially elongate at the point of exposure to slightly clavate at the adoral end of the phragmocone.

Ventrolateral tubercles persist onto the body chamber. They gradually become more widely spaced, attaining their maximum spacing on the adoral end of the shaft, and become more closely spaced again on the hook. In the holotype, the distance between consecutive ventrolateral tubercles is 6 mm at midshaft, 7.5 mm on the adoral end of the shaft, and 4.5 mm on the hook (fig. 19E–H). Three or four ribs loop between tubercles on opposite sides of the venter at midshaft, with an equal number of ribs intercalating between them. Because the venter is broadly rounded to nearly flat, the tubercles appear at or just below the ventrolateral shoulder. The number of ventrolateral tubercles on the body chamber ranges from 10 to 25 in our measured sample (16 in the holotype). The tubercles are clavate on the adoral end of the shaft where they attain their maximum height.

FIGURE 19. *Hoploscaphites macer*, macroconchs. A–D. AMNH 108487, AMNH loc. 3278, *Baculites baculus* or *B. grandis* Zone, Pierre Shale, Weston County, Wyoming. **A,** Right lateral; **B,** apertural; **C,** ventral; **D,** left lateral. **E–H.** AMNH 71839, holotype, AMNH loc. 3921, lower *Baculites grandis* Zone, Pierre Shale, Cedar Creek Anticline, east-central Montana. **E,** Right lateral; **F,** apertural; **G,** ventral; **H,** left lateral. **I–K.** AMNH 71931, AMNH loc. 3921, upper *Baculites baculus* or lower *B. grandis* Zone, Pierre Shale, Cedar Creek Anticline, east-central Montana. **I,** Right lateral; **J,** ventral, **K,** left lateral. Arrows indicate the base of the body chamber. Specimens ×1.

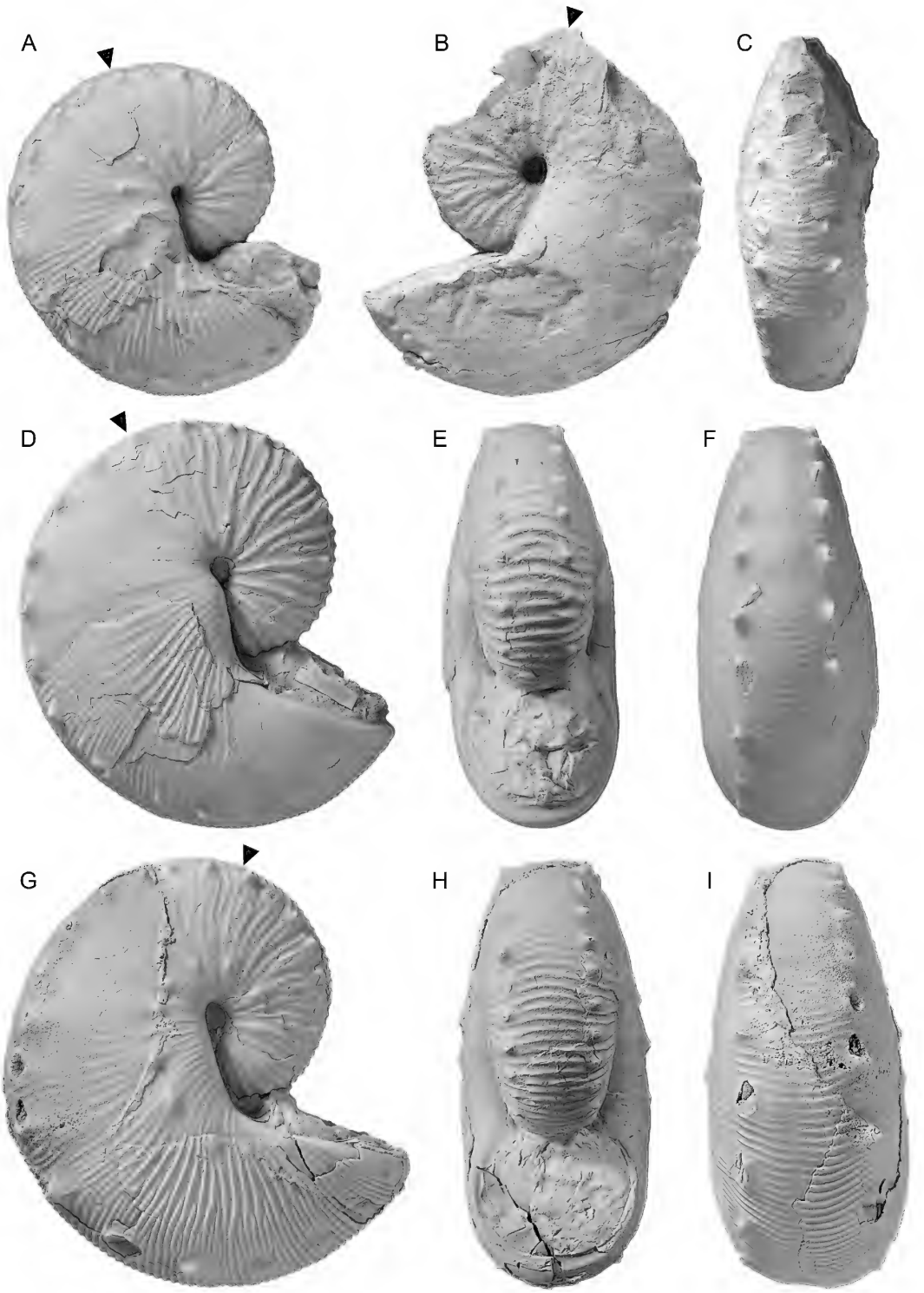
A
B
C
D
E
F
G
H
I

They become smaller on the hook and, in some instances, slightly radially elongate.

In a few specimens, small lateral tubercles occur on the adapical end of the exposed phragmocone. They form a single row at two-thirds whorl height and persist for as much as one-quarter whorl. For example, in USNM 713623 (not figured), a single row of five lateral tubercles is present beginning at the point of exposure. They occur on every rib and are evenly spaced at intervals of 2.5 mm. Similarly, in AMNH 113323 (fig. 20D–F), a single row of five lateral tubercles appears on the adapical end of the phragmocone and persists for one-eighth whorl.

The suture is deeply incised, with a broad, asymmetrically bifid first lateral saddle (E/L) and a narrow, symmetrically to asymmetrically bifid first lateral lobe (L) (fig. 23A, B).

Microconch Description: In comparison with macroconchs, microconchs are characterized by a more openly coiled shell with a larger umbilicus. In addition, the umbilical shoulder is concave in lateral view and the umbilicolateral tubercles are more prominent. LMAX averages 45.1 mm and ranges from 35.4 to 56.6 mm (table 2). The ratio of the average size of microconchs to that of macroconchs is 0.73. The size distribution is unimodal with a peak at 35–40 mm (fig. 13).

Microconchs are oval in lateral view. The phragmocone usually terminates at or below the line of maximum length. Microconchs are less tightly coiled than macroconchs with a gap between the phragmocone and hook. $LMAX/H_{P2}$ averages 2.90 and ranges from 2.56 to 3.22. AMNH 72624 (fig. 25E–G) is an example of an openly coiled specimen ($LMAX/H_{P2}$ = 3.19) and AMNH 76383 (fig. 24I–L) is an example of a more tightly coiled specimen ($LMAX/H_{P2}$ = 2.90). The body chamber occupies slightly more than one-half whorl. The umbilicus is relatively large. UD/LMAX averages 0.08 and ranges from 0.06 to 0.11. The average value of UD/LMAX is significantly higher in microconchs than it is in macroconchs (UD/LMAX = 0.06).

The whorl section of the exposed phragmocone is compressed subquadrate. W_{P1}/H_{P1} averages 0.89 and ranges from 0.64 to 1.16; W_{P2}/H_{P2} averages 0.86 and ranges from 0.70 to 1.01. The umbilical wall is steep and nearly vertical, the umbilical shoulder is sharply rounded, and the flanks are broadly rounded and gently converge to the ventrolateral shoulder. The ventrolateral shoulder is sharply rounded and the venter is broadly rounded.

Whorl width gradually increases from the phragmocone into the body chamber, attaining its maximum value on the hook. Whorl height also increases gradually from the phragmocone into the body chamber, but reaches its maximum value at midshaft and remains nearly the same thereafter. The whorl section at midshaft is compressed subquadrate with maximum width at one-quarter whorl height. W_S/H_S averages 0.86 and ranges from 0.75 to 0.99 (table 2). The umbilical wall is steep and slopes outward at an acute angle. The flanks are broadly rounded and converge gently toward the ventrolateral shoulder. The ventrolateral shoulder is sharply rounded and the venter is nearly flat. V_S/H_S averages 0.41 and ranges from 0.31 to 0.54. The whorl section at the hook is more ovate than that at midshaft. W_H/H_H averages 0.99 and ranges from 0.82 to 1.17. The venter is broadly rounded, which is accentuated by the disappearance of the ventrolateral tubercles.

FIGURE 20. *Hoploscaphites macer*, macroconchs. **A.** AMNH 74331, right lateral, AMNH loc. 3921, upper *Baculites baculus* or lower *B. grandis* Zone, Pierre Shale, Cedar Creek Anticline, east-central Montana (used for ontogenetic breakdown). **B, C.** DMNH EPI 19920, DMNH loc. 1405, *Baculites baculus* or *B. grandis* Zone, Pierre Shale, Jefferson County, Colorado. **B,** Left lateral; **C,** ventral. **D–F.** AMNH 113323, paratype, upper *Baculites baculus* or lower *B. grandis* Zone, Pierre Shale, Cedar Creek Anticline, east-central Montana. **D,** Right lateral; **E,** apertural; **F,** ventral. **G–I.** AMNH 113324, paratype, AMNH loc. 3921, upper *Baculites baculus* or lower *B. grandis* Zone, Pierre Shale, Cedar Creek Anticline, east-central Montana. **G,** Right lateral; **H,** apertural; **I,** ventral. Arrows indicate the base of the body chamber. Specimens ×1.

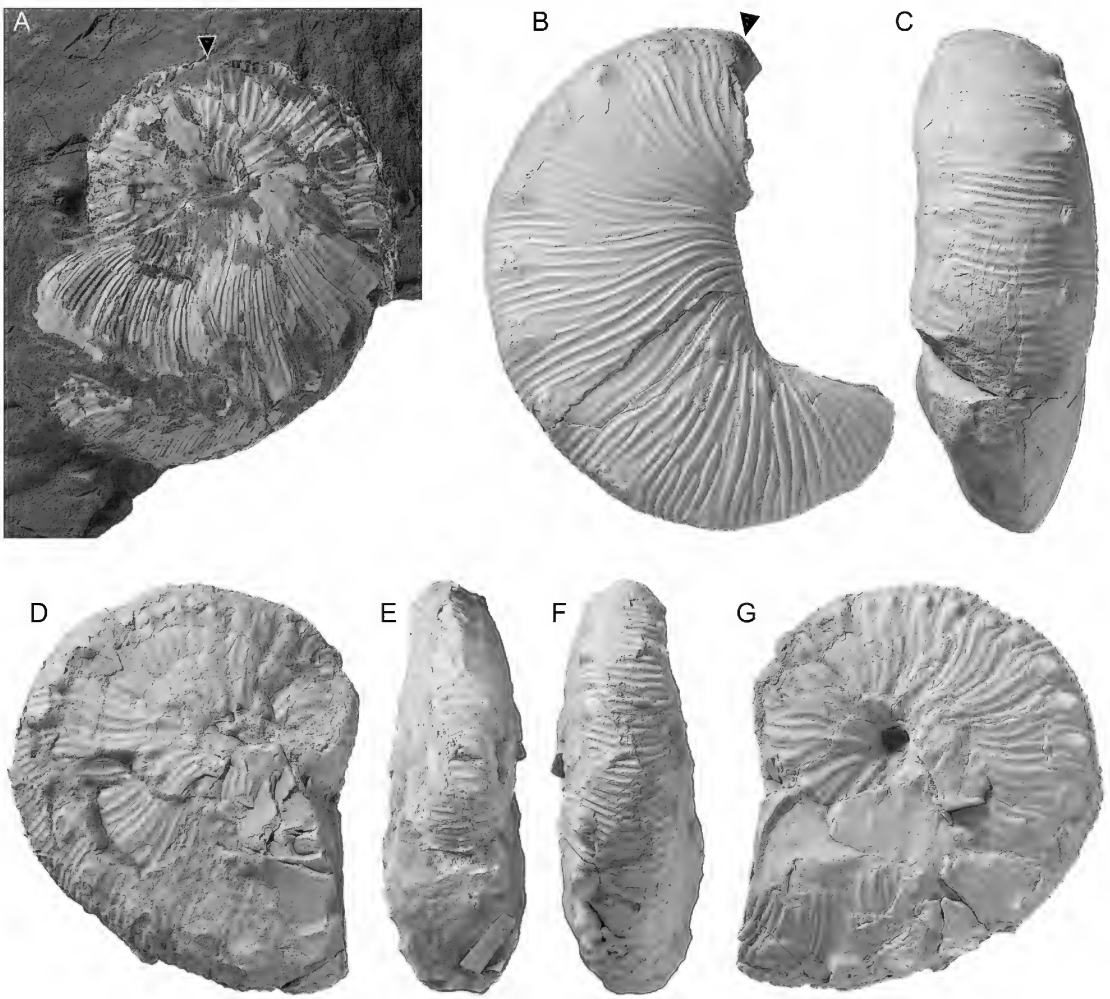

FIGURE 21. *Hoploscaphites macer*, macroconchs. **A.** DMNH EPI 19946, left lateral, finely ribbed specimen with a lethal injury at the aperture, DMNH loc. 1405, *Baculites baculus* or *B. grandis* Zone, Pierre Shale, Jefferson County, Colorado. **B, C.** DMNH EPI 22915, DMNH loc. 1405, *Baculites baculus* or *B. grandis* Zone, Pierre Shale, Jefferson County, Colorado. **B,** Right lateral; **C,** ventral. **D–G.** DMNH EPI 36444, incomplete specimen, DMNH loc. 5751, *Baculites baculus* or *B. grandis* Zone, Pierre Shale, Jefferson County, Colorado. **D,** Right lateral; **E,** apertural; **F,** ventral; **G,** left lateral. Arrows indicate the base of the body chamber. Specimens ×1.

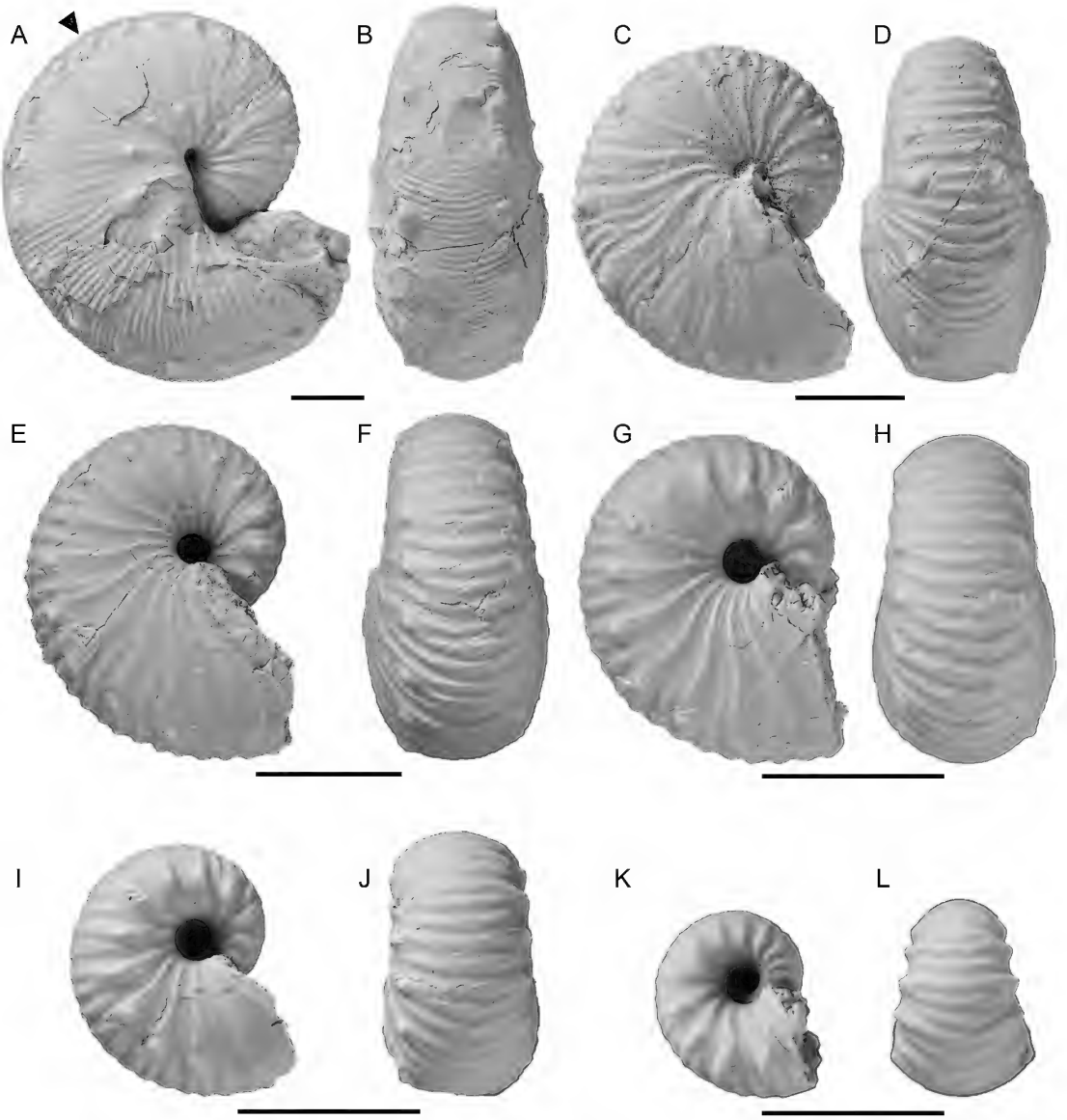

FIGURE 22. Ontogenetic breakdown of *Hoploscaphites macer*, macroconch, AMNH 74331, AMNH loc. 3921, upper *Baculites baculus* or lower *B. grandis* Zone, Pierre Shale, Cedar Creek Anticline, east-central Montana. **A–L.** Six sizes through ontogeny in lateral and ventral views showing The change in ornamentation from early ontogeny (K, L) to maturity (A, B). Arrow indicates the base of the body chamber. Scale bar = 1 cm.

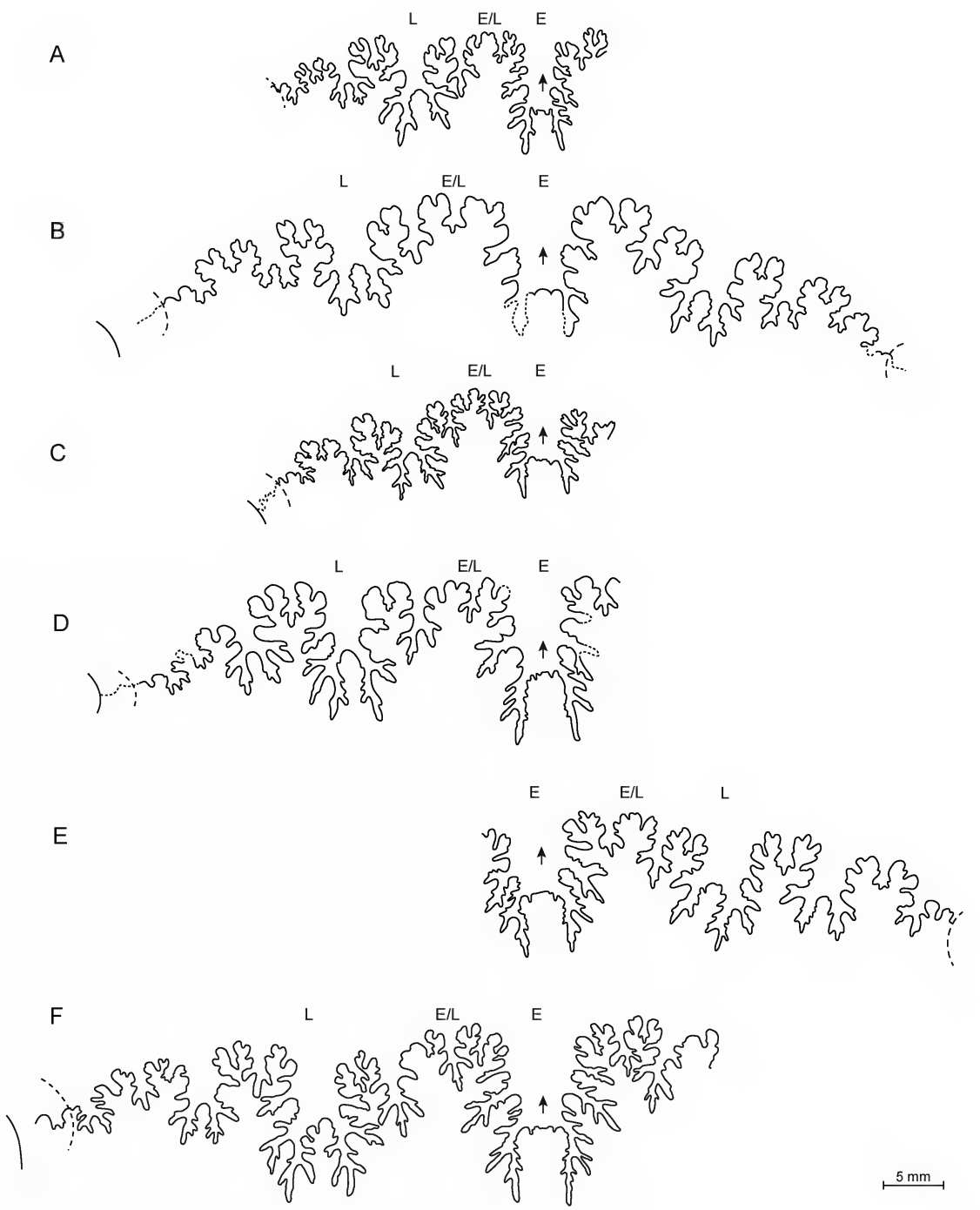
A
L
E/L
E
B
L
E/L
E
C
L
E/L
E
D
L
E/L
E
E
E
E/L
L
F
L
E/L
E
5 mm

On the exposed phragmocone, ribs emerge at the umbilical seam and are slightly rursiradiate on the umbilical wall. They are weakly flexuous on the flanks, swinging gently backward on the inner flanks, gently forward on the midflanks, and gently backward again on the outer flanks. Ribs are uniformly strong on the venter, which they cross with a weak adoral projection. They are relatively closely spaced with an average of 8 ribs/cm on both the adapical and adoral portions of the phragmocone.

Ribs are long and prorsiradiate on the shaft, swinging gently forward on the midflanks and backward again on the outer flanks. In general, ribs are much weaker on the shaft than on the phragmocone. Intercalation and branching occur at two-thirds whorl height. Ribs cross the venter with a strong adoral projection and become more closely spaced on the hook. For example, in AMNH 108314 (fig. 24E–H), the rib density increases from 9 to 11 ribs/cm in passing from the midshaft to the hook.

Umbilicolateral tubercles are absent on the adapical end of the phragmocone, and usually appear on the adoral end, and continue onto the body chamber up to the aperture. They are perched on the umbilical shoulder, which constitutes one of the distinctive features of microconchs. The tubercles are small, radially elongate, and evenly spaced. The distance between consecutive tubercles at midshaft is 4.6 mm in AMNH 108314 (fig. 24E–H) and 4.2 mm in AMNH 72634 (fig. 24M–P). The number of umbilicolateral tubercles on the body chamber ranges from 5 to 8 in our measured sample, e.g., 5 in AMNH 108314 (fig. 24E–H) and 7 in AMNH 72634 (fig. 24M–P).

Ventrolateral tubercles are usually present at the point of exposure. They are initially closely spaced but become more widely spaced toward the adoral end of the phragmocone. In AMNH 72634 (fig. 24M–P), the distance between consecutive tubercles is 4.1 mm at the adapical end of the phragmocone and 6.3 mm at the adoral end of the phragmocone. The tubercles are small and conical. The number of ventrolateral tubercles on the phragmocone ranges from 4 to 8 in our measured sample, e.g., 4 in AMNH 108314 (fig. 24E–H) and 7 in AMNH 72634 (fig. 24M–P). Two ribs loop between ventrolateral tubercles on opposite sides of the venter with as many as three ribs intercalating between them.

Ventrolateral tubercles persist onto the body chamber and become more widely spaced toward the adoral end of the shaft. The distance between ventrolateral tubercles at midshaft is 8.2 mm in AMNH 108314 (fig. 24E–H) and 7.2 mm in AMNH 72634 (fig. 24M–P). The number of ventrolateral tubercles on the body chamber ranges from 7 to 10 in our measured sample. The total number of ventrolateral tubercles on the adult shell ranges from 12 to 19, e.g., a total of 12 tubercles in AMNH 108314 (fig. 24E–H) and 15 tubercles in AMNH 72634 (fig. 24M–P). They are clavate on the midshaft, with steeply sloping adapical sides and more gently sloping adoral sides. In

FIGURE 23. Sutures. **A.** *Hoploscaphites macer*, macroconch, AMNH 71839, holotype, third suture from the last, AMNH loc. 3921, lower *Baculites grandis* Zone, Pierre Shale, Cedar Creek Anticline, east-central Montana. **B.** *Hoploscaphites macer*, macroconch, USNM 713624, third suture from the last, USGS Mesozoic loc. D2118, lower *Baculites grandis* Zone, Pierre Shale, Niobrara County, Wyoming. **C.** *Hoploscaphites macer*, microconch, AMNH 76381, third suture from the last, AMNH loc. 3921, upper *Baculites baculus* or lower B. *grandis* Zone, Pierre Shale, Cedar Creek Anticline, east-central Montana. **D.** *Hoploscaphites criptonodosus* (Riccardi, 1983), macroconch, AMNH 95766, third suture from the last, AMNH loc. 3278, *Baculites baculus* or *B. grandis* Zone, Pierre Shale, Weston County, Wyoming. **E.** *Hoploscaphites criptonodosus* (Riccardi, 1983), macroconch, AMNH 82725, third suture from the last, AMNH loc. 3268, *Baculites baculus* Zone, Pierre Shale, Weston County, Wyoming. **F.** *Hoploscaphites* sp., AMNH 76187, macroconch, last suture of a closely related, undescribed species, AMNH loc. 3921, lower *Baculites baculus* Zone, Pierre Shale, Cedar Creek Anticline, east-central Montana.

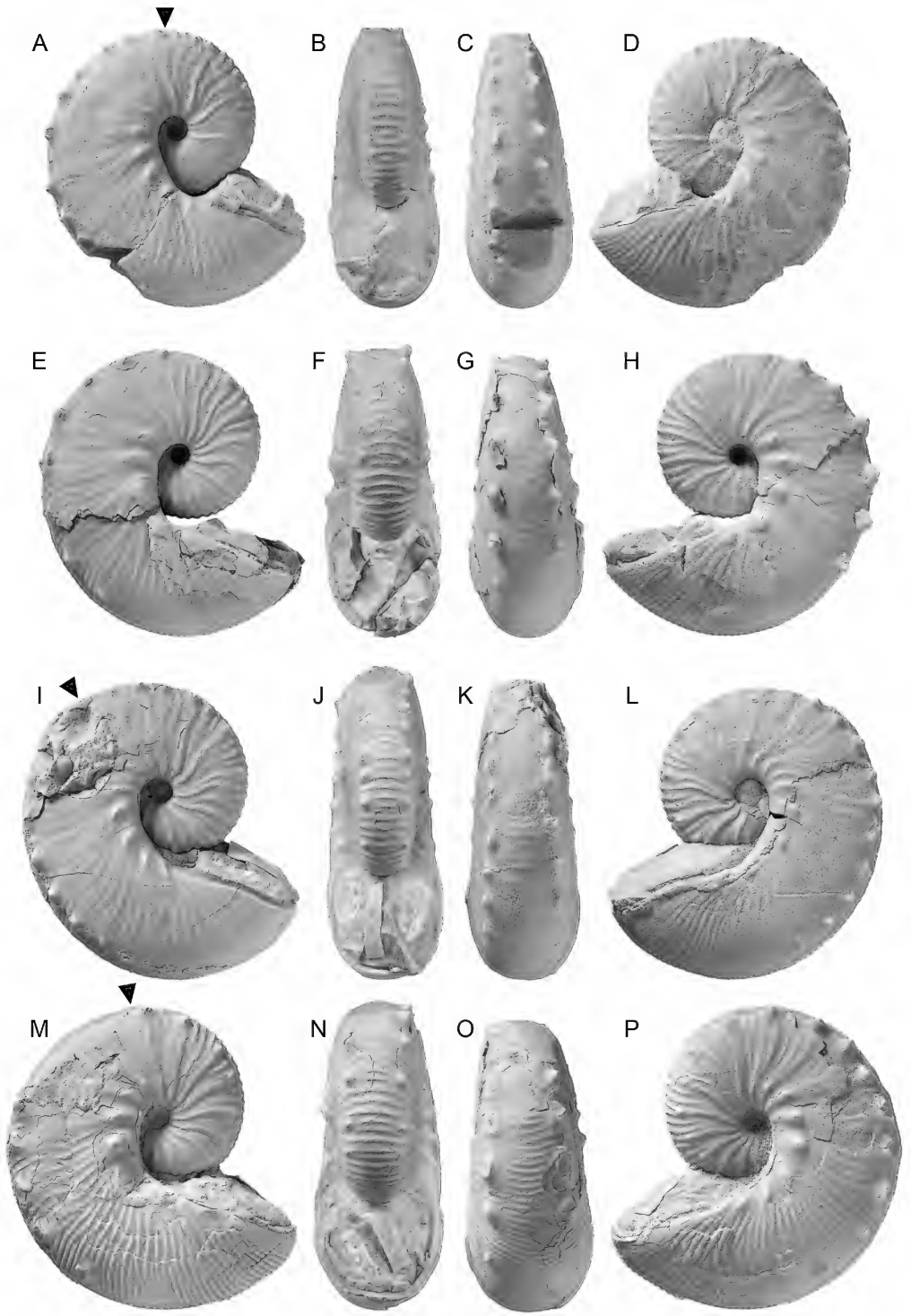
A
B
C
D
E
F
G
H
I
J
K
L
M
N
O
P

larger specimens, as many as four ribs loop between ventrolateral tubercles on opposites sides of the venter, with up to five ribs intercalating between them. In smaller specimens, as many as three ribs loop between tubercles on opposite sides of the venter, with up to five ribs intercalating between them. Tubercles disappear on the adoral end of the shaft.

Two specimens (AMNH 72589 and 74354) in our measured set exhibit a single row of lateral tubercles on the adapical end of the phragmocone (not figured). The tubercles are closely and evenly spaced and nearly the same size as the ventrolateral tubercles. However, the ventrolateral tubercles persist onto the body chamber whereas the lateral tubercles disappear on the adoral end of the phragmocone.

Occurrence: This species occurs in the upper part of the *Baculites baculus* Zone and lower part of the *B. grandis* Zone in the Pierre Shale in Montana, Colorado, and Wyoming. Nearly all the specimens that were collected with precise biostratigraphic information (down to zone) are from the lower part the *B. grandis* Zone.

Discussion: Among older species from the Western Interior of North America, small specimens of *Hoploscaphites macer* most closely resemble small specimens of *H. brevis* from the *Baculites compressus–B. cuneatus* zones. However, *H. macer* differs from *H. brevis* in its more tightly coiled shell, with more inflated flanks, its less flexuous ribs, and its smaller, more numerous, and more closely spaced ventrolateral tubercles. Among younger species from the Western Interior, *H. macer* most closely resembles *H. criptonodosus* and *H. sargklofak*. It differs from *H. criptonodosus* in its finer ribbing and, in general, the absence of lateral tubercles on the exposed phragmocone. However, as noted above, in some specimens of *H. macer* such as USNM 713623 from the *B. grandis* Zone, a few lateral tubercles appear on the adapical end of the exposed phragmocone. It differs from *H. sargklofak* in its more inflated shell, with more broadly rounded flanks, and its fewer and more widely spaced ventrolateral tubercles. However, in some specimens of *H. macer*, such as BHI 4346 (fig. 14) from the *B. grandis* Zone, the spacing of the ventrolateral tubercles begins to approach that of *H. sargklofak*.

Outside the Western Interior, *Hoploscaphites macer* most closely resembles *H. youngi* Larson, 2016, from the upper Campanian Coon Creek Member of the Ripley Formation, McNairy County, Tennessee (Larson, 2016: fig. 11F–I), and the Nacatoch Sand, Red River County, Texas (Stephenson, 1941: pl. 90, figs. 7, 8). However, it differs from this species in its more inflated whorl section with more broadly rounded flanks. Outside North America, *H. macer* most closely resembles *H. constrictus* from northern Europe (see Kennedy, 1986: pl. 13, figs. 1–3, 16–24; pl. 14, figs. 1–38; pl. 15, figs. 1–31; text-figs. 9, 11; Machalski, 2005: figs. 5–7, 10, 12), which ranges from the base of the Maastrichtian to the Cretaceous-Paleogene boundary and possibly into the lower Paleocene (Machalski and Heinberg, 2005). However, *H. macer* differs from *H. constrictus* in having more numerous ventrolateral tubercles on the exposed phragmocone. In addition, the distance between ventrolateral tubercles on opposite sides of the venter at midshaft is greater in *H. macer* than in *H. constrictus*.

FIGURE 24. *Hoploscaphites macer*, microconchs. A-D. YPM 35657, YPM loc. A4745, *Baculites baculus* or *B. grandis* Zone, Pierre Shale, Niobrara County, Wyoming. **A,** Right lateral; **B,** apertural; **C,** ventral; **D,** left lateral. **E–H.** AMNH 108314, paratype, AMNH loc. 3244, lower *B. grandis* Zone, Pierre Shale, Dawson County, Montana. **E,** Right lateral; **F,** apertural; **G,** ventral; **H,** left lateral. **I–L.** AMNH 76383, AMNH loc. 3921, upper *Baculites baculus* or lower *B. grandis* Zone, Pierre Shale, Cedar Creek Anticline, east-central Montana. **I,** Right lateral; **J,** apertural; **K,** ventral; **L,** left lateral. **M–P.** AMNH 72634, paratype, AMNH loc. 3921, upper *Baculites baculus* or lower *B. grandis* Zone, Pierre Shale, Cedar Creek Anticline, east-central Montana. **M,** Right lateral; **N,** apertural; **O,** ventral; **P,** left lateral. Arrows indicate the base of the body chamber. Specimens ×1.

Hoploscaphites criptonodosus (Riccardi, 1983)

Figures 8C, D, 9, 11A, B, 23D, E, 26–38

1983. *Jeletzkytes criptonodosus*. Riccardi, p. 28, pl. 6, fig. 10; pl. 7, figs. 1, 2; pl. 8, figs. 7–9; text-figs. 25–27.

1983. *Jeletzkytes* cf. *criptonodosus*. Riccardi, p. 30, pl. 11, figs. 1–11, 15–21; text-figs. 28, 29b, 30, 31.

non 1983. *Jeletzkytes* cf. *criptonodosus*. Riccardi, p. 30, pl. 11, figs. 12–14; text-fig. 29a (= *Hoploscaphites sargklofak*).

1994. *Jeletzkyites* (*Karlwaageites*) *criptonodosus* Riccardi. Cooper, p. 181.

1995. *Jeletzkytes criptonodosus* Riccardi, 1983. Cobban and Kennedy, p. 31, figs. 6.4, 6.5, 22.5–22.12, 23.1–23.5.

1997. *Jeletzkytes criptonodosus* Riccardi, 1983. Larson et al., p. 81, fig. on bottom; p. 82. top (= Riccardi, 1983, pl. 6, fig. 10, pl. 7, fig. 1).

2000. *Jeletzkytes criptonodosus* Riccardi, 1983. Kennedy et al., p. 26, fig. 12A, B.

2016. *Jeletzkytes criptonodosus* Riccardi, 1983. Klein, p. 138.

Emended Diagnosis: Macroconchs oval in lateral view; robust, with compressed subquadrate whorl section of shaft consisting of broadly rounded flanks and nearly flat venter; small umbilicus commonly with umbilical bulge; apertural angle averaging approximately 60°; ribbing coarse on the adapical end of the phragmocone, becoming finer on the body chamber; moderately closely spaced, medium sized ventrolateral tubercles; small umbilicolateral tubercles on phragmocone and body chamber; one or two rows of lateral tubercles on the outer flanks on the adapical end of the phragmocone; microconchs oval in lateral view; whorl section of shaft subquadrate with broadly rounded flanks converging toward ventrolateral shoulder; large umbilicus exposing earlier whorls; moderately closely spaced, medium sized ventrolateral tubercles; relatively prominent umbilicolateral tubercles on body chamber; one or two rows of lateral tubercles on the adapical end of the phragmocone; suture deeply incised, with a broad, asymmetrically bifid first lateral saddle and a narrow, symmetrically to asymmetrically bifid first lateral lobe (slightly modified from Riccardi, 1983).

Types: The holotype and paratype are GSC 67104 and 67105, respectively, illustrated in Riccardi (1983: pl. 6, fig. 10; pl. 7, figs. 1, 2; pl. 8, figs. 7–9). They are both from GSC loc. 10374 from the *Baculites baculus* Zone of the Belanger Member of the Bearpaw Shale, on the north side of Frenchman River, sec. 14, T. 6, R. 25, W3rd Mer., Saskatchewan, Canada.

Material: The collection consists of approximately 90 specimens of which 61 comprise the measured set (tables 3, 4) representing 43 macroconchs and 18 microconchs. The specimens in our collection are from the upper part of the *Baculites baculus* and *B. grandis* zones of the Pierre Shale in Wyoming, Colorado, Montana, and possibly South Dakota, and the Bearpaw Shale in Montana.

Macroconch Description: In the measured sample, LMAX averages 79.2 mm and ranges from 60.9 to 102.4 mm (table 3). The ratio of the size of the largest specimen to that of the smallest is 1.68. The specimens form a broad size distribution, with a primary peak at 65–70 mm and a secondary peak at 75–80 mm (fig. 26). Adults are stout with an oval outline in side view. $LMAX/H_S$ averages 2.09 and ranges from 1.86 to 2.32 (2.04 in the holotype). USNM 463215 (fig. 33) is an example of a specimen with an oval outline ($LMAX/H_S = 2.27$) and AMNH 108445 (fig. 30) is an example of a specimen with a more rounded outline ($LMAX/H_S = 1.98$).

The umbilicus is small and deep. The umbilical diameter averages 5.0 mm and ranges from 3.7 to 7.6 mm. UD/LMAX averages 0.06 and ranges from 0.05 to 0.10. The umbilicus is unusually large (7.6 mm) in AMNH 108456 (fig. 31). In lateral view, the umbilical shoulder is straight and usually exhibits a pronounced umbilical bulge. Most specimens are tightly coiled with little or no gap between the phragmocone and hook. $LMAX/H_{P2}$ averages 2.83 and ranges from 2.59 to 3.04 (2.79 in the holotype). AMNH 95771 (fig. 32A–C) is an

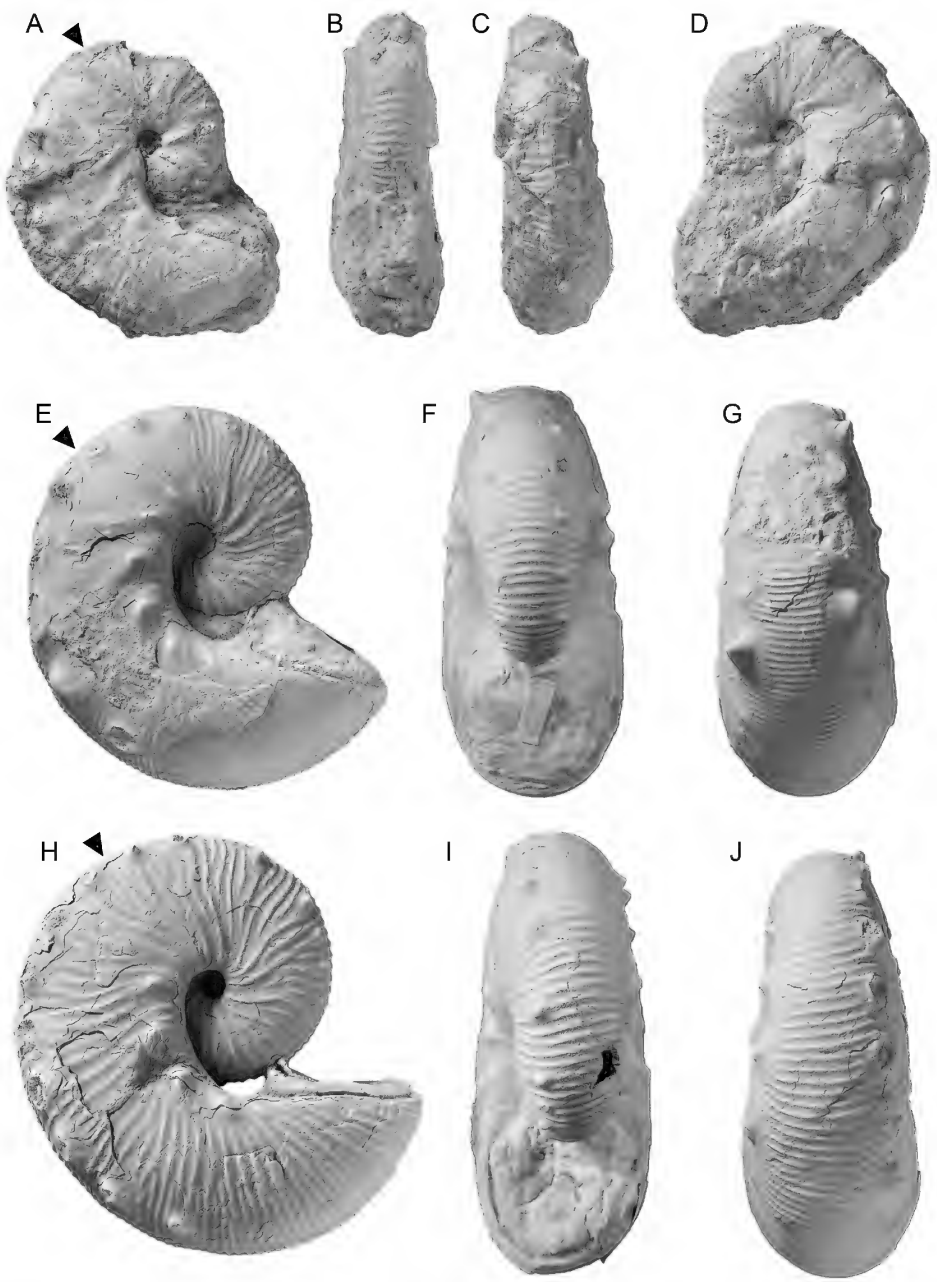

FIGURE 25. *Hoploscaphites macer*, microconchs. **A–D.** DMNH EPI 22907, DMNH loc. 1405, *Baculites baculus* or *B. grandis* Zone, Pierre Shale, Jefferson County, Colorado. **A,** Right lateral; **B,** apertural; **C,** ventral; **D,** left lateral. **E–G.** AMNH 72624, AMNH loc. 3921, upper *Baculites baculus* or lower *B. grandis* Zone, Pierre Shale, Cedar Creek Anticline, east-central Montana. **E,** Right lateral; **F,** apertural; **G,** ventral. **H–J.** USNM 713625, ?AMNH loc. 3921, upper *Baculites baculus* or lower *B. grandis* Zone, Pierre Shale, Cedar Creek Anticline, east-central Montana. **H,** Right lateral; **I,** apertural; **J,** ventral. Arrows indicate the base of the body chamber. Specimens ×1.

TABLE 3

***Hoploscaphites criptonodosus* (Riccardi, 1983), macroconchs**

See figure 12 for description of measurements. All measurements are in mm, except for apertural angle. * = close to *H. macer*; b = *B. baculus* Zone; g= *B. grandis* Zone; b/g = *Baculites baculus* or *B. grandis* Zone; ub= upper *B. baculus* Zone; lg = lower *B. grandis* Zone; ug = upper *B. grandis* Zone; ub/lg= upper *B. baculus* or lower *B. grandis* Zone; C = illustrated in Cobban and Kennedy (1995); [1] = suture; [2] = scanned; [3] = locality details appear in the appendix.

Specimen no.	Photo	Sample no.	Loc.	Zone	LMAX	LMAX/ H_{P2}	LMAX/ H_S	AA	UD	UD/ LMAX	W_{P1}/ H_{P1}	W_{P2}/ H_{P2}	W_S/ H_S	W_H/ H_H	V_S/H_S
AMNH 71830		271 (JG 233)	3921	ub/lg	78.6	2.97	2.14	76	5.4	0.07	1.12	1.06	–	1.22	–
AMNH 71834		(JG606)	3921	lg	84.6	2.72	2.03	57	5.2	0.06	1.08	0.96	0.92	1.18	0.46
AMNH 71859		268 (JG 114)	3921	ub/lg	88.6	2.69	2.00	59	5.5	0.06	1.04	0.98	0.89	1.07	0.41
AMNH 74286		1058	3732	g	62.5	2.80	2.00	–	5.2	0.08	0.93	0.89	0.74	0.93	0.33
AMNH 77029		791	3732	g	79.8	2.75	2.06	58.5	4.6	0.06	0.94	0.90	0.84	1.20	0.32
AMNH 77031		864	3730	g	68.1	2.69	1.98	55	4.3	0.06	–	0.87	0.85	–	0.39
AMNH 82725[1]		1240	3278	b	69.8	2.87	2.11	–	4.4	0.06	1.12	0.96	0.95	1.16	0.37
AMNH 95766[1]		1420	3278	b/g	69.5	2.76	2.01	61	4.2	0.06	1.02	0.85	0.82	1.08	0.34
AMNH 95771	x	1337	3269	b/g	69.1	2.76	2.06	52	4.0	0.06	1.09	0.98	0.93	1.23	0.46
AMNH 95773*	x	1293	3921	ub/lg	77.9	2.78	2.02	61.5	3.7	0.05	1.09	0.90	0.87	1.20	0.39
AMNH 108309		674	3727	g	98.2	–	2.07	75	4.9	0.05	–	–	0.98	1.23	0.44
AMNH 108310		618	3921	ub/lg	78.2	2.72	2.05	60.5	4.2	0.05	1.18	0.98	0.89	1.24	0.51
AMNH 108311		1251	3264	lg	71.7	2.89	2.19	55	4.9	0.07	0.96	0.84	0.90	1.01	0.41
AMNH 108312	x	1447	3265	b/g	85.9	2.88	2.03	55.5	5.0	0.06	1.08	1.02	0.97	1.33	0.43
AMNH 108313[2]	x	1300	3269	g	78.8	2.84	2.11	68	4.6	0.06	1.03	0.90	0.87	1.10	0.38
AMNH 108424		695	3730	b	87.2	2.78	2.13	62	4.4	0.05	–	0.94	–	–	–
AMNH 108425		1306	3268	b/g	73.2	2.85	2.18	63	4.0	0.05	1.22	1.00	0.95	1.23	0.46
AMNH 108426*		1005	3732	b	75.6	2.71	1.86	60.5	4.9	0.06	0.91	0.85	–	1.21	0.31
AMNH 108445	x	374	3730	b	86.5	3.00	1.98	62	5.6	0.06	1.15	1.06	0.89	1.25	0.48
AMNH 108456	x	1231	3278	g	83.3	2.63	2.14	26	7.6	0.09	1.19	1.10	1.02	1.04	0.43
AMNH 161810		1224	3278	b/g	76.0	2.88	2.22	–	6.2	0.08	0.92	0.88	0.87	1.03	0.34

Specimen no.	Photo	Sample no.	Loc.	Zone	LMAX	LMAX/ H_{P2}	LMAX/ H_S	AA	UD	UD/ LMAX	W_{P1}/ H_{P1}	W_{P2}/ H_{P2}	W_S/ H_S	W_H/ H_H	V_S/H_S
AMNH 161814		–	3278	b	88.7	2.87	2.02	–	5.9	0.07	1.15	1.10	0.95	1.12	0.34
BHI 4094		397	3278	g	71.6	2.84	2.24	40	5.4	0.07	1.23	1.05	–	–	–
BHI 4131*		251	3921	ub/lg	76.9	2.91	2.06	61.5	3.9	0.05	1.05	0.94	0.88	1.18	0.52
BHI 4300	x	274	3278	g	68.9	2.97	2.03	60	4.2	0.06	1.07	1.11	0.94	1.17	0.36
BHI 4309		256	3921	ub/lg	83.8	3.04	2.08	68	5.6	0.07	0.98	1.04	0.74	1.02	0.44
FM 10689	x		AK	?	69.9	2.86	2.04	66	–	–	–	–	0.83	1.01	0.49
GSC 67104 (10374) holotype			SK[3]	b	85.5	2.79	2.04	47.5	4.3	0.05	1.06	0.94	0.88	1.16	0.44
GSC 67105 paratype		406	SK[3]	b	85.4	–	1.89	51	5.6	0.06	–	–	0.85	1.02	0.40
MSNS-IP 7881.3*	x		MS	g?	66.7	–	2.08	78	–	–	–	–	0.84	–	–
USNM 463214	C	622	D771	g	94.0	–	2.24	58	4.7	0.05	–	–	0.98	1.04	0.50
USNM 463215	x	158	12700	g	91.5	2.91	2.27	66	6.1	0.07	1.04	0.97	1.07	1.15	0.73
USNM 713614			D1018	b	81.4	2.82	2.17	59	4.3	0.05	1.18	0.92	0.90	–	0.45
USNM 713615		854	D1986	ug	68.2	2.95	2.19	68	5.0	0.07	1.22	1.00	0.91	1.18	0.43
USNM 713616*		161	23628	?	80.2	2.80	2.03	–	3.7	0.05	1.16	0.94	0.84	1.12	0.42
USNM 713617	x	153	12757	g	92.5	2.80	2.20	50	6.5	0.07	1.03	0.87	1.00	–	0.44
USNM 713618		152	12757	g	102.4	–	2.32	50.5	6.6	0.06	–	–	0.96	1.09	0.44
USNM 713619		–	12757	g	60.9	2.87	2.12	64	5.8	0.10	1.07	0.98	0.90	1.12	0.41
USNM 713620		151	10764	g	102.2	2.72	2.02	48	6.5	0.06	1.12	1.02	0.91	1.13	0.44
USNM 713621		149	D1984	ub	84.6	2.76	1.89	56	5.2	0.06	1.17	0.96	0.89	1.26	0.34
USNM 713622		853	D1985	lg	82.2	2.59	2.22	59	–	–	–	0.95	0.96	1.30	0.42
YPM 35602		532	A4768	lg	67.5	2.91	2.15	57.5	3.9	0.06	1.09	1.00	0.90	1.05	0.39
YPM 35604		1062	A4768	l g	–	–	–	56	–	–	–	–	0.96	1.15	0.41
Average					79.2	2.83	2.09	58.8	5.0	0.06	1.08	0.96	0.90	1.14	0.43
Standard Deviation					10.7	0.13	0.10	9.2	0.9	0.01	0.09	0.08	0.07	0.09	0.07

TABLE 4

***Hoploscaphites criptonodosus* (Riccardi, 1983), microconchs**

See Figure 12 for description of measurements. All measurements are in mm. b = *B. baculus* Zone; g= *B. grandis* Zone; b/g = *Baculites baculus* or *B. grandis* Zone; ub= upper *B. baculus* Zone; lg = lower *B. grandis* Zone; ub/lg= upper *B. baculus* or lower *B. grandis* Zone; [1] = found in gravel pit.

Specimen no.	Photo	Sample no.	Loc.	Zone	LMAX	LMAX/ H_{P2}	LMAX/H_S	UD	UD/ LMAX	W_{P1}/ H_{P1}	W_{P2}/ H_{P2}	W_S/ H_S	W_H/ H_H	V_S/H_S
AMNH 74346	x	1045	3921	ub/lg	46.4	2.99	2.73	4.8	0.10	0.89	0.99	–	–	0.51
AMNH 74355	x	580	3921	ub/lg	47.5	3.14	2.32	4.0	0.08	1.04	1.00	0.94	1.09	0.43
AMNH 74357	x	1041	3921	ub/lg	50.2	3.01	2.49	4.8	0.10	0.90	1.00	0.91	1.02	0.39
AMNH 76214		996 (JG176)	3921	ub/lg	53.5	3.07	2.62	4.6	0.09	0.98	0.95	0.95	1.10	0.43
AMNH 76224		998 (JG261)	3921	ub/lg	48.7	3.01	2.53	4.4	0.09	0.98	0.99	0.93	1.08	0.44
AMNH 108315		–	3728	g	56.2	3.04	2.33	4.8	0.08	1.04	1.05	1.01	–	0.39
AMNH 108316	x	1229	3278	b/g	46.3	2.81	2.47	4.7	0.10	0.94	0.87	0.92	1.02	0.41
AMNH 108317		–	3487	g	50.9	3.33	2.67	5.1	0.10	0.94	0.94	0.93	0.93	0.35
AMNH 108318		–	3487	g	56.2	3.27	–	6.5	0.12	0.91	0.84	–	0.96	–
AMNH 108327			3921	ub/lg	55.5	2.97	2.48	6.1	0.11	0.97	0.89	–	–	–
BHI 4296		576	3278	b/g	52.0	2.96	2.53	5.7	0.11	0.97	0.87	0.91	1.10	0.39
BHI 4345	x	700	Fall River Co., SD[1]	g	50.0	3.23	2.45	6.1	0.12	0.99	0.97	0.87	0.94	0.42
USNM 713626	x	–	D12208	b?	68.2	3.09	2.60	5.1	0.08	0.91	0.93	0.77	0.85	0.49
USNM 713635	x	851	D2118	lg	51.6	3.39	2.44	6.1	0.12	0.90	0.94	0.83	1.02	0.42
USNM 713636		–	D1033	g	43.6	3.05	2.39	5.0	0.11	1.00	1.00	0.93	0.99	0.43
USNM 713637		247	6528	g	49.4	3.10	2.54	5.2	0.10	–	0.89	0.84	0.92	0.39
USNM 713638		–	24312	b?	45.0	3.14	2.51	6.4	0.14	1.09	0.99	0.95	1.09	0.35
YPM 35649		571	A4768	lg	43.2	3.11	2.56	4.8	0.11	0.82	0.82	0.83	0.93	0.46
Average					51.0	3.10	2.52	5.3	0.10	0.96	0.95	0.92	1.01	0.42
Standard Deviation					5.68	0.13	0.12	0.7	0.02	0.07	0.07	0.08	0.08	0.05

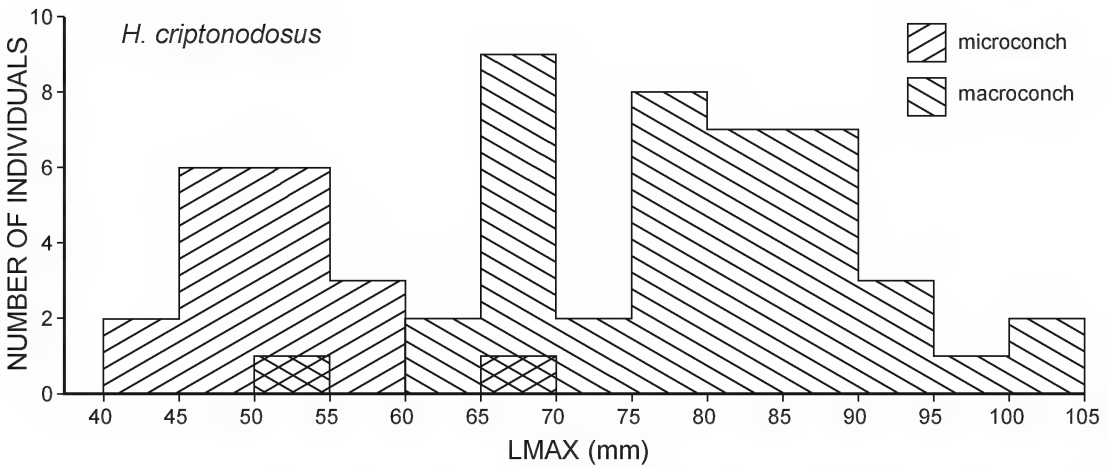

FIGURE 26. Size frequency histogram of *Hoploscaphites criptonodosus* (Riccardi, 1983) based on the sample in tables 3 and 4.

example of a tightly coiled specimen ($LMAX/H_{P2}$ = 2.76) and USNM 463215 (fig. 33) is an example of a more loosely coiled specimen ($LMAX/H_{P2}$ = 2.91). The exposed phragmocone occupies approximately one-half whorl and generally terminates just below the line of maximum length. The body chamber consists of a short shaft and recurved hook totaling slightly more than one-half whorl. The apertural lip is flexuous with a dorsal projection (fig. 8C, D). The apertural angle averages 58.8° and ranges from 26.0 to 78.0° (47.5° in the holotype). AMNH 108456 (fig. 31) exhibits a very low apertural angle (26.0°) and is associated with a very large umbilicus (7.6 mm diameter).

The whorl section of the phragmocone near the point of exposure is depressed subquadrate with maximum whorl width at one-third whorl height. W_{P1}/H_{P1} averages 1.08 and ranges from 0.91 to 1.23 (1.06 in the holotype). The umbilical wall is steep and subvertical and the umbilical shoulder is sharply rounded. The flanks are broadly rounded and converge toward the ventrolateral shoulder starting at two-thirds whorl height. The ventrolateral shoulder is sharply rounded and the venter is broadly rounded. The whorl section of the phragmocone at the line of maximum length is slightly more compressed than that at the point of exposure, reflecting a steep increase in whorl height. W_{P2}/H_{P2} averages 0.96 and ranges from 0.84 to 1.11 (0.94 in the holotype). The flanks are very broadly rounded and the venter is nearly flat.

The whorl width increases as the shell passes from the phragmocone into the body chamber and reaches its maximum value on the adoral part of the shaft but does not produce a conspicuous bulge in this area. Whorl height increases much more markedly during this transition and reaches its maximum value at midshaft. Thereafter, it diminishes to the point of recurvature and remains nearly the same up to the aperture. These changes in whorl width and height result in a slightly more compressed whorl section at midshaft than at the adoral end of the phragmocone. W_S/H_S averages 0.90 and ranges from 0.74 to 1.07 (0.88 in the holotype). The whorl section is subquadrate with maximum whorl width at one-quarter whorl height. The umbilical wall is steep and subvertical and the umbilical shoulder is sharply rounded. The whorls are very high and broadly rounded, and gently converge toward the venter. The ventrolateral shoulder is sharply rounded and the venter is broadly rounded. V_S/H_S averages 0.43 and ranges from 0.31 to 0.73 (0.44 in the holotype). In USNM 463215 (fig. 33), the value of V_S/H_S is very high (0.73) because the ventrolateral tubercles occur slightly

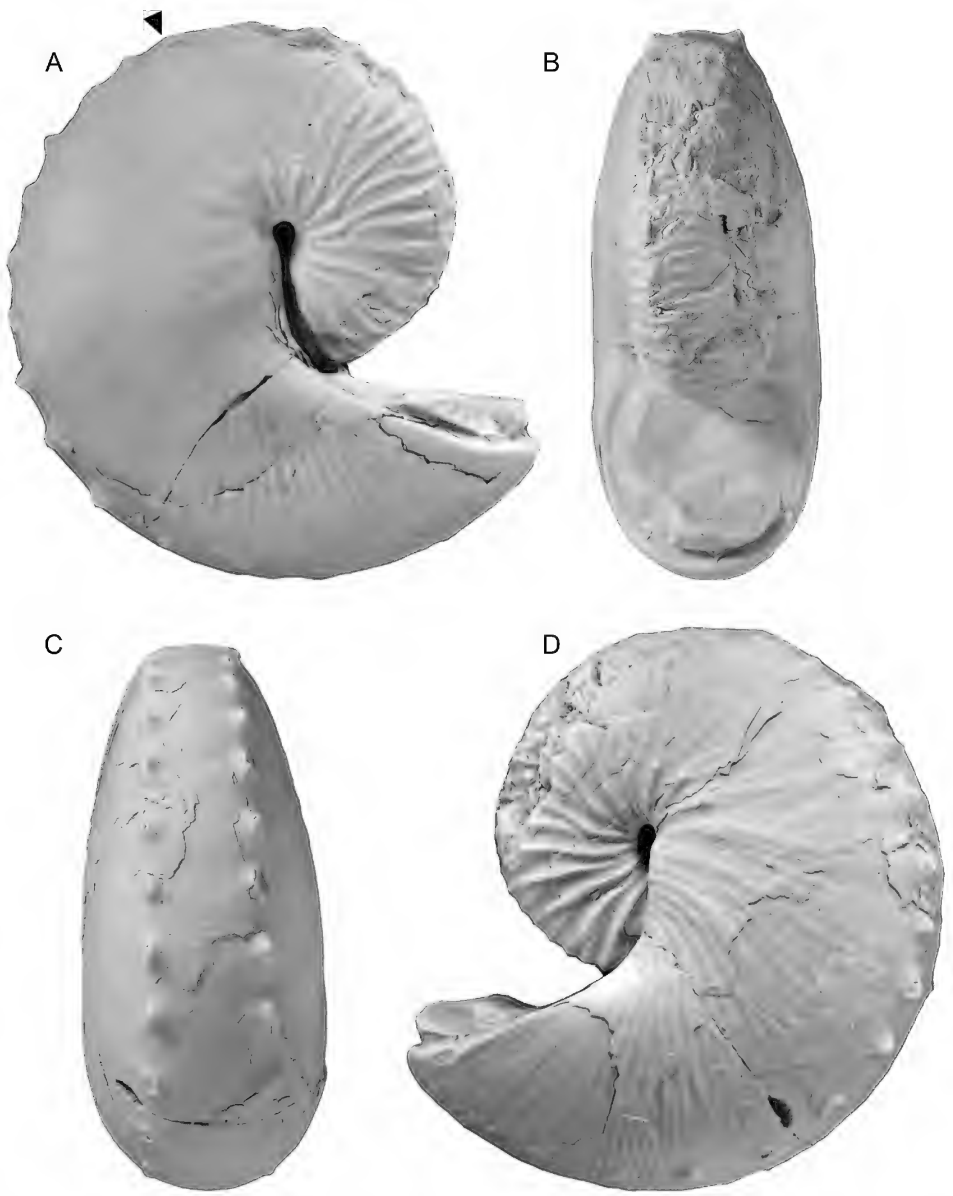

FIGURE 27. *Hoploscaphites criptonodosus* (Riccardi, 1983), macroconch. **A–D.** AMNH 95773, AMNH loc. 3921, upper *Baculites baculus* or lower *B. grandis* Zone, Pierre Shale, Cedar Creek Anticline, Montana. **A,** Right lateral; **B,** apertural; **C,** ventral; **D,** left lateral. Arrow indicates the base of the body chamber. Specimens ×1.

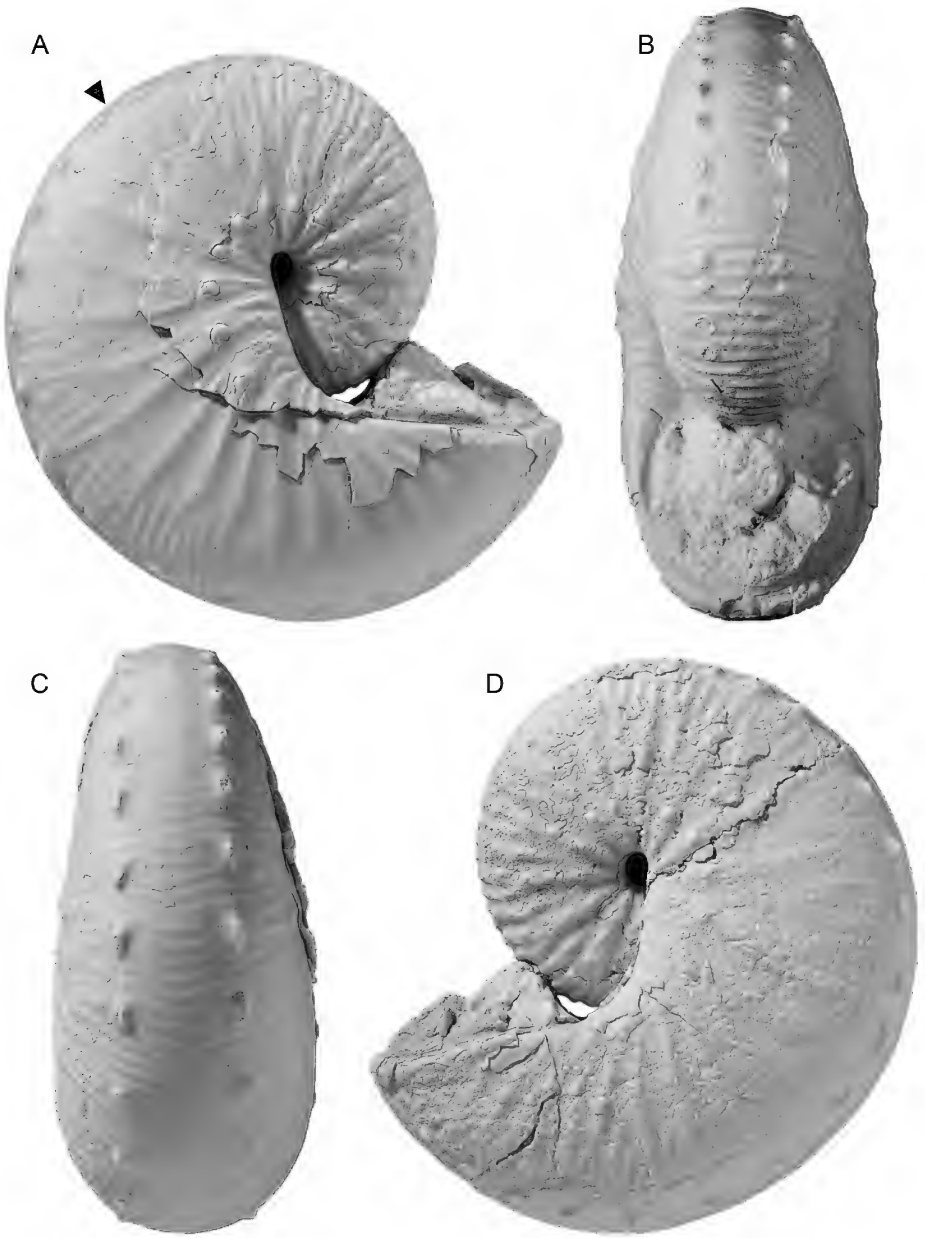

FIGURE 28. *Hoploscaphites criptonodosus* (Riccardi, 1983), macroconch. **A–D.** AMNH 108313, AMNH loc. 3269, *Baculites grandis* Zone, Pierre Shale, Weston County, Wyoming. **A,** Right lateral; **B,** apertural; **C,** ventral; **D,** left lateral. Arrow indicates the base of the body chamber. Specimens ×1.

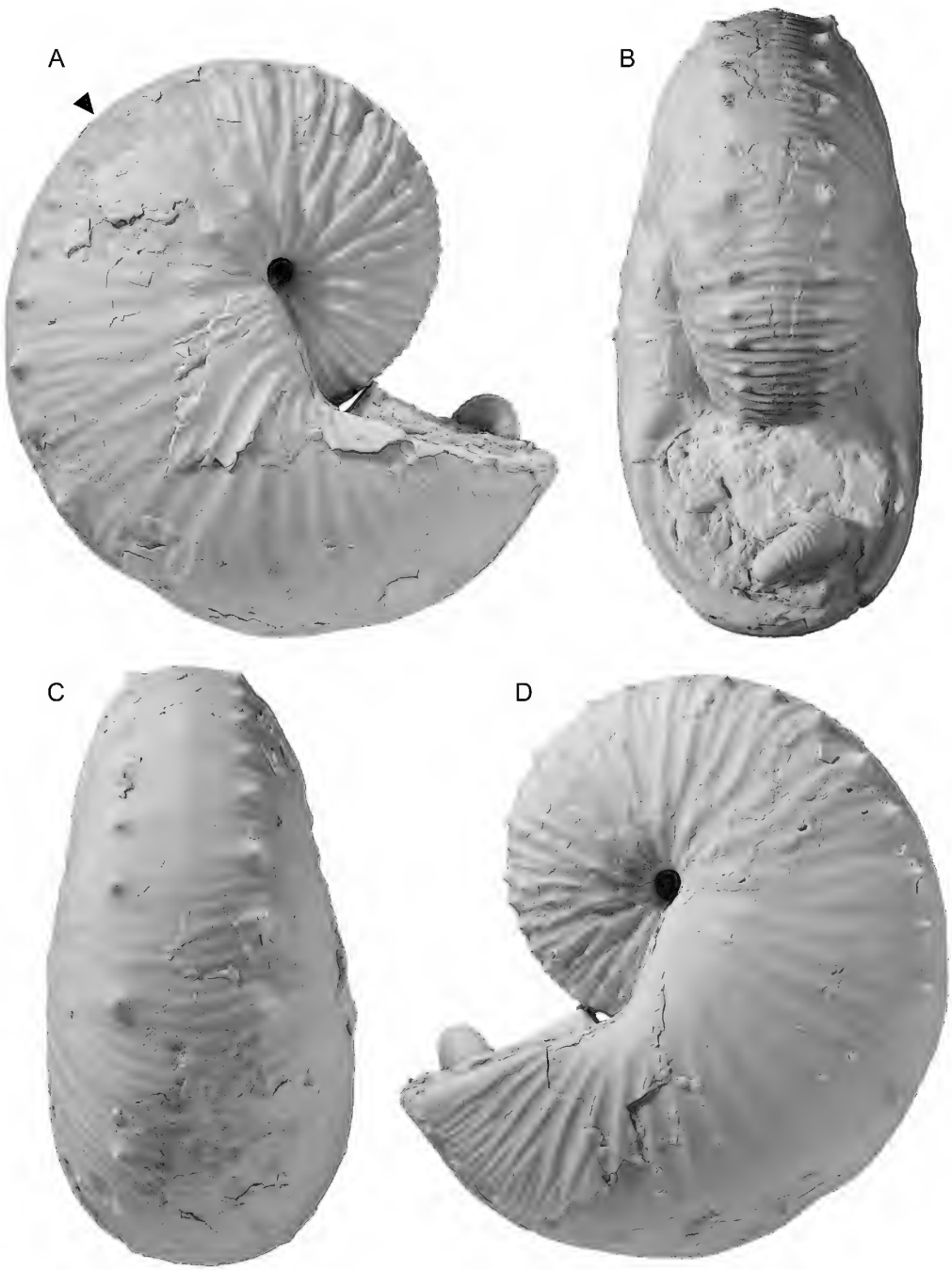

FIGURE 29. *Hoploscaphites criptonodosus* (Riccardi, 1983), macroconch. **A-D.** AMNH 108312, AMNH loc. 3265, *Baculites baculus–B. grandis* zones, Pierre Shale, Weston County, Wyoming. **A,** Right lateral; **B,** apertural; **C,** ventral; **D,** left lateral. Arrow indicates the base of the body chamber. Specimens ×1.

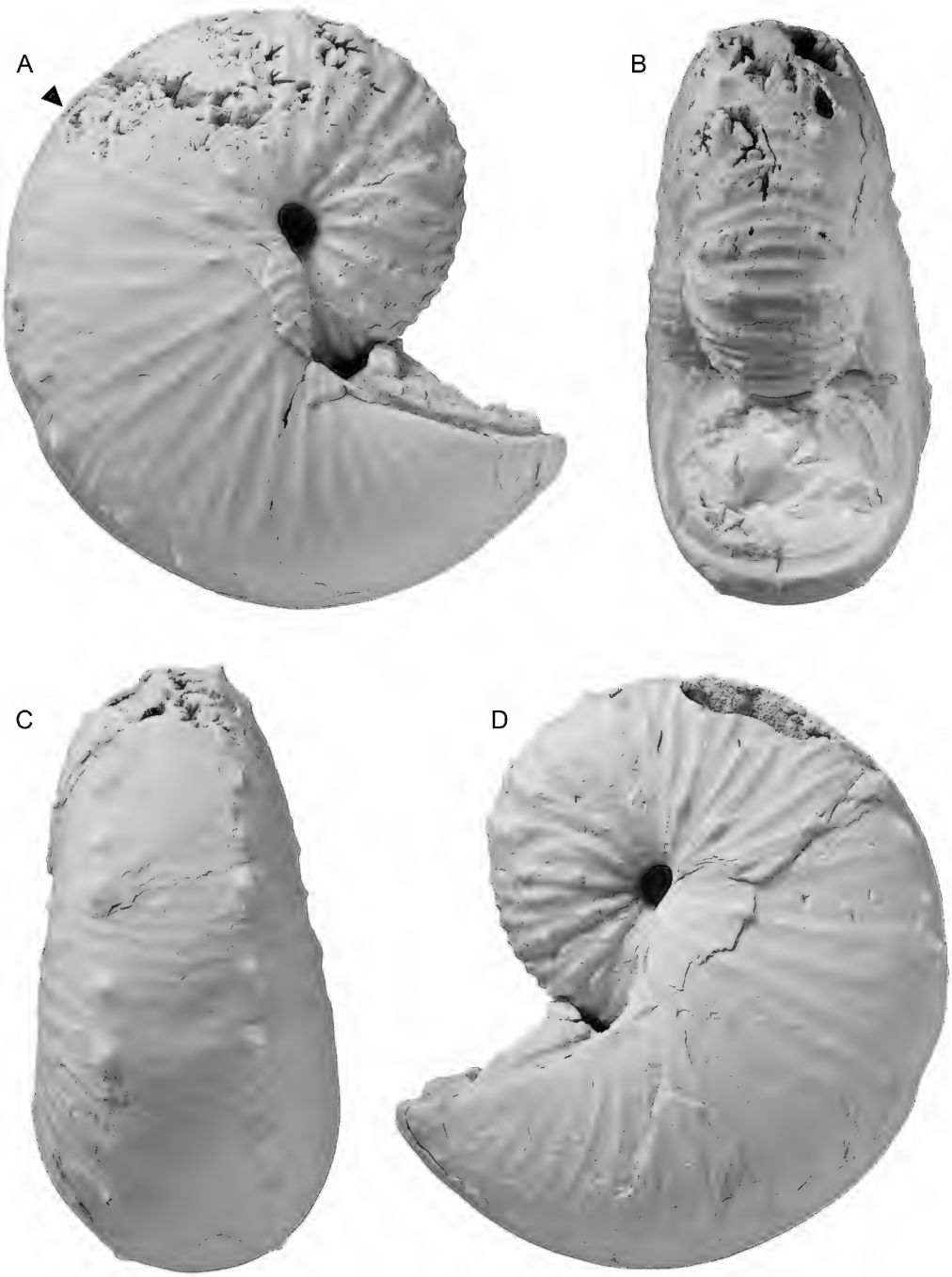

FIGURE 30. *Hoploscaphites criptonodosus* (Riccardi, 1983), macroconch. **A–D.** AMNH 108445, AMNH loc. 3730, *Baculites baculus* Zone, Pierre Shale, Niobrara County, Wyoming. **A,** Right lateral; **B,** apertural; **C,** ventral; **D,** left lateral. Arrow indicates the base of the body chamber. Specimens ×1.

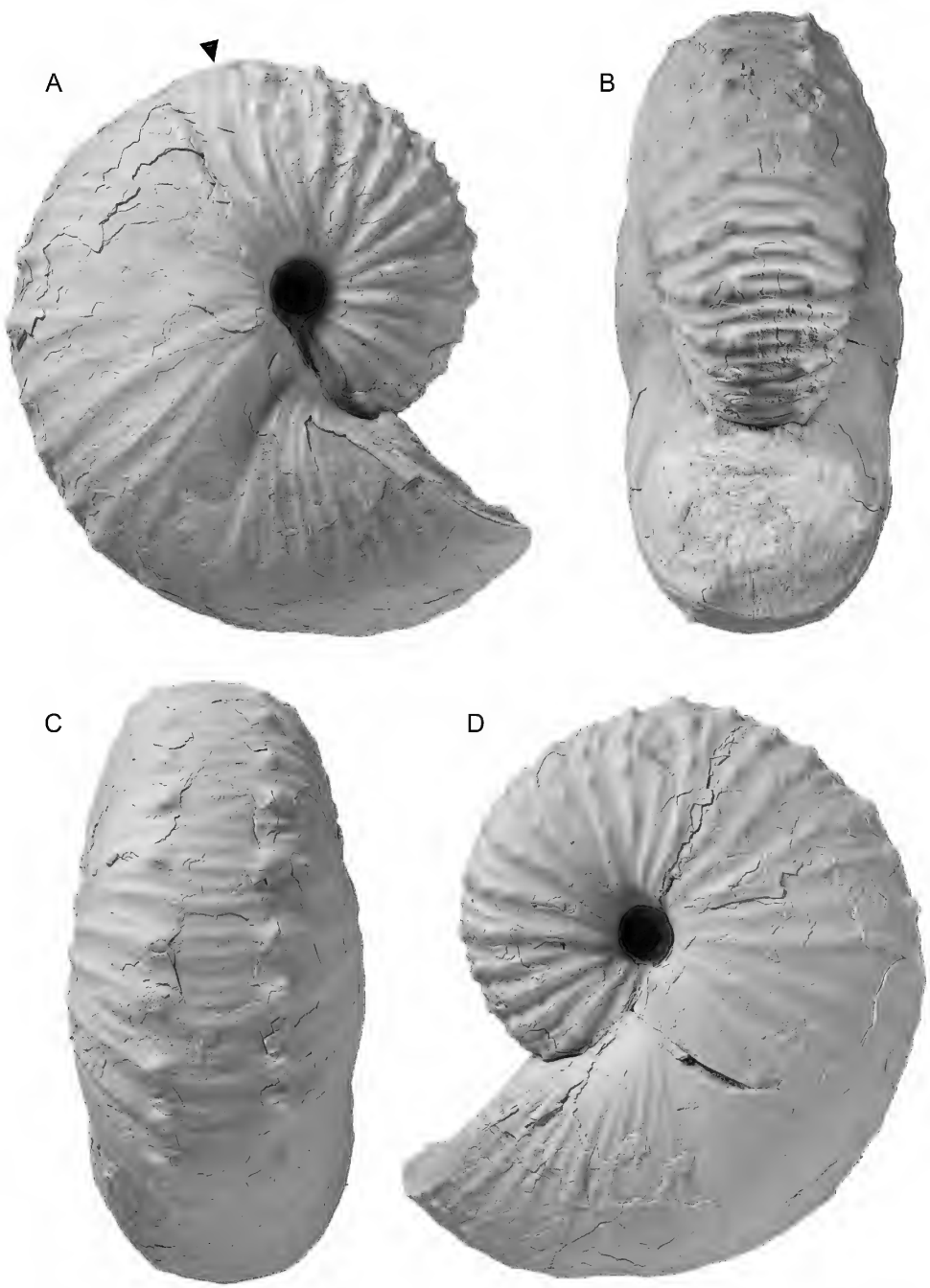

FIGURE 31. *Hoploscaphites criptonodosus* (Riccardi, 1983), macroconch. **A–D.** AMNH 108456, AMNH loc. 3269, *Baculites grandis* Zone, Pierre Shale, Niobrara County, Wyoming. **A,** Right lateral; **B,** apertural; **C,** ventral; **D,** left lateral. Arrow indicates the base of the body chamber. Specimens ×1.

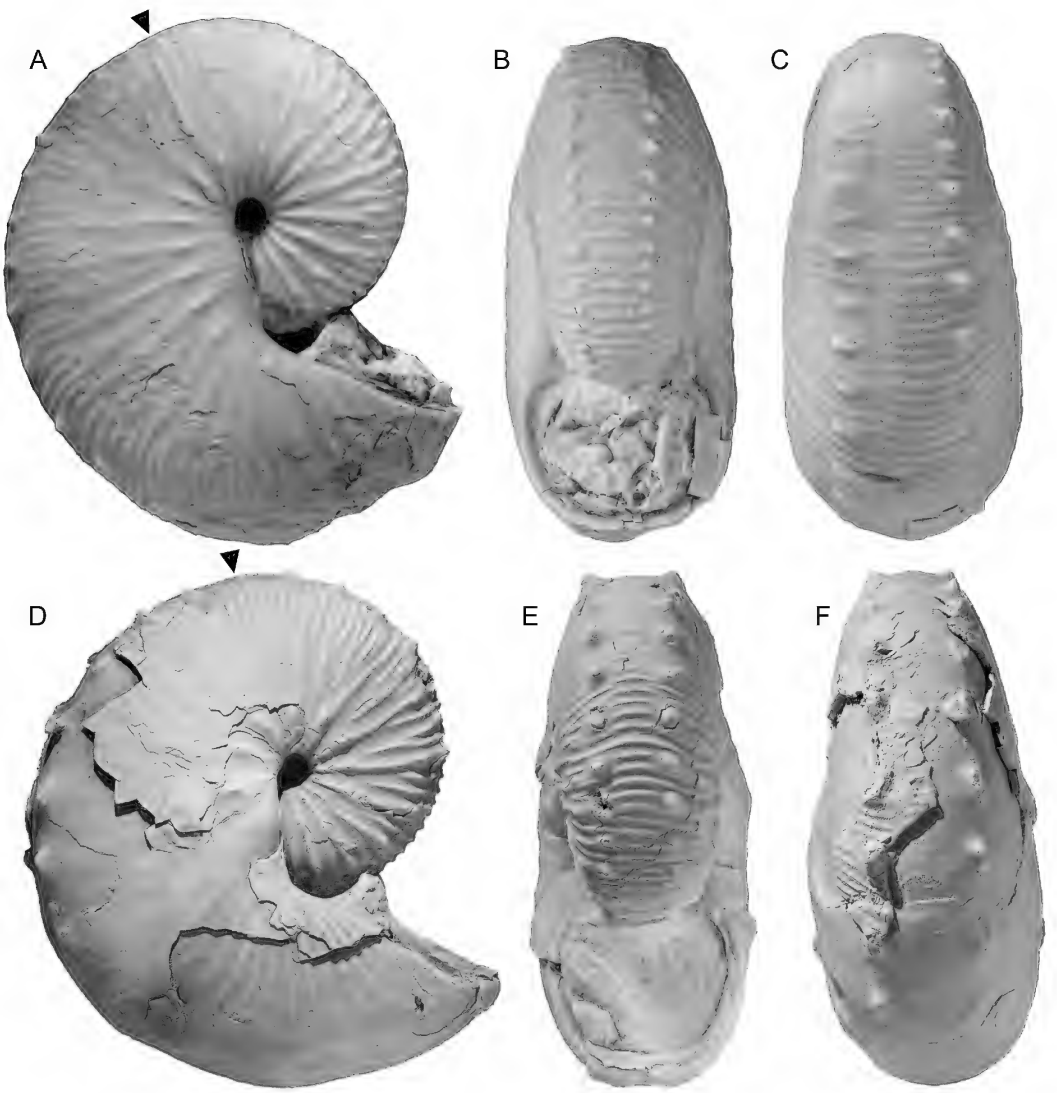

FIGURE 32. *Hoploscaphites criptonodosus* (Riccardi, 1983), macroconchs. **A–C.** AMNH 95771, AMNH loc. 3278, *Baculites baculus–B. grandis* zones, Pierre Shale, Weston County, Wyoming. **A,** Right lateral; **B,** apertural; **C,** ventral. **D–F.** BHI 4300, AMNH loc. 3278, *Baculites grandis* Zone, Pierre Shale, Weston County, Wyoming. **D,** Right lateral; **E,** apertural; **F,** ventral. Arrows indicate the base of the body chamber. Specimens ×1.

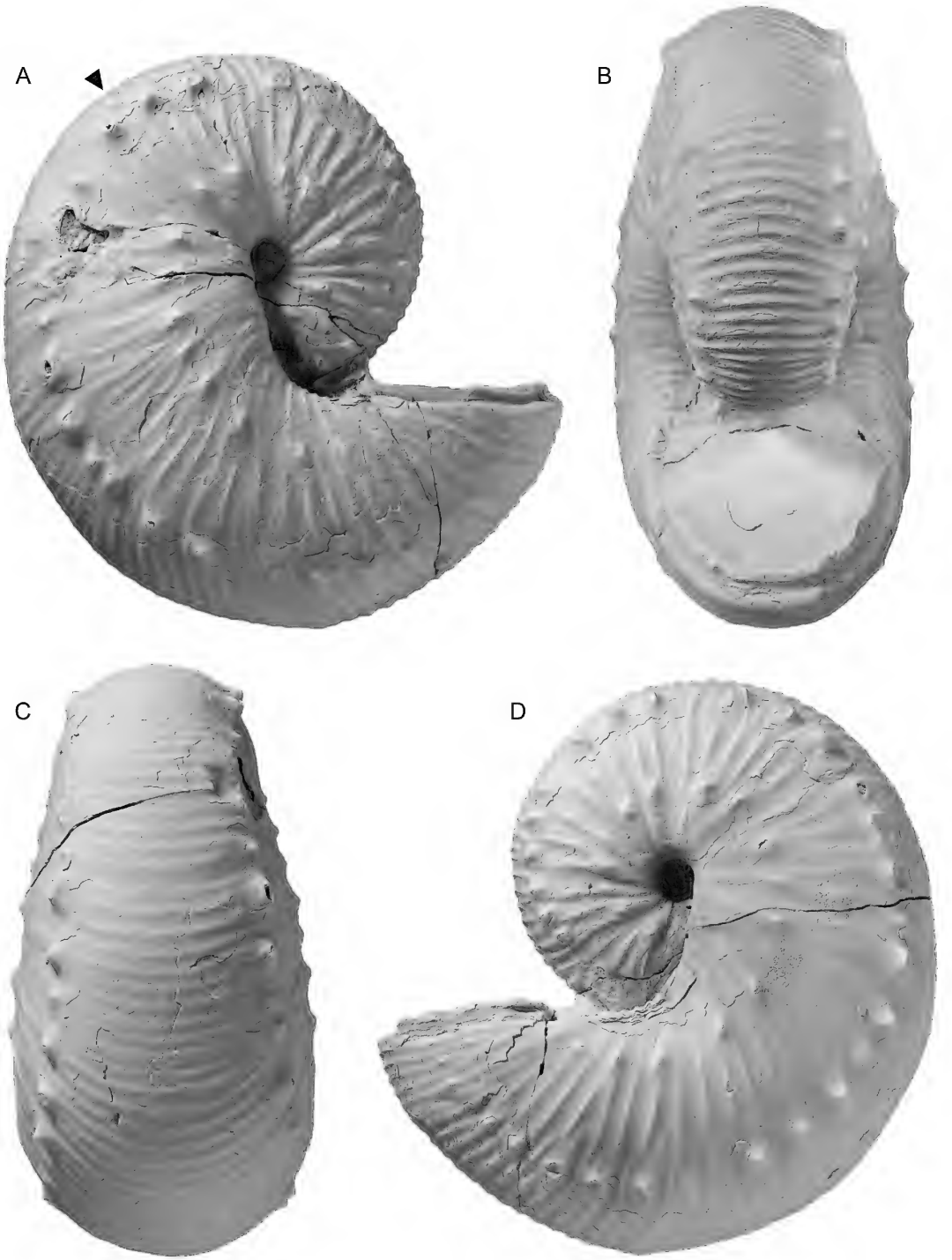
A
B
C
D

below the ventrolateral shoulder, so that the distance between ventrolateral tubercles on opposite sides of the venter is unusually high.

The whorl section at the point of recurvature is less compressed than that at midshaft, mainly due to a decrease in whorl height. W_H/H_H averages 1.14 and ranges from 0.93 to 1.33 (1.16 in the holotype). The whorl section at the point of recurvature is subovoid with maximum whorl width at one-third whorl height. The umbilical wall is slightly concave and the umbilical shoulder is sharply rounded. The flanks are broadly rounded and gently converge toward the venter.

At the adapical end of the exposed phragmocone, ribs emerge at the umbilical seam. They are strong and widely spaced on the flanks and bend slightly forward at two-thirds whorl height. They attain their maximum strength at one-third whorl height and develop into small umbilicolateral tubercles at this point. Ribs are equally spaced on the venter, which they cross with a slight adoral projection. In the holotype, the rib density on the adapical end of the phragmocone is 4.5 ribs/cm. The rib density is nearly the same on the adoral end of the phragmocone (e.g., 5 ribs/cm in the holotype).

On the body chamber, ribs arise at the umbilical seam and are rursiradiate on the umbilical wall and shoulder. They are long, broad, straight, and rectiradiate at midshaft, becoming more prorsiradiate toward the adoral end of the shaft. Umbilicolateral tubercles are usually present on the body chamber, but given the large size and robust cross section of the shell, they are surprisingly small. In the holotype, the distance between consecutive umbilicolateral tubercles at midshaft is 4.9 mm. Branching and intercalation occur at two-thirds whorl height, with the result that the outer flanks are more densely covered with ribs than the inner flanks. Ribs are usually not preserved on the venter of the shaft, but in AMNH 108313 (fig. 28) in which they are preserved, the rib density is 6 ribs/cm. Ribs are narrow and closely spaced on the venter of the hook, which they cross with a strong adoral projection. In AMNH 108313, the rib density on the hook is 9 ribs/cm (fig. 28).

Ventrolateral tubercles appear early in ontogeny at a diameter of approximately 6 mm and continue onto the exposed phragmocone (fig. 36). They are closely and evenly spaced, occurring on every rib or every other rib. In the holotype, the distance between consecutive tubercles is 4.3 mm on the adapical end and 6.3 mm on the adoral end of the exposed phragmocone, yielding a total of 17 tubercles. The tubercles are conical in shape and change from slightly radially elongate at the point of exposure to slightly clavate on the adoral end of the phragmocone.

Ventrolateral tubercles are closely and evenly spaced on the midshaft, becoming slightly more widely spaced on the adoral end of the shaft, and slightly more closely spaced again near the aperture. In the holotype, the distance between consecutive ventrolateral tubercles is 9.6 mm on the midshaft, 12.7 mm on the adoral end of the shaft, and 7.4 mm on the hook, yielding a total of 15 tubercles on the body chamber (32 tubercles on the whole exposed shell). In AMNH 108313 (fig. 28) in which the ribs are well preserved on the venter at midshaft, two or three ribs loop between ventrolateral tubercles on opposite sides of the venter with one or two ribs intercalating between them. The tubercles are slightly clavate on the adoral end of the shaft where they attain their maximum height.

A single row of outer lateral tubercles appears early in ontogeny at approximately 10 mm diameter (fig. 36). It is joined by another row of inner lateral tubercles, both of which continue onto the exposed phragmocone for an additional one-eighth to one-half whorl. The tubercles are

FIGURE 33. *Hoploscaphites criptonodosus* (Riccardi, 1983), macroconch. **A–D.** USNM 463215, USGS loc. 12700, *Baculites grandis* Zone, Pierre Shale, Campbell County, Wyoming. **A,** Right lateral; **B,** apertural; **C,** ventral; **D,** left lateral. Arrow indicates the base of the body chamber. Specimens ×1.

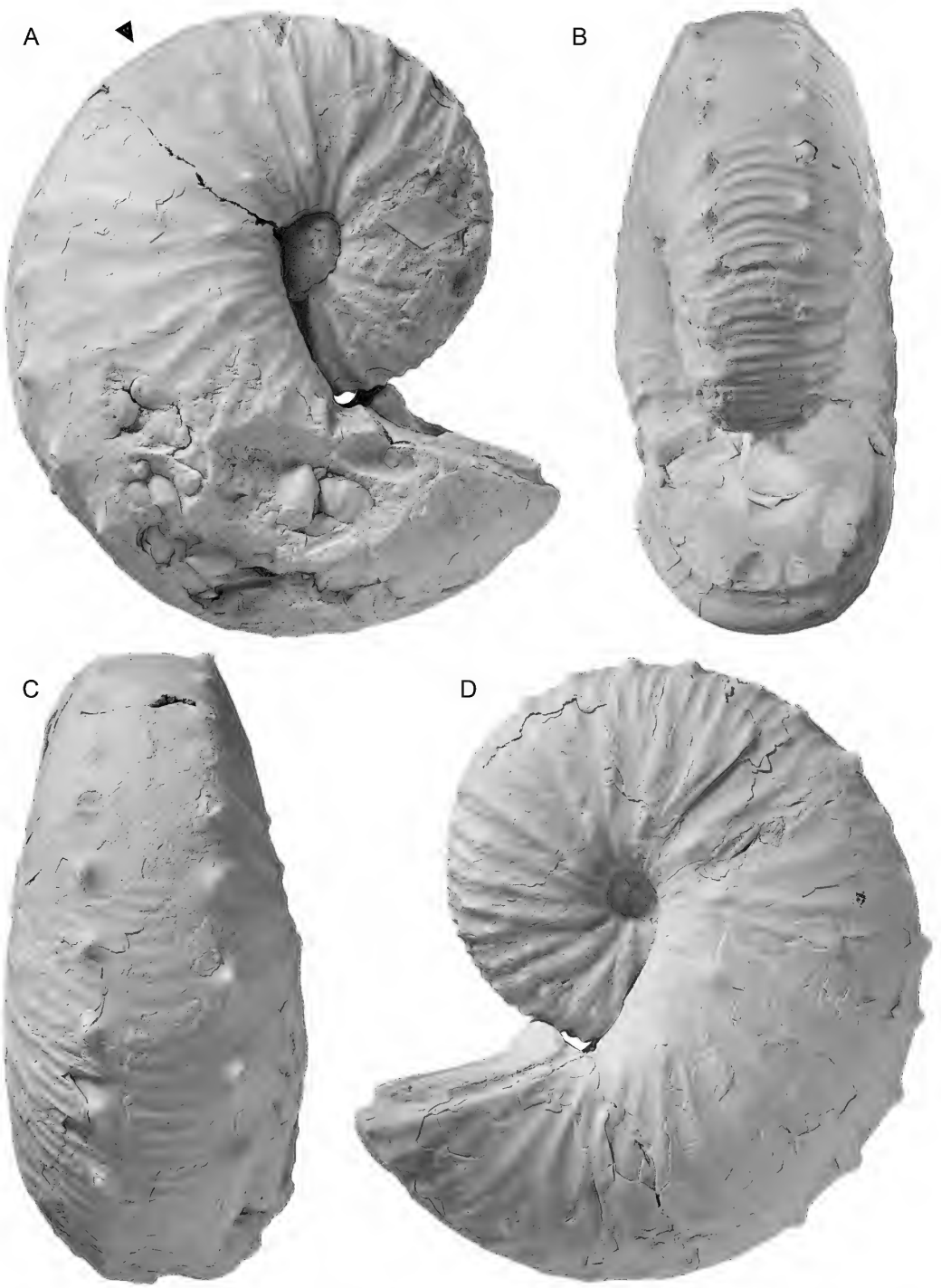

FIGURE 34. *Hoploscaphites criptonodosus* (Riccardi, 1983), macroconch. **A–D.** USNM 713617, USGS loc. 12757, *Baculites grandis* Zone, Pierre Shale, Weston County, Wyoming. **A,** Right lateral; **B,** apertural; **C,** ventral, **D,** left lateral. Arrow indicates the base of the body chamber. Specimens ×1.

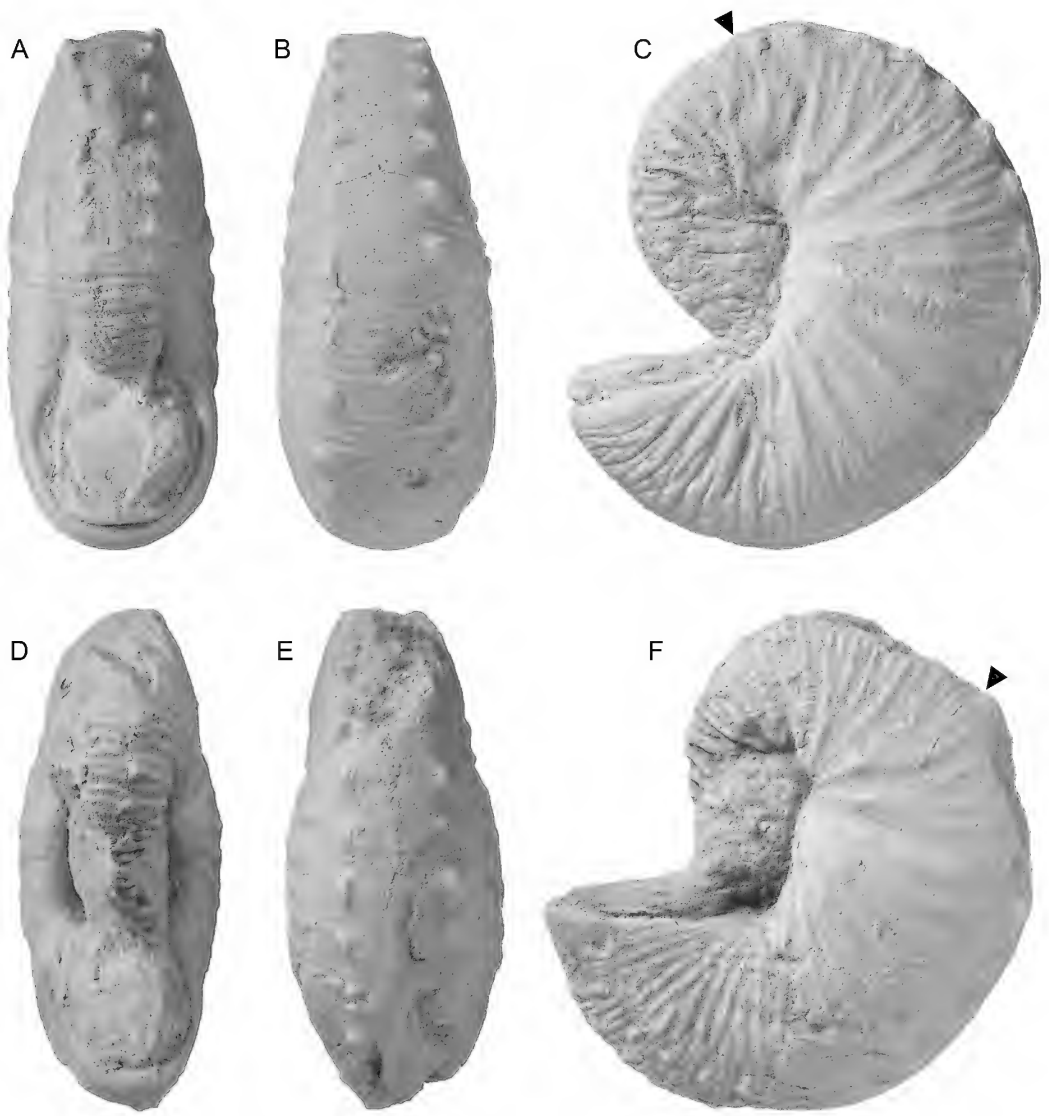

FIGURE 35. *Hoploscaphites criptonodosus* (Riccardi, 1983), macroconchs. **A–C.** FM 10689, erroneously labeled Pierre Shale, but probably Nacatoch Sand, Clark County, Arkansas. **A,** Apertural; **B,** ventral; **C,** left lateral. **D–F.** MSNS-IP 7881.3, ?*Baculites grandis* Zone, Coon Creek Member of the Ripley Formation, Union County, Mississippi. **D,** Apertural; **E,** ventral; **F,** left lateral. Arrows indicate the base of the body chamber. Specimens ×1.

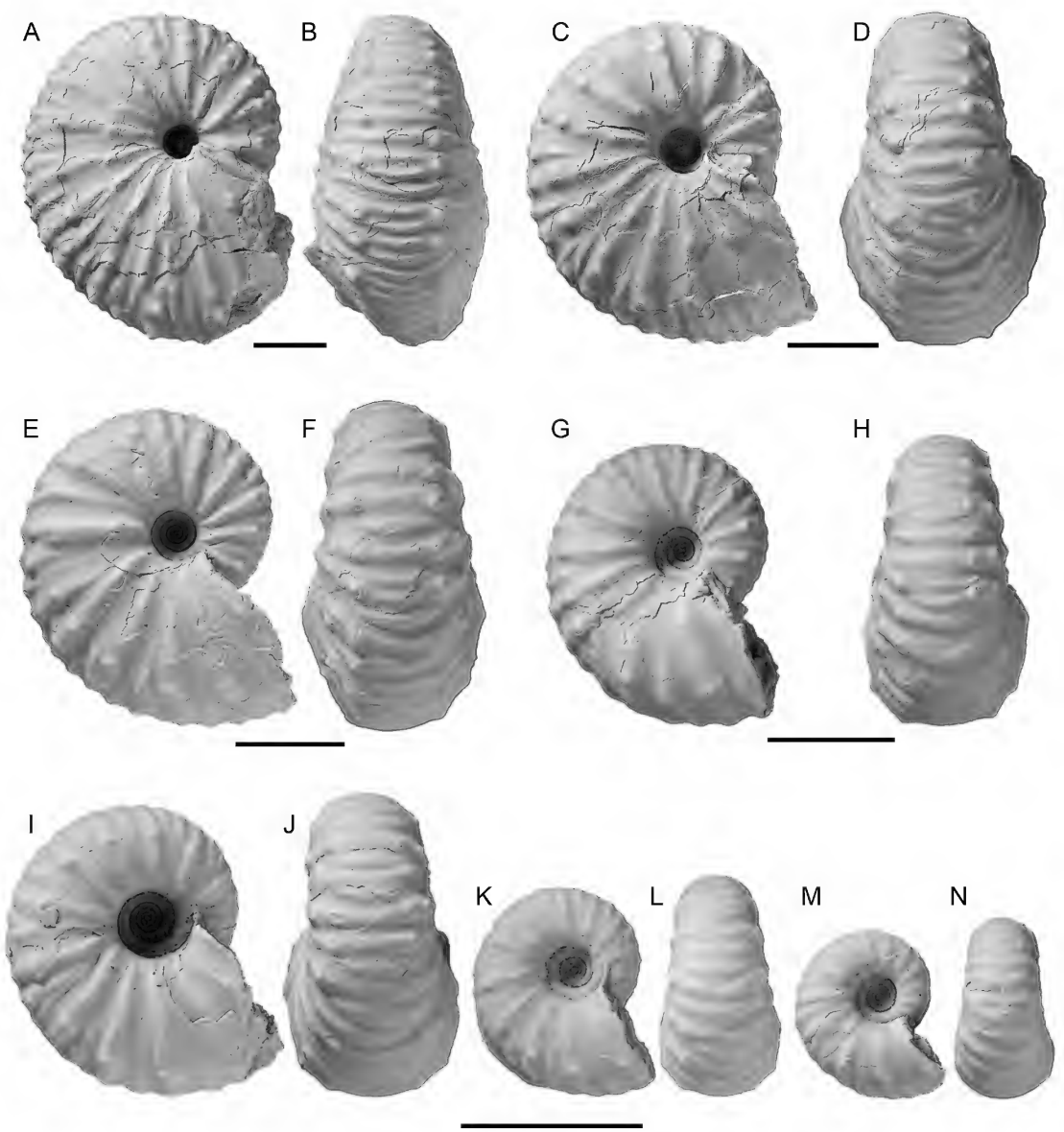

FIGURE 36. Ontogenetic breakdown of *Hoploscaphites criptonodosus* (Riccardi, 1983), macroconch, AMNH 94607, AMNH loc. 3729, *Baculites grandis* Zone, Pierre Shale, Niobrara County, Wyoming. **A–N.** Seven sizes through ontogeny in lateral and ventral views showing the change in ornamentation from the early whorls (M, N) to the adult phragmocone (A, B). Scale bar = 1 cm.

closely spaced and occur on every rib or every other rib. The tubercles in the outermost row are only slightly smaller than those in the ventrolateral row.

The suture is deeply incised, with a broad, asymmetrically bifid first lateral saddle (E/L) and a narrow, symmetrically to asymmetrically bifid first lateral lobe (L) (fig. 23D, E).

Microconch Description: Microconchs are smaller than macroconchs. LMAX averages 51.0 mm and ranges from 43.2 to 68.2 mm (table 4). The size distribution is unimodal with a broad peak at 45–55 mm (fig. 26). The ratio of the average size of microconchs to that of macroconchs is 0.64. This is lower than that in most species of *Hoploscaphites* and may reflect the fact that the sample of microconchs is biased because of its small size.

Microconchs are oval in lateral view with a large gap between the phragmocone and hook. $LMAX/H_{P2}$ averages 3.10 and ranges from 2.81 to 3.39. The average value of $LMAX/H_{P2}$ in microconchs is significantly higher than that in macroconchs (2.83). The phragmocone occupies slightly more than one-half whorl and terminates just below the line of maximum length. The umbilical diameter is relatively larger in microconchs than in macroconchs. UD/LMAX averages 0.10 in microconchs whereas it averages 0.06 in macroconchs. In addition, the umbilical seam in microconchs is concave in side view. The body chamber occupies slightly more than one-half whorl and terminates in a constriction and accompanying varix.

The whorl section at the adapical end of the phragmocone is robust and subquadrate with maximum whorl width at one-quarter whorl height. W_{P1}/H_{P1} averages 0.96 and ranges from 0.82 to 1.09. The umbilical wall is nearly vertical and the umbilical shoulder is sharply rounded. The flanks are broadly rounded and gently converge toward the ventrolateral shoulder. In costal cross section, the flanks flatten out between the inner lateral and ventrolateral tubercles. The venter is broadly rounded. The whorl section at the adoral end of the phragmocone is more quadrate than that at the adapical end of the phragmocone, with flatter flanks and more sharply rounded ventrolateral shoulder. However, the average value of W_{P2}/H_{P2} (0.95) is nearly the same as that of W_{P1}/H_{P1} (0.96).

In passing from the phragmocone to the body chamber, both whorl width and height gradually increase, but the increase in whorl height is much less dramatic than in macroconchs. Whorl height attains its maximum value at midshaft and remains nearly the same thereafter, but whorl width attains its maximum value on the hook and decreases slightly thereafter. The whorl section at midshaft is compressed subquadrate, with maximum width at one-quarter whorl height. W_S/H_S averages 0.92 and ranges from 0.77 to 1.01. The umbilical wall is broad and slopes gently outward culminating in the umbilicolateral tubercles. The flanks are nearly flat and converge toward the ventrolateral shoulder. The ventrolateral shoulder is abruptly rounded and the venter is nearly flat. The whorl section at the point of recurvature is compressed subovate. W_H/H_H averages 1.01 and ranges from 0.85 to 1.10. The flanks are broadly rounded with maximum width at one-quarter whorl height. The venter is broadly rounded, which is accentuated in specimens without ventrolateral tubercles.

On the adapical end of the phragmocone, ribs emerge at the umbilical seam and strengthen on the flanks. They are strong and widely spaced. In more finely ribbed specimens such as AMNH 74357 (fig. 38B–D), they bend slightly backward on the inner flanks, slightly forward on the midflanks, and slightly backward again on the outer flanks. However, in more coarsely ornamented specimens such as USNM 713635 (fig. 38E–H), the ribs are nearly straight and bend only slightly backward on the outer flanks. Ribs are uniformly strong on the venter, which they cross with a slight adoral projection. They are relatively closely spaced with an average of 7 ribs/cm. They are equally coarse on the adoral end of the phragmocone, with branching and interca-

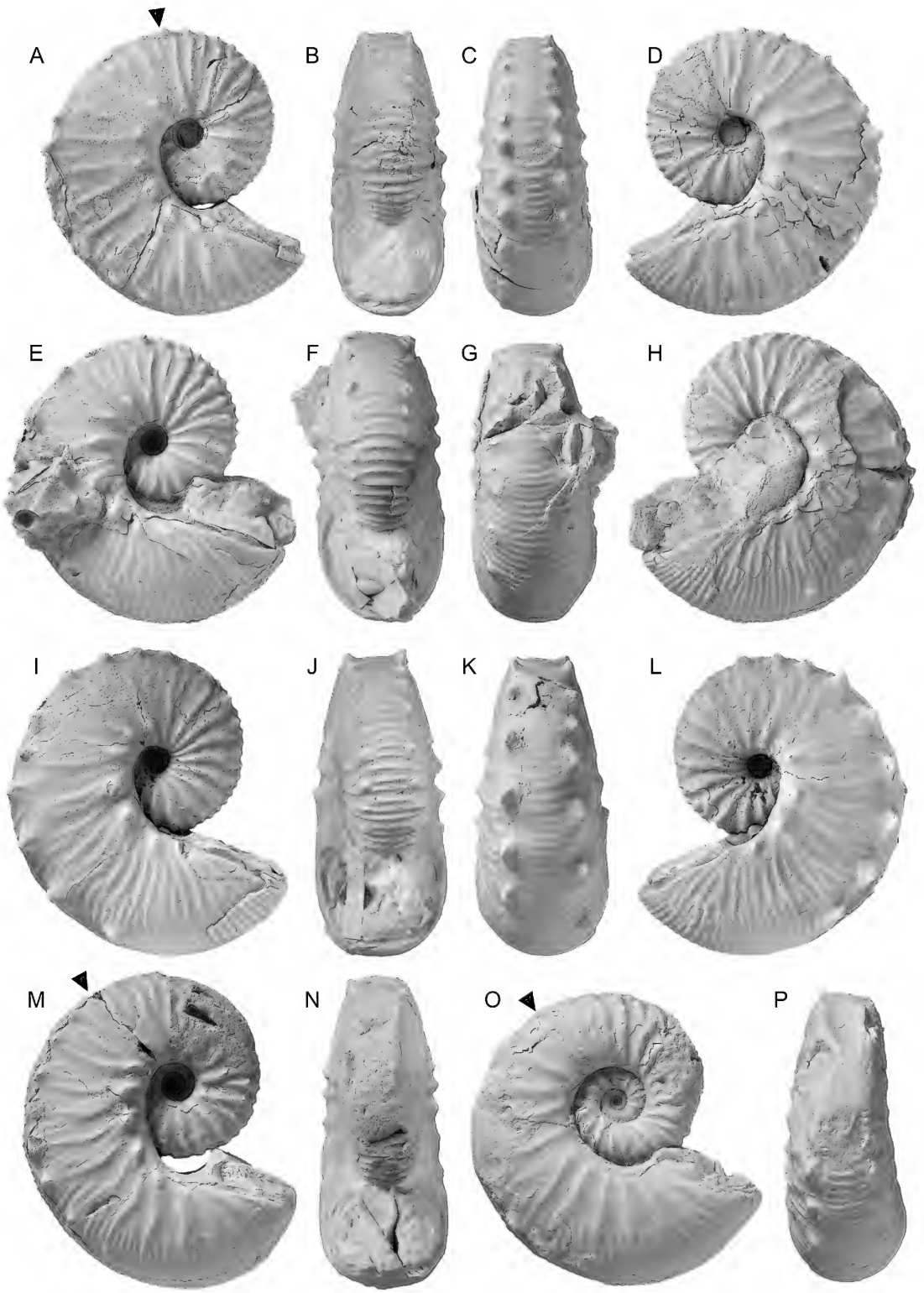
A
B
C
D
E
F
G
H
I
J
K
L
M
N
O
P

lation occurring at one-third and two-thirds whorl height.

Ribs are strong and prorsiradiate on the shaft and cross the flanks with a broad adoral convexity. Branching and intercalation occur at one-third whorl height (at and between the umbilicolateral tubercles) and, again, at two-thirds whorl height. Ribs are generally not preserved on the venter. However, in USNM 713635 (fig. 38E–H) in which they are preserved, they are closely spaced (9 ribs/cm), with a strong adoral projection. Ribs are prorsiradiate on the hook, with branching and intercalation occurring at one-quarter whorl height (at and between the umbilicolateral tubercles) and at one-half whorl height. The outer flanks and venter are covered with fine, closely spaced ribs. The rib density ranges from 8 to 10 ribs/cm in our measured sample.

Umbilicolateral tubercles appear on the adoral end of the phragmocone and continue uninterruptedly to the aperture. They become slightly more widely spaced adorally, attaining their maximum spacing on the adoral end of the shaft, e.g., 6 mm in USNM 713635 (fig. 38E–H), 7 mm in AMNH 74357 (fig. 38B–D), and 8 mm in USNM 713626 (fig. 38I–K). The tubercles are radially elongate on the adoral end of the phragmocone, conical on the midshaft, and clavate on the adoral end of the shaft and hook.

Ventrolateral tubercles are present at the point of exposure. They are initially closely and evenly spaced, becoming slightly more widely spaced on the adoral end of the phragmocone. For example, in USNM 713635 (fig. 38E–H), the distance between consecutive tubercles is 2.5 mm and 4.5 mm on the adapical and adoral ends of the phragmocone, respectively. In contrast, in AMNH 74346 (fig. 37E–H), the tubercles are uniformly spaced at distances of 3–4 mm, except for two gaps of 5–6 mm each on the adapical end of the phragmocone. One or two ribs loop between tubercles on opposite sides of the venter, with up to three ribs intercalating between them. The number of ventrolateral tubercles on the phragmocone ranges from 9 to 13 in our measured sample.

Ventrolateral tubercles continue onto the body chamber and gradually become more widely spaced until the adoral end of the shaft, after which they disappear. The distance between consecutive tubercles on the adoral end of the shaft is 7.5 mm in smaller specimens such as AMNH 74357 (fig. 38B–D) and 11.5 mm in larger specimens such as USNM 713626 (fig. 38I–K). The number of ventrolateral tubercles on the body chamber ranges from 6 to 10 in our measured sample, so that the total number of ventrolateral tubercles on the adult shell ranges from 17 to 24. In specimens in which the ribs are well preserved on the venter of the shaft such as USNM 713635 (fig. 38E–H), as many as four ribs loop between ventrolateral tubercles on opposite sides of the venter, with two or three nontuberculate ribs intercalating between them. The tubercles become progressively larger and more clavate toward the adoral end of the shaft. They are asymmetric in profile. with steeply sloping adapical faces and more gently sloping adoral faces.

One or two lateral rows of tubercles are usually present at the point of exposure. As a result,

FIGURE 37. *Hoploscaphites criptonodosus* (Riccardi, 1983), microconchs. **A–D.** AMNH 108316, AMNH loc. 3278, *Baculites baculus* or *B. grandis* Zone, Pierre Shale, Weston County, Wyoming. **A,** Right lateral; **B,** apertural; **C,** ventral; **D,** left lateral. **E–H.** AMNH 74346, AMNH loc. 3921, *B. grandis* Zone, Pierre Shale, Cedar Creek Anticline, east-central Montana. **E,** Right lateral; **F,** apertural; **G,** ventral; **H,** left lateral. **I–L.** AMNH 74355, AMNH loc. 3921, upper *Baculites baculus* or lower *B. grandis* Zone, Pierre Shale, Cedar Creek Anticline, east-central Montana. **I,** Right lateral; **J,** apertural; **K,** ventral; **L,** left lateral. **M, N.** BHI 4345, *Baculites grandis* Zone, Pierre Shale, Fall River County, South Dakota (found in gravel pit). **M,** Right lateral; **N,** apertural. **O, P.** AMNH 108325, pathologic specimen with unusually openly coiled whorls, *Baculites grandis* Zone, Pierre Shale, Weston County, Wyoming. Gift of Jordan K. Sawdo, Northglen, Colorado, **O,** Right lateral; **P,** apertural. Arrows indicate the base of the body chamber. Specimens ×1.

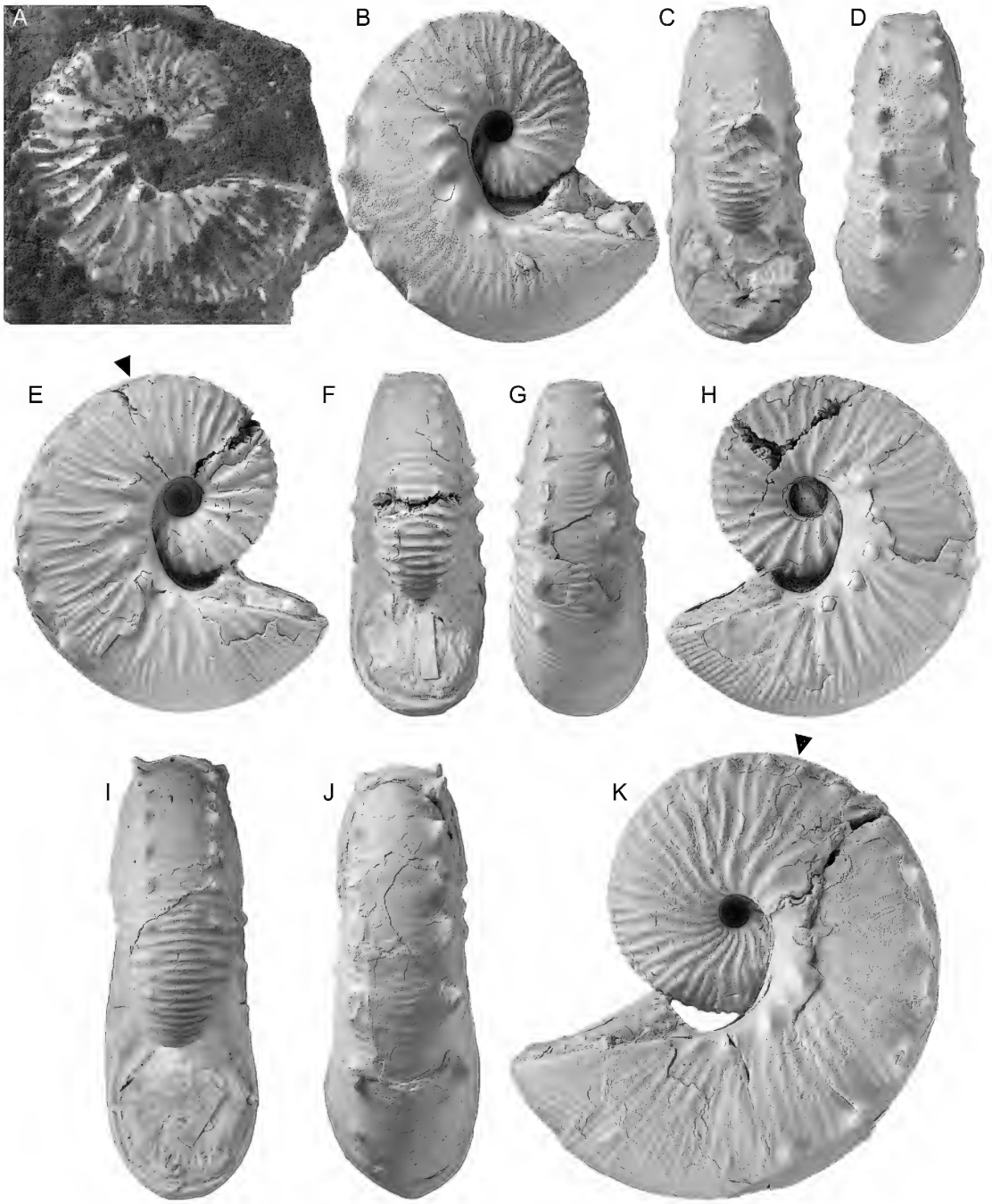
A
B
C
D
E
F
G
H
I
J
K

most of the surface of the shell in this area is covered with tubercles (umbilicolateral, lateral, and ventrolateral tubercles). The lateral tubercles persist to the middle of the phragmocone, but if two rows are present, the inner lateral row usually dies out first. The lateral and ventrolateral tubercles occur on the same rib, with the height of the rib dipping between tubercles. The lateral tubercles are more or less evenly spaced; for example, in USNM 713635 (fig. 38E–H), the distance between consecutive outer lateral tubercles is 5 mm.

Occurrence: This species occurs in the upper part of the *Baculites baculus* Zone and *B. grandis* Zone in the Pierre Shale of Montana, Colorado, and Wyoming and in the Bearpaw Shale of Montana. It is also possible that it occurs in the Pierre Shale of South Dakota but our only specimen from this area (BHI 4345) is from a gravel pit, and its provenance is unknown (fig. 37M, N). Riccardi (1983) also recorded it from the *B. baculus* Zone in the Bearpaw Shale of Saskatchewan, Canada. On the U.S. Gulf Coastal Plain, it occurs in the Coon Creek Member of the Ripley Formation of Mississippi, in the Prairie Bluff Chalk of Alabama (Cobban and Kennedy, 1995), and possibly in the Nacatoch Sand of Arkansas. On the U.S. Atlantic Coastal Plain, it occurs in the Navesink Formation of New Jersey (Kennedy et al., 2000).

Discussion: Most of the microconchs in our measured sample are small. The largest microconch is USNM 713626 (fig. 38I–K), which presumably corresponds to one of the larger macroconchs in our sample, for example, AMNH 108445 (fig. 30). All the microconchs illustrated by Riccardi (1983: pl. 11, figs. 1–21) are equally small and, in this context, it is worth noting that the illustrations of some of his specimens are magnified and, in reality, the specimens are much smaller than they appear (Riccardi, 1983: pl. 11, figs. 7–11). The absence of larger microconchs in both collections may be a preservational bias. We also illustrate a pathologic specimen (AMNH 108325), which is very openly coiled even for a microconch (fig. 37O, P).

The specimens illustrated by Riccardi (1983) are from the *Baculites baculus* Zone, but most of the specimens that we describe are from the *B. grandis* Zone. We also illustrate two specimens of this species from the U.S. Gulf Coastal Plain. FM 10689 (fig. 35A–C) is a macroconch erroneously labelled as coming from the Pierre Shale, Arkadelphia, Clark County, Arkansas, but probably from the Nacatoch Sand. MMNS-IP 7881.3 (fig. 35D–F) and 8825.1 (fig. 38A) are a macroconch and microconch, respectively, from the Coon Creek Member of the Ripley Formation, Union County, Mississippi. Cobban and Kennedy (1995: fig. 22.5–12) illustrated fragments of similar material from the Prairie Bluff Chalk, Wilcox County, Alabama.

Among older species in the Western Interior, *Hoploscaphites criptonodosus* is most closely similar to large specimens of *H. brevis* from the *Baculites compressus–B. cuneatus* Zones. It differs, however, in its more closely coiled shell and, notably, multituberculate phragmocone, the character from which its name is derived (Riccardi, 1983). As noted above, *H. criptonodosus* is also similar to *H. sargklofak* (fig. 10), which occurs in the same biostratigraphic zone. Indeed, lateral tubercles appear on the adapical end of the exposed phragmocone in both species. However, *H. criptonodosus* is larger and more coarsely ornamented than *H. sargklofak*, although it is possible that the two forms represent the coarsely and finely ornamented end members of a single species.

FIGURE 38. *Hoploscaphites criptonodosus* (Riccardi, 1983), microconchs. **A.** MSNS-IP 8825.1, right lateral, ?*Baculites grandis* Zone, Coon Creek Member of the Ripley Formation, Union County, Mississippi. **B–D.** AMNH 74357, AMNH loc. 3921, upper *Baculites baculus* or lower *B. grandis* Zone, Pierre Shale, Cedar Creek Anticline, Montana. **B,** apertural; **C,** ventral; **D,** left lateral. **E–H.** USNM 713635, USGS Mesozoic loc. D2118, lower *Baculites grandis* Zone, Pierre Shale, Niobrara County, Wyoming. **E,** Right lateral; **F,** apertural; **G,** ventral; **H,** left lateral. **I–K.** USNM 713626, USGS Mesozoic loc. D12208, ?*B. baculus* Zone, Bearpaw Shale, Garfield County, Montana. **I,** Apertural; **J,** ventral; **K,** left lateral. Arrows indicate the base of the body chamber. Specimens ×1.

ACKNOWLEDGMENTS

At the American Museum of Natural History, we thank Bushra Hussaini, Mary Conway, Kathleen Sarg, and Marion Savas for accessioning material and assigning AMNH numbers, Mariah Slovacek for collecting fossils in the field and preparing specimens, Carolyn Merril for surface-scanning several specimens, William Harcourt-Smith for interpreting these scans, Mary Knight for editing the manuscript for publication, and Stephen Thurston for photographing specimens and preparing figures. We thank the landowners Donley and Nancy Darnell and Bobbie Blackenship for permission to collect on their property and Barbara A. Beasley for arranging permits to collect on the Buffalo Gap National Grassland, South Dakota. Many students, colleagues, and family members have helped us collect in the field and interpret the results, and we wish to express our thanks to Jamie Brezina, Barry and Aimee Brown, J. Kirk Cochran, Matthew P. Garb, Kate F. Grier, Isabella Kruta, Ekaterina Larina, Luke Larson, Kimberly C. Meehan, Corinne Myers, Jack Petersen, Kristin Polizzotto, Anastasia Rashkova, Isabelle Rouget, Remy Rovelli, Al Rowe, Joshua Slattery, Kazushige Tanabe, and James Witts. We thank K.C. McKinney for facilitating use of the USGS collections and for hunting down locality data. We thank Susan H. Butts and Jessica Utrup (YPM), George Phillips (MMNS), Kristen MacKenzie (DMNH), and Kathy Hollis (USNM) for arranging loans of specimens from their institutions. An earlier version of this manuscript was reviewed by Margaret (Peg) M. Yacobucci (Bowling Green State University) and Royal H. Mapes (Ohio University), both of whom made very helpful suggestions that improved the quality of the manuscript. This research was supported by the N.D. Newell Fund (AMNH) and personal funds of J.C. and J.W. Grier, T. Linn, and N.L. Larson.

REFERENCES

Atabekian, A.A. 1979. Correlation of the Campanian stage in Kopetdag and western Europe. *In* Aspekte der Kreide europas, International Union of Geological Sciences A6: 511–526. Stuttgart: Schweizerbart.

Birkelund, T. 1965. Ammonites from the Upper Cretaceous of West Greenland. Meddelelser om Grønland 179 (7): 1–192.

Bishop, G.A. 1967. Biostratigraphic mapping in the upper Pierre Shale utilizing the cephalopod genus *Baculites,* Cedar Creek Anticline, Montana. M.S. thesis in Geology, South Dakota School of Mines and Technology, Rapid City, 18 pp.

Bishop, G.A. 1973. Geology, stratigraphy, and biostratigraphy of the north end of the Cedar Creek Anticline, Dawson County, Montana. Montana Bureau of Mines and Geology Special Publication 61.

Calvert, W.R. 1910. Geology of certain lignite fields in eastern Montana. U.S. Geological Survey Bulletin 441: 187–201.

Clement, J.H. 1986. Cedar Creek: a significant paleotectonic feature of the Williston Basin. Part II. Northern Rocky Mountains. *In* J.A. Peterson (editor), Paleotectonics and sedimentation in the Rocky Mountain region, United States: 213–240. Tulsa, OK: American Association of Petroleum Geologists.

Cobban, W.A., 1952. Scaphitoid cephalopods of the Colorado Group. U.S. Geological Survey Professional Paper 239: 1–39.

Cobban, W.A. 1958. Two new species of *Baculites* from the Western Interior Region. Journal of Paleontology 36 (1): 126–135.

Cobban, W.A., and W.J. Kennedy. 1995. Maastrichtian ammonites chiefly from the Prairie Bluff Chalk in Alabama and Mississippi. Paleontological Society Memoir 44: 1–40.

Cobban, W.A., E.A. Merewether, T.D. Fouch, and J.D. Obradovich. 1994. Some Cretaceous shorelines in the Western Interior of the United States. *In* M.V. Caputo, J.A. Peterson, and K.J. Franczyk (editors), Mesozoic systems of the Rocky Mountain region, USA: 393–413. Denver: Rocky Mountain Section of Society for Sedimentary Geology.

Cobban, W.A., I. Walaszczyk, J.D. Obradovich, and K.C. McKinney. 2006. A USGS zonal table for the Upper Cretaceous middle Cenomanian–Maastrichtian of the Western Interior of the United States based on ammonites, inoceramids, and radiometric ages. U.S. Geological Survey Open-File Report 2006-1250: 1–46.

Cooper, M.R. 1994. Towards a phylogenetic classification of the Cretaceous ammonites. III. Scaphitaceae. Neues Jahrbuch für Geologie und Paläontologie Abhandlungen 193 (2): 165–193.

Coryell, H.N., and E.S. Salmon. 1934. A molluscan faunule from the Pierre Formation in eastern Montana. American Museum of Natural History Novitates 746: 1–18.

Cuvier, G. 1797. Tableau élémentaire de l'histoire naturelle des animaux. Paris: Baudouin, xvi + 710 pp.

Delaney, R.R., J.D. Witts, and N.H. Landman. 2018. The geologically youngest methane seep in the Late Cretaceous Western Interior Seaway. Geological Society of America, Abstracts with Programs 50 (6).

DeWolf, F.W., and W.W. West. 1939. Stratigraphic studies of Baker-Glendive Anticline, eastern Montana. American Association of Petroleum Geologists Bulletin 23: 461–475.

Elias, M.K. 1933. Cephalopods of the Pierre Formation of Wallace County, Kansas, and adjacent area. University of Kansas Science Bulletin 21 (9): 289–363.

Erdmann, C.E., C.E. Dobbin, and R.M. Larson. 1936. Geologic and structure contour map of the Cedar Creek Anticline, Dawson, Prairie, Wibaux and Fallon Counties, Montana, and Bowman County, North Dakota. U.S. Geological Survey General Mineral Resources Map.

Gill, J.R., and W.A. Cobban. 1966. The Red Bird section of the Upper Cretaceous Pierre Shale in Wyoming. U.S. Geological Survey Professional Paper 393-A: 1–73.

Gill, J.R., and W.A. Cobban. 1973. Stratigraphy and geologic history of the Montana Group and equivalent rocks, Montana, Wyoming, and North and South Dakota. U.S. Geological Survey Professional Paper 776: 1–37.

Gill, T. 1871. Arrangement of the families of mollusks. Smithsonian Miscellaneous Collections 227: 1–49.

Grier, J.C., and J.W. Grier. 1998. New findings of the ammonite *Rhaeboceras*, including a new species, from the Pierre Shale of eastern Montana. Journal of Paleontology 72: 473–476.

Grier, J.C., J.W. Grier, and J.G. Petersen. 1992. Occurrence of the Upper Cretaceous ammonite *Rhaeboceras* in the *Baculites eliasi* Zone of the Pierre Shale. Journal of Paleontology 66: 521–523.

Grier, J.W., J.C. Grier, N.L. Larson, and J.G. Petersen. 2007. Synonymy of the ammonite genus *Ponteixites* Warren with *Rhaeboceras* Meek. Rocky Mountain Geology 42: 123–136.

Gries, J.P. 1954. Cretaceous rocks of Williston Basin. American Association of Petroleum Geologists Bulletin 38: 443–453.

Hall, J., and F.B. Meek. 1855. Descriptions of new species of fossils from the Cretaceous formations of Nebraska, with observations upon *Baculites ovatus* and *Baculites compressus*, and the progressive development of the septa in baculites, ammonites and scaphites. American Academy of Arts and Science Memoir, new series 5: 379–411.

Hicks, J.F., J.D. Obradovich, and L. Tauxe. 1999. Magnetostratigraphy, isotopic age calibration, and intercontinental correlation of the Red Bird section of the Pierre Shale, Niobrara County, Wyoming, USA. Cretaceous Research 20: 1–27.

Jacobs, D.K., N.H. Landman, and J.A. Chamberlain. 1994. Ammonite shell shape covaries with facies and hydrodynamics: Iterative evolution as a response to changes in basinal environment. Geology 22: 905–908.

Kauffman, E.G., and W.G.E. Caldwell. 1993. The Western Interior Basin in space and time. *In* W.G.E. Caldwell and E.G. Kauffman (editors), Evolution of the Western Interior Basin. Geological Association of Canada Special Paper 39: 1–30.

Kennedy, W.J. 1986. The ammonite fauna of the Calcaire à *Baculites* (Upper Maastrichtian) of the Cotentin Peninsula (Manche, France). Palaeontology 29: 25–83.

Kennedy, J.W., N.H. Landman, W.A. Cobban, and R.O. Johnson. 2000. Additions to the ammonite fauna of the Upper Cretaceous Navesink Formation of New Jersey. American Museum Novitates 3306: 1–30.

Keupp, H. 2006. Sublethal punctures in body chambers of Mesozoic ammonites (*forma aegra fenestra* n. f.), a tool to interpret synecological relationships, particularly predator-prey interactions. Paläontologische Zeitschrift 80/2:112–123.

Kier, P.M. 1966. A new echinoid from the Cretaceous Pierre Shale of eastern Wyoming. United States Geological Survey Professional Paper 393-A: A62–65.

Klein, J. 2016. Lower Cretaceous Ammonites X Scaphitoidea, including the Upper Cretaceous representatives. Fossilium catalogus I: Animalia, pars 157: 1–203. Leiden: Backhuys.

Kröger, B. 2002. Antipredatory traits of the ammonoid shell—indications from Jurassic ammonoids with sublethal injuries. Paläontologische Zeitschrift 76 (2): 223–234.

Krystinik, L.F., and B.B. DeJarnett. 1995. Lateral variability of sequence stratigraphic framework in the Campanian and lower Maastrichtian of the Western Interior Seaway. *In* J.C. Van Wagoner and G.T. Bertram (editors), Sequence stratigraphy of foreland basin deposits: outcrop and subsurface examples

from the Cretaceous of North America. American Association of Petroleum Geologists Memoir 64: 11–25.

Landman, N.H., and K.M. Waage. 1986. Shell abnormalities in scaphitid ammonites. Lethaia 19 (3): 211–224.

Landman, N.H., and K.M. Waage. 1993a. Scaphitid ammonites of the Upper Cretaceous (Maastrichtian) Fox Hills Formation in South Dakota and Wyoming. Bulletin of the American Museum of Natural History 215: 1–257.

Landman, N.H., and K.M. Waage. 1993b. Morphology and environment of Upper Cretaceous (Maastrichtian) scaphites. Geobios, Mémoire Spécial 15: 227–265.

Landman, N.H., W.J. Kennedy, W.A. Cobban, and N.L. Larson. 2010. Scaphites of the "*nodosus* group" from the Upper Cretaceous (Campanian) of the Western Interior of North America. Bulletin of the American Museum of Natural History 342: 1–242.

Landman, N.H., W.A., Cobban, and N.L. Larson. 2012a. Mode of life and habitat of scaphitid ammonites, *In* P. Neige and I. Rouget (editors), 8th International Symposium, Cephalopods—present and past, Dijon, Aug. 30–Sept. 2, 2010. Geobios 45: 87–98.

Landman, N.H., et al. 2012b. Methane seeps as ammonite habitats in the U.S. Western Interior Seaway revealed by isotopic analyses of well-preserved shell material. Geology 40 (6): 507–510.

Landman, N.H., J.C. Grier, J.W. Grier, J.K. Cochran, and S.M. Klofak. 2015a. 3-D orientation and distribution of ammonites in a concretion from the Upper Cretaceous Pierre shale of Montana. Swiss Journal of Paleontology 134 (2): 257–279.

Landman, N.H., W.J. Kennedy, and N.L. Larson. 2015b. A new species of scaphitid ammonite from the lower Maastrichtian of the Western Interior of North America, with close affinities to *Hoploscaphites constrictus* Sowerby, 1817. American Museum Novitates 3833: 1–40.

Landman, N.H., J.S. Slatterty, and P.J. Harries. 2016. Encrustation of inarticulate brachiopods on scaphitid ammonites and inoceramid bivalves from the Upper Cretaceous U. S. Western Interior. Acta Geologica Polonica 66 (4): 645–662.

Landman, N.H., A.G. Plint, and I. Walaszczyk. 2017. Scaphitid ammonites from the Upper Cretaceous (Coniacian-Santonian) Western Canada Foreland Basin. Bulletin of the American Museum of Natural History 414: 105–172.

Landman, N.H., et al. 2018a. Isotope sclerochronology of ammonites (*Baculites compressus*) from methane seep and non-seep sites in the Late Cretaceous Western Interior Seaway, USA: implications for ammonite habitat and mode of life. American Journal of Science 318: 603–639.

Landman, N.H., et al. 2018b. Nautilid nurseries: hatchlings and juveniles of *Eutrephoceras dekayi* from the lower Maastrichtian (Upper Cretaceous) Pierre Shale of east-central Montana. Lethaia: 51 (1): 48–74.

Larson, N.L. 2003. Predation and pathologies in the Late Cretaceous ammonite family Scaphitidae. MAPS 26 (3): 1–30. Malcolm, IL: Mid-America Paleontology Society.

Larson, N.L. 2016. The Late Cretaceous (upper Campanian) cephalopod fauna from the Coon Creek Science Center, McNairy County, Tennessee. Bulletin of the Alabama Museum of Natural History 33: 21–58.

Larson, N.L., S.D. Jorgensen, R.A. Farrar, and P.L. Larson. 1997. Ammonites and the other cephalopods of the Pierre Seaway. Tucson, AZ: Geoscience Press, 148 pp.

Linn, T. 2010. Biostratigraphic zonation of fossil cephalopods in the upper unnamed shale member of the Pierre Shale in the Cedar Creek Anticline of Dawson County, MT. Senior research paper, B.S. in Geology, South Dakota School of Mines and Technology, Rapid City, 28 pp.

Machalski, M. 2005. Late Maastrichtian and earliest Danian scaphitid ammonites from central Europe: taxonomy, evolution, and extinction. Acta Palaeontologica Polonica 50 (4): 653–696.

Machalski, M., and C. Heinberg. 2005. Evidence for ammonite survival into the Danian (Paleogene) from the Cerithium Limestone at Stevns Klint, Denmark. Bulletin of the Geological Society of Denmark 52: 97–111.

Machalski, M.J., J.W.M. Jagt, N.H. Landman, and N. Motchurova-Dekova. 2007. The highest records of North American scaphitid ammonites in the European Maastrichtian (Upper Cretaceous) and their stratigraphic implications. Acta Geologica Polonica 2: 169–185.

Meek, F.B. 1876. A report on the invertebrate Cretaceous and Tertiary fossils of the upper Missouri country. United States Geological Survey of the Territories Report 9: 1–629, pls. 1–45.

Meek, F.B., and F.V. Hayden 1856. Descriptions of new species of Gasteropoda and Cephalopoda from the Cretaceous formations of Nebraska Territory. Proceedings of the Academy of Natural Sciences, Philadelphia 8: 63–126.

Meek, F.B., and F.V. Hayden. 1861. Descriptions of new Lower Silurian (Primordial), Jurassic, Cretaceous and Tertiary fossils collected in Nebraska by the exploring expedition under the command of Captain W.F. Raynolds, U.S. Topographical Engineer, with some remarks on the rocks from which they were obtained. Philadelphia Academy of Natural Science Proceedings: 415–447.

Nowak, J. 1911. Untersuchungen über die Cephalopoden der oberen Kreide in Polen. II Teil: die Skaphiten. Bulletin de l'Académie des Sciences de Cracovie Séries B 7: 547–589.

Owen, D.D. 1852. Report of a geological survey of Wisconsin, Iowa, and Minnesota; and incidentally of a portion of Nebraska Territory made under instructions from the United States Treasury Department. Philadelphia: Lippincott, Grambo, & Co., 2 vols., 638 pp.

Quaas, A. 1902. II. Die Fauna der Overwegischichten und der Blätterthone in der libyschen Wüste. Palaeontographica 30 (2): 153–336, 14 pl.

Reiskind, J. 1975. Marine concretionary faunas of the uppermost Bearpaw Shale (Maestrichtian) in eastern Montana and southwestern Saskatchewan. Geological Association of Canada Special Paper 13: 235–252.

Riccardi, A.C. 1983. Scaphitids from the Upper Campanian–lower Maastrichtian Bearpaw Formation of the Western Interior of Canada. Geological Survey of Canada Bulletin 354: 1–51.

Robinson, C.S., W.J. Mapel, and W.A. Cobban. 1959. Pierre Shale along western and northern flanks of the Black Hills, Wyoming, and Montana. American Association of Petroleum Geologists Bulletin 43: 101–123.

Sageman, B.S., and M.A. Arthur. 1994. Early Turonian paleogeographic/paleobathymetric map, Western Interior, U. S. *In* M. Caputo, J.A. Peterson, and K.J. Franczyk (eds.), Mesozoic Systems of the Rocky Mountain Region, U.S. Rocky Mountain Section, SEPM (Society for Sedimentary Geology) Special Publication: 457–470.

Sessa, J.A., et al. 2015. Ammonite habitat revealed via isotopic composition and comparisons with co-occurring benthic and planktonic organisms. Proceedings of the National Academy of Sciences of the United States of America: 112 (51) 15562–15567. [www.pnas.org/cgi/doi/10.1073/pnas.1507554112]

Slattery, J.S., W.A. Cobban, K.C. McKinney, P.J. Harries, and A.L. Sandness. 2013. Early Cretaceous to Paleocene paleogeography of the Western Interior Seaway: the interaction of eustasy and tectonism. *In* M.J. Bingle-Davis (editor), Guidebook (68th Annual Field Conference): Cretaceous Conference: evolution and revolution: Casper, Wyoming, June 1–4, 2013. Casper: Wyoming Geological Association.

Slattery, J.S., P.J. Harries, and A.L. Sandness. 2018. Do marine faunas track lithofacies? Faunal dynamics in the Upper Cretaceous Pierre Shale, Western Interior, USA. Palaeogeography, Palaeoclimatology, Palaeoecology 496: 205–224.

Sowerby, J. 1817. The mineral conchology of Great Britain, vol. 2. London: the author. [7 vols.]

Stephenson, L.W. 1941. The larger invertebrates of the Navarro Group of Texas (exclusive of corals and crustaceans and exclusive of the fauna of the Escondido Formation). University of Texas Bulletin 4101: 1–641.

Takeda, Y., L. Tanabe, T. Sasaki, and N.H. Landman. 2016. Durophagous predation on scaphitid ammonoids in the Late Cretaceous Western Interior Seaway of North America. Lethaia 49 (1): 28–42.

Vuke, S.M., E.M. Wilde, R.B. Colton, and M.S. Stickney. 2003. Geologic map of the Wibaux 30′ × 60′ Quadrangle eastern Montana and adjacent North Dakota. Montana Bureau of Mines and Geology, Open File Report MBMG 465, 11 pp.

Walaszczyk, I., W.A. Cobban, and P.J. Harries. 2001. Inoceramids and inoceramid biostratigraphy of the Campanian and Maastrichtian of the United States Western Interior Basin. Revue Paléobiologie, Genève 20 (1): 117–234.

Whitfield, R.P. 1877. Preliminary report on the paleontology of the Black Hills, containing descriptions of new species of fossils from the Potsdam, Jurassic, and Cretaceous formations of the Black Hills of Dakota. U.S. Geographical and Geological Survey Rocky Mountain Region Report (Powell), 49 pp.

Wiedmann, J. 1966. Stammesgeschichte und System der postriadischen Ammonoideen: ein Überblick. Neues Jahrbuch für Geologie und Paläontologie Abhandlungen 125: 49–79; 127: 13–81.

Williams, G.D., and C.R. Stelck. 1975. Speculations on the Cretaceous palaeogeography of North America. *In* W.G.E. Caldwell (editor), The Cretaceous system in the Western Interior of North America. Geological Association of Canada Special Paper 13: 1–20.

Wright, C.W. 1996. Treatise on invertebrate paleontology: part L, Mollusca 4 (revised), Cretaceous Ammonoidea: 362 pp. Boulder, CO: Geological Society of America.

Zittel, K.A. von. 1884. Handbuch der Paläontologie. Abteilung 1. Band 2: 329–522. Munich: R. Oldenbourg.

APPENDIX

List of Localities

Localities are from the American Museum of Natural History (AMNH), the Denver Museum of Nature and Science (DMNH), the Geological Survey of Canada (GSC), the U.S. Geological Survey (USGS), and the Yale Peabody Museum (YPM). Several localities specify a range of biozones, but some specimens from these localities were collected with more precise information (within a single biozone or part thereof). The biostratigraphic information is listed in a column next to the specimens in tables 1–4. The names of collectors and dates of collection are indicated at the end of each entry, where known. In the USGS numbers, the prefix D refers to Denver locality numbers and the others refer to Washington, D.C., locality numbers.

AMNH Localities

1. 3244. *Baculites baculus–B. grandis* zones, Pierre Shale, secs. 2, 34, and 35 T. 14 N., R. 55 E. and sec. 1, T. 13 N., R. 55 E., approximately 10 km south of Glendive, Dawson County, Montana.

2. 3264. Upper *Baculites baculus*–lower *B. grandis* zones, Pierre Shale, W½ sec. 15, T. 42 N., R. 62 W., west of Newcastle, Weston County, Wyoming. July 8, 1998.

3. 3265. *Baculites baculus–B. grandis* zones, Pierre Shale, SE¼ sec. 15, T. 42 N., R. 62 W., west of Newcastle, Weston County, Wyoming.

4. 3268. *Baculites baculus–B. grandis* zones, Pierre Shale, S½ sec.19, T. 43N., R. 62W., west of Newcastle, Weston County, Wyoming.

5. 3269. *Baculites baculus–B. grandis* zones, Pierre Shale, SE¼ sec. 30, SW¼ sec. 29, NE¼ sec. 31 and NW¼ sec. 32, T. 43 N., R. 62 W., west of Newcastle, Weston County, Wyoming.

6. 3278. *Baculites baculus–B. grandis* zones, Pierre Shale, near Newcastle, Weston County, Wyoming.

7. 3487. *Baculites grandis* Zone, upper part of Pierre Shale, 43° 35′ 36″ N, -104° 16′ 42″ W, Weston County, Wyoming.

8. 3727 (= G71188). *Baculites grandis–B. clinolobatus* zones, mostly in and below 8 ft (2.4 m) thick bentonite noted by Gill and Cobban (1966), upper unnamed shale member, Pierre Shale, SW¼ to NW¼NE¼NE¼ sec. 14, T. 38 N., R. 62 W., in an area trending northeast across Brewster Draw, 2.1–2.5 mi (3.4–4.0 km) north-northeast of Red Bird, Niobrara County, Wyoming. N. H. Landman and K. M. Waage, July11, 1988.

9. 3728 (= G71288). *Baculites grandis–B. clinolobatus* zones, mostly in and below 8 ft (2.4 m) thick bentonite noted by Gill and Cobban (1966), upper unnamed shale member, Pierre Shale, SW¼ to NW¼NE¼NE¼ sec. 14, T. 38 N., R. 62 W., in an area trending northeast across Brewster Draw, 2.1–2.5 mi (3.4–4.0 km) north-northeast of Red Bird, Niobrara County, Wyoming. N. H. Landman and K. M. Waage, July 12, 1988.

10. 3730 (= G71488). *Baculites baculus–B. grandis* zones, mostly in and below 8 ft (2.4 m) thick bentonite noted by Gill and Cobban (1966), upper unnamed shale member, Pierre Shale, SW¼ to NW¼NE¼NE¼ sec. 14, T. 38 N., R. 62 W., in an area trending northeast across Brewster Draw, 2.1–2.5 mi (3.4–4.0 km) north-northeast of Red Bird, Niobrara County, Wyoming. N. H. Landman and K. M. Waage, July 14, 1988.

11. 3732 (= G71688). *Baculites baculus–B. clinolobatus* zones, mostly in and below 8 ft (2.4 m) thick bentonite noted by Gill and Cobban (1966), upper unnamed shale member, Pierre Shale, SW¼ to NW¼NE¼NE¼ sec. 14, T. 38 N., R. 62 W., in an area trending northeast across Brewster Draw, 2.1–2.5 mi (3.4–4.0 km) north-northeast of Red Bird, Niobrara County, Wyoming. N. H. Landman, July 16, 1988.

12. 3921. *Baculites eliasi–B. grandis* zones, Pierre Shale, Cedar Creek Anticline, Wibaux, Dawson, Fallon, and Prairie counties, Montana.

Denver Museum of Nature and Science Localities

13. 1405. *Baculites baculus–B. grandis* zones, Pierre Shale, Western Aggregate Pit, near Golden, Jefferson County, Colorado. W. D. Bateman, 1998 (approximately the same site as below).

14. 5751. *Baculites baculus–B. grandis* zones, Pierre Shale, TXI Clay Quarry, near Golden, Jefferson County, Colorado. W. D. Bateman, 1995 (approximately the same site as above).

GSC Localities

15. 10374. *Baculites baculus* Zone, Bearpaw Shale, north side of Frenchman River, just west of road from Caton's Ranch to Robsart, sec. 14, T. 6, R. 25, W 3rd Mer., Saskatchewan. G.M Furnival, 1940.

USGS Localities

16. 5440. Bearpaw Shale, near Poplar, Roosevelt County, Montana.

17. 6528. *Baculites grandis* Zone, Pierre Shale, 3 mi (4.8 km) southeast of Moorcroft, Crook County, Wyoming. T. W. Stanton, 1910.

18. 10189. Upper part of Pierre Shale, SW¼ sec. 32, T. 36 N., R. 63 W., Niobrara County, Wyoming.

19. 10764. Bearpaw Shale, 200 ft (71 m) below top, sec. 30, T. 21 N., R. 34 E., drainage of Seven Blackfoot Creek, breaks of Missouri River, Garfield County, Montana. Dobbin, Thom, and Stanton, 1921.

20. 12700. *Baculites grandis* Zone, Pierre Shale, NE¼ T. 56 N., R. 69 W., Campbell County, Wyoming.

21. 12757. Upper 100 ft (30.5 m) of Pierre Shale, 43.8540882° N., -104.4027328° W., 10 mi (16 km) west of Newcastle, Weston County, Wyoming. C.E. Dobbin and J. B. Reeside, 1924.

22. 23628. Bearpaw Shale, SW¼SW¼ sec. 6, T. 27 N., R. 52 E., Roosevelt County, Montana.

23. 24312. Bearpaw Shale, 38 ft (11.6 m) below top, E½NW¼ sec. 2, T. 26 N., R. 50 E., 5 mi (8 km) south-southwest of Poplar, on west side of Redwater Creek Valley, Roosevelt County, Montana. W.A. Cobban, 1951.

24. D771. *Baculites grandis* Zone, Pierre Shale, NE¼NE¼sec. 9, T. 3 S., R. 70 W., north of Golden, Jefferson County, Colorado.

25. D1018. *Baculites baculus* Zone, Pierre Shale, brownish calcareous concretions about 412–422 ft (125.6–128.6 m) below top, SE ¼ NW ¼ sec. 24, T. 39 N., R. 62 W., south side of U.S. Highway 85, 2.1 mi (3.4 km) southwest of bridge over Mule Creek, Niobrara County, Wyoming. W.A. Cobban, 1956.

26. D1033. *Baculites grandis* Zone, Pierre Shale, brown and gray calcareous concretions 364–394 ft (110.9–120.1 m) below top, NW¼ sec. 25, T. 39 N., R. 62 W., about 1 mi (1.6 km) southeast of U. S. Highway 85, Niobrara County, Wyoming. W.A. Cobban, September 29, 1956.

27. D1047. *Baculites baculus* Zone, Pierre Shale, gray calcareous concretions 77–87 ft (23.5–26.5 m) below top, E½ E½ sec. 27 T. 14 N., R. 55 E., approximately 10 mi (16.1 km) south of Glendive, Dawson County, Montana.

28. D1984. *Baculites baculus* Zone, Pierre Shale, 150 ft (45.7 m) below top of uppermost bentonitic unit, SW¼SE¼SE¼ SW¼ sec. 14, T. 38 N., R. 62 W., Niobrara County, Wyoming. J.R. Gill, W.J. Mapel, C.S. Robinson, and H. A. Tourtelot, 1958.

29. D1985. *Baculites grandis* Zone, Pierre Shale, 110 ft (33.5 m) below top of uppermost bentonitic unit, NW¼SE¼ sec. 14, T. 38 N., R. 62 W., Niobrara County, Wyoming. J.R. Gill, W.J. Mapel, C.S. Robinson, H. A. Tourtelot, and W.A. Cobban, 1958.

30. D1986. Upper part of *Baculites grandis* Zone, upper unnamed shale member, Pierre Shale, NW¼SE¼ sec. 14, T. 38 N., R. 62 W., Niobrara County, Wyoming.

31. D2118. Lower part of *Baculites grandis* Zone, brown limestone concretions, upper unnamed shale member, Pierre Shale, NW¼SE¼ sec. 14, T. 38 N., R. 62 W., Niobrara County,Wyoming.

32. D12208. Bearpaw Shale, NW¼ sec. 32, T. 24 N., R. 42 E., south side of peninsula on Big Dry Creek arm of Ft. Peck Reservoir, Garfield County, Montana. R. J. Sutton, 1971.

33. D14195. Base of Fox Hills Formation, NE¼ sec. 11, T.12 N., R. 56 E., Dawson County, Montana.

YPM Localities

34. A4745. *Baculites baculus–B. grandis* zones, upper part of Pierre Shale, in gulleys from 0.3 mi (0.5 km) south of old road from Lance Creek to U.S. Rt. 85, and 0.5 mi (0.8 km) east of East Fork Buck Creek, and 8.3 mi (13.4 km) east-northeast of Lance Creek, Wyoming. K. M. Waage.

35. A4768. Lower part of *Baculites grandis* Zone, in and below 8 ft (2.4 m)-thick bentonite noted by Gill and Cobban (1966), upper unnamed shale member, Pierre Shale, SW¼ to NW¼ NE¼NE¼ sec.14, T. 38 N., R. 62 W., in an area trending northeast across Brewster Drawer, 2.1–2.5 mi (3.4–4.0 km) north-northeast of Red Bird, Niobrara County, Wyoming.

Scientific Publications of the American Museum of Natural History

American Museum Novitates
Bulletin of the American Museum of Natural History
Anthropological Papers of the American Museum of Natural History

Submission procedures can be found at http://research.amnh.org/scipubs

All issues of *Novitates* and *Bulletin* are available on the web (http://digitallibrary.amnh.org/dspace). Order printed copies on the web from:
http://shop.amnh.org/a701/shop-by-category/books/scientific-publications.html

or via standard mail from:
American Museum of Natural History—Scientific Publications
Central Park West at 79th Street
New York, NY 10024

♾ This paper meets the requirements of ANSI/NISO Z39.48-1992 (permanence of paper).

On the cover: Sample of macroconchs (females?) of *Hoploscaphites macer*, n. sp., from the Upper Cretaceous (lower Maastrichtian) Pierre Shale of the Cedar Creek Anticline, east-central Montana. This species forms part of an evolutionary lineage of ammonites that inhabited the Western Interior Seaway of North America for approximately 12 million years. Reduced ×0.5. Photo: Stephen Thurston (AMNH).